

Proposal to Measure
 $\bar{\nu}_\mu e^-$ and $\nu_\mu e^-$ Elastic Scattering,
Neutrino Oscillations, and Decays of
Long-Lived Neutral Particles
at
The Tevatron of Fermilab

Submitted by
A. Abashian, L. W. Mo^{*}, T. A. Nunamaker, R. Orr,
T. Toohig, and C. H. Wang
Fermilab-N.S.F.-V.P.I. & S.U.-I.H.P. (P.R.C.)

*Spokesman

145

Table of Contents

I.	Introduction	1
II.	Physics	5
	(A) Neutrino-Electron Elastic Scattering.....	5
	(B) Neutrino Masses and Neutrino Oscillations	10
	(C) Decay of Long-Lived Neutral Particles	13
III.	Experimental Apparatus	14
	(A) The Non-Magnetic Detector	15
	(1) The MWPC	15
	(2) The CCD Digitizer	16
	(3) The Planned Test	17
	(4) The Resolutions	18
	(B) The Magnetic Muon Detector	19
	(C) The Neutrino Beam	20
	(D) Equipment Calibration	20
	(E) Beam Normalization	20
IV.	Counting Rates and Backgrounds	23
	(A) Counting Rate for $\nu_{\mu} e^{-}$ and $\bar{\nu}_{\mu} e^{-}$ Elastic Scattering	23
	(B) Background for $\nu_{\mu} e^{-}$ and $\bar{\nu}_{\mu} e^{-}$ Elastic Scattering	24
	(C) Neutrino Oscillations	26
	(D) Neutral Particle Decays	27
V.	Other Possibilities	28
	(1) $\bar{\nu}_e e^{-}$ Elastic Scattering	28
	(2) Search of ν_{τ}	29

VI. Program of Test	31
(1) Hadron and Electron Beam	31
(2) Cosmic Ray Test	31
(3) Muon Test	31
VII. Proposal and Request	32
Appendix 1 Cost Estimate	34
Appendix 2 Manpower, Resources and Support	35
References	37
Figure Captions	40
Figures 1-11	42

I. Introduction

During the past decade, the nature of high energy neutrino experiments has changed markedly. Experiments have advanced from being of low statistics and largely qualitative to being of high statistics and quantitatively and theoretically definitive. Particularly notable among the major accomplishments of neutrino experiments during that period were the discovery of weak neutral currents^(1,2), detailed information on the properties of the weak charged-currents through inelastic neutrino scattering^(3,4), tests of the electroweak unifying gauge theories of Weinberg and Salam⁽⁵⁾, and direct measurements of lepton-lepton couplings⁽⁶⁾.

With the expected turn-on of the Tevatron within the next few years, neutrino beams of hitherto unavailable energies and fluxes will be available to physicists for further experimentation. We can anticipate that with technological improvements in detectors, the prospects for better understanding of weak interactions will be substantially enhanced.

Already, provocative questions are being generated and are capable of being answered. Among these are the following:

1. How many generations of neutrinos are there and what are their properties?
2. Do the various neutrinos have a mass and are there mass differences? If there are mass differences, is it possible to determine them through oscillations between generations in much the same way as for the K_L^0 - K_S^0 system?
3. What are the forms of the couplings between the leptons?

Independent of particular models such as that of Weinberg-Salam, can the vector and axial vector couplings be accurately determined?

4. What theories, alternate to the standard $SU(2)_L \times U(1)$, can provide the unification scheme of the four known forces?
5. In details, how do the weak neutral currents differ from the weak charged currents?
6. Are there long-lived objects, such as axions, which could be observed in a well instrumented neutrino detector?

The list above is only intended to be representative of fundamental questions which can be addressed using today's advanced technology. When compared to physics justification of proposals submitted in the beginning of 1970's it is clear that new directions are being emphasized.

Given the many exciting possibilities presented, it is oftentimes tempting, to design an experiment which will address all questions of interest with a single detector. We have resisted the temptation to proceed along this path in the belief that a well designed apparatus intended to answer a limited but interesting set of questions has, in the long run, a better chance to yield precise measurements which can sensitively test theoretical ideas and models. We propose, therefore, a detector about which we have developed substantial expertise and which we feel can meet the goals described above.

In our considerations, we have attempted to retain the following features for the detector:

1. The technology should be advanced state of the art capable

of yielding improved precision and information not achievable with earlier generation detectors.

2. The detector should be capable of handling high data rates to eliminate the loss of events due to equipment dead-time, since tens of neutrino events per pulse are anticipated.
3. Digitization should be performed in a manner in which the essential data can be extracted in a short time. This has two components; the first is for on-line sampling to monitor the experiment, and the second is for off-line data processing.
4. The detector should have good energy, angular, and spatial resolutions so that rare processes can be cleanly separated from backgrounds arising from more abundant processes. Also, good resolution will permit precision measurements of high rate reactions.
5. A modular design, easy to understand, maintain and operate, and for which Monte Carlo calculations will be easy to perform should be preferred. This will lead to fewer uncertainties about systematic effects which will ultimately be the limiting factor with this new generation of neutrino experiments.
6. Finally, economy in costs without major compromises in capability must be sought. In this regard, ingenuity coupled together with high technical ability are requisite.

In the following sections of this proposal, we shall attempt to define and specify a particular area of neutrino physics and to demonstrate how a unique and powerful detector we have designed is capable of address-

ing, Section II will discuss the physics of interest. Section III will describe the detector in detail. Section IV will deal with rates, backgrounds, biases, calibrations and normalizations. Section V points out the possibility of using the proposed detector on beam dump experiments. Section VI discusses the program of testing and preparation between the present and 1983 when the Tevatron program is expected to commence. Section VII will deal with the proposal and request to the Laboratory. Detailed information is provided in the appendices.

II. Physics

Among the many possibilities in the field of neutrino physics, we focus upon the study of only a few important topics which may contribute to the fundamental understanding of weak interactions. These topics include neutrino-electron elastic scattering, neutrino oscillations, and the decays of long-lived particles.

(A) Neutrino-Electron Elastic Scattering:

The reactions

$$\nu_{\mu} + e^{-} \rightarrow \nu_{\mu} + e^{-}, \text{ and} \quad (1)$$

$$\bar{\nu}_{\mu} + e^{-} \rightarrow \bar{\nu}_{\mu} + e^{-} \quad (2)$$

are particularly important for the study of electroweak interactions. These reactions are particularly simple in the determination of the two parameters, ρ and $\sin^2\theta_W$, in the W-S model as no complications due to quarks are involved. These two parameters are defined by the following expression for the neutral current,

$$J_{\mu}^{NC} = \rho (I_{\mu}^3 - \sin^2\theta_W J_{\mu}^{EM}), \quad (3)$$

where ρ is the ratio of neutral to charged current; I_{μ}^3 , the third isospin component of weak current; $\sin^2\theta_W$, the mixing parameter in W-S model; J_{μ}^{EM} , the electromagnetic current. The cross sections for these two reactions are given by⁽⁷⁾

$$\frac{d\sigma^{\nu, \bar{\nu}}}{dy} = \frac{G_V^2 m_e E^{(-\nu)}}{2\pi} [(g_V \pm g_A)^2 + (g_V \mp g_A)^2 (1-y)^2], \quad (4)$$

where $y \equiv E_e/E^{(-\nu)}$; E_e , the outgoing electron energy; $E^{(-\nu)}$, the energy of incoming ν_μ (or $\bar{\nu}_\mu$); $G_V \approx 10^{-5}/M_p^2$, the Fermi coupling constant; M_p and m_e , the mass of proton and electron; g_V and g_A , the vector and axial-vector coupling constants; and the upper signs inside the brackets are for ν_μ , while the lower ones for $\bar{\nu}_\mu$. Equation (4) is the most general expression for neutrino-electron scattering, and it requires only the existence of leptonic neutral currents. We can integrate this expression between experimental limits in electron energy, E_e , to obtain the total cross section. Using the total cross sections, $\sigma(\nu_\mu e^-)$ and $\sigma(\bar{\nu}_\mu e^-)$, the leptonic coupling constants, g_V and g_A , can be empirically determined independent of any theoretical model. Alternatively, we can use the $\nu_\mu e^-$ cross sections to determine the two independent parameters, ρ and $\sin^2\theta_W$, in the W-S model. It should be recalled that there exists also in the W-S model the condition

$$\rho \equiv \left| \frac{M_Z}{M_W \cos\theta_W} \right|^2 = 1, \quad (5)$$

where M_Z and M_W are the masses of the intermediate vector bosons, Z^0 and W^\pm , respectively. Under such circumstances, g_A is definitely predicted to be

$$g_A = -1/2, \quad (6)$$

and g_V is related to the single remaining parameter, $\sin^2\theta_W$, by the relationship

$$g_V = 2\sin^2\theta_W - 1/2. \quad (7)$$

There exist theoretical models, e.g., the symmetric left-right gauge models $SU(2)_L \times SU(2)_R \times U_{B-L}(1)$ and $U_L(2) \times U_R(2)$ ⁽⁸⁾, or the graded gauge model $SU(2/1)$ ⁽⁹⁾, in which the value of $\sin^2\theta_W$ can be calculated, rather than leaving it as an experimental parameter. They all predict $\sin^2\theta_W = 1/4$, which is equivalent to $g_V = 0$ and $g_A = -1/2$. This prediction implies that, in purely leptonic weak interactions, the electron current is a purely axial vector. The left-handed and the right-handed couplings are equal in magnitudes, but opposite in sign. However, some of the grand unification schemes, such as $SU(5)$, call for $\sin^2\theta_W \leq 0.19$ ⁽¹⁰⁾. It is imperative to resolve this issue by an $(\bar{\nu}_\mu^-) e$ elastic scattering experiment of good statistics.

During the past years, substantial progress has been made in the measurement of $(\bar{\nu}_\mu^-) e^-$ elastic scattering. The results are summarized in Table 1.

Table 1

Experiment	Experimental Group	No. of Events
$\nu_{\mu} + e^{-} \rightarrow \nu_{\mu} + e^{-}$	GGM ⁽¹¹⁾	<0.7
	Aachen-Padova ⁽¹²⁾	11.5
	BNL-Columbia ⁽¹³⁾	11.0
	GGM ⁽¹⁴⁾	8.6
	CHARM ⁽¹⁵⁾	6.5
	E-253 (Fermilab) ⁽¹⁶⁾	34.0
$\bar{\nu}_{\mu} + e^{-} \rightarrow \bar{\nu}_{\mu} + e^{-}$	GGM ⁽¹⁷⁾	3.0
	Aachen-Padova ⁽¹⁸⁾	9.6
$\bar{\nu}_{e} + e^{-} \rightarrow \bar{\nu}_{e} + e^{-}$	Savannah River ⁽¹⁹⁾	~460*

*See footnote in reference 19.

These purely leptonic scattering experiments can provide definitive results, free from hadronic complications; but they lack adequate statistics. Also, the prediction of $g_A = -1/2$ in the standard $SU(2)_L \times U(1)$ model of W-S has not been critically tested in these reactions. Further, the ambiguity in $g_V \neq g_A$ cannot be resolved by the study of $\bar{\nu}_{\mu} e^{-}$ elastic scattering alone. Because Eq.(4) is an expression quadratic in g_V and g_A , its plot in the $g_V - g_A$ plane is an ellipse. The intersections of the two ellipses, corresponding to $\nu_{\mu} e^{-}$ and $\bar{\nu}_{\mu} e^{-}$ elastic scattering, yield four pairs of solutions on g_V and g_A . This four-fold ambiguity can be resolved if we include also the following two reactions:

$$\nu_e + e^- \rightarrow \nu_e + e^- \quad (8)$$

and

$$\bar{\nu}_e + e^- \rightarrow \bar{\nu}_e + e^-. \quad (9)$$

In these two reactions, both charged and neutral current contribute. Their cross sections can also be calculated by Eq.(4) with the substitutions $g_V \rightarrow 1 + g_V$ and $g_A \rightarrow 1 + g_A$. Without doing all four purely leptonic scattering experiments, the uniqueness of the solution for g_V and g_A can only be obtained by using the interference term between the electromagnetic and weak interaction currents in the experiment of $e^+ + e^- \rightarrow \mu^+ + \mu^-$; or by the factorization relationship⁽²⁰⁾ together with the data from polarized eD scattering⁽²¹⁾ and $(\bar{\nu})N$ reactions⁽²²⁾. Summary of the present status is shown in Figure 1.

Within the context of the standard $SU(2)_L \times U(1)$ theory of W-S, with spontaneous symmetry breaking being induced by Higgs doublets, or alternatively with a γ - W^0 interference scheme a la Sakurai, the value of $\rho \equiv \left| \frac{m_W}{m_Z \cos \theta_W} \right|^2$ can be unity. However, higher order radiative corrections⁽²³⁾, which are calculable and finite in the gauge theory, could cause a finite value for $(\rho-1)$. For instance, the loop corrections to the W^\pm propagator can be different from those to the Z^0 propagator as shown in figure 2. As $q^2 \rightarrow 0$, the W^\pm and Z^0 self energy parts will differ, and we will have

$$\rho = 1 + 8\pi^2 G_V^2 m_f^2 + (\text{logarithmic terms}), \quad (10)$$

where m_f refers to the mass of the fermion which circulates in the loop.

If we use the presently available value for ρ from the $(\bar{\nu})N$ experiments:

$$\rho = 1.01 \pm 0.03^{(24)} \quad (11)$$

then we obtain $m_f \leq 500$ GeV. A better limit on ρ would therefore improve the upper bound on the mass of the heaviest quark allowed.

The new experiment we plan to perform at Fermilab on the Tevatron anticipate obtaining $\approx 1,000 \nu_\mu e^-$ and $\approx 200 \bar{\nu}_\mu e^-$ events. This should allow us to determine both ρ and $\sin^2 \theta_W$ to an accuracy of ± 0.01 , or alternatively g_A and g_V to an accuracy of about ± 0.02 . Results of such an accuracy will allow us to make definitive comparisons with the predictions of various gauge models, e.g., $g_A = -1/2$ in the standard model, $\sin^2 \theta_W \leq 0.19$ in SU(5), $\sin^2 \theta_W = 0.25$ in the left-right symmetric models; and to establish better limits on the right-handed couplings and the masses of the heavier gauge bosons. It should be noted that the experimental accuracy can be further improved by increasing the number of $\bar{\nu}_\mu e^-$ events.

(B) Neutrino Masses and Neutrino Oscillations

The question of the finiteness of the neutrino mass, for each of the three known generations, has been most crucial to a number of theories. It can answer the question whether the neutrinos could be Majorana particles, or whether there exist right-handed neutrinos. The experimental values of the neutrino masses at the present time are:

$$\begin{aligned} m(\nu_e) &< 0.00007 \text{ MeV,} \\ m(\nu_\mu) &< 0.51 \text{ MeV,} \\ m(\nu_\tau) &< 250 \text{ MeV.} \end{aligned}$$

On the assumption that the neutrinos of each generation are Majorana particles, Mohapatra and Senjanovic⁽²⁵⁾ have derived an expression for the neutrino mass in terms of the right-handed weak vector boson W_R :

$$m_{\nu_\ell} = \frac{m_\ell^2}{gm_{WR}^2}$$

where g is the coupling constant in the standard gauge theory; m_ℓ , the charged lepton mass; m_{WR} , mass of the right-handed weak vector boson.

If the neutrino masses are indeed unequal and non-zero, we could write⁽²⁶⁾ (consider two generations of neutrinos here only for the sake of brevity):

$$\begin{aligned} \nu_e &= \nu_1 \cos\theta_\nu + \nu_2 \sin\theta_\nu \\ \nu_\mu &= -\nu_1 \sin\theta_\nu + \nu_2 \cos\theta_\nu \end{aligned} \quad (13)$$

where θ_ν is an empirical mixing parameter; ν_1 and ν_2 , the neutrino mass eigen-states. In the event that $\theta_\nu \neq 0$, we might have a neutrino oscillation process, $\nu_\mu \rightleftharpoons \nu_e$, very much similar to the $K_L^0 - K_S^0$ system. The probability of finding the neutrino as an ν_e from an originally ν_μ beam is given by

$$P(\nu_e) = \sin^2(2\theta_\nu) \sin^2 \left[\frac{(m_1^2 - m_2^2) \ell}{4p} \right] P(\nu_\mu) \quad (14)$$

where ℓ is the distance traversed by the neutrino; p , the momentum of the neutrino; m_1 and m_2 , the mass of ν_1 and ν_2 ; $P(\nu_e)$, the probability of finding the neutrino in the state $|\nu_e\rangle$. Previously, physicists used to envisage doing a neutrino oscillation experiment by mounting a detector on a vehicle and vary the length ℓ away from the neutrino source. At lower energies, low fluxes and small cross sections lead to low event rates and make the experiments apparently impractical. With the advent of the Tevatron, the neutrino spectrum can extend to energies as high as 600 GeV and about 1000 neutrino interactions/hr. can be observed. The technique is to use a low effective density detector of ~100 meters in length,

and to compare the charged current interactions induced by electron neutrinos of different energies as a function of distance. If the mass difference is too large, the oscillation wavelength is too small to allow any observation and vice versa for too small a mass difference. Within a window of $\Delta m \approx 1 \sim 10^3 \text{ eV}^{(27)}$, there is a chance to observe the neutrino oscillations.

As a numerical example, we consider a hypothetical case:

$$m_1 = 0 \text{ eV},$$

$$m_2 = 100 \text{ eV},$$

$$\Delta x = 100 \text{ m (detector length)},$$

$$p = 600 \text{ GeV/c}.$$

The oscillation phase angle is given by

$$\Delta\phi = \frac{(m_2^2 - m_1^2)\Delta x}{4p} \approx \frac{(10^{-7})^2 \times 10^4}{4 \times 600 \times (2 \times 10^{-14})} \approx 2 \text{ rad.}$$

The oscillation wavelength is given by

$$\lambda \approx \frac{2\pi}{\Delta\phi} \times 100 \text{ m} \approx 300 \text{ m}.$$

The corresponding quantities for $p = 100 \text{ GeV/c}$ will be

$$\Delta\phi \approx 12 \text{ rad.},$$

$$\lambda \approx 30 \text{ m}.$$

Therefore, by comparing the charged current interaction rates as a

function of distance, l , for neutrinos of different momenta, there could be a possibility of observing the neutrino oscillations and establish a much lower mass limits for the neutrinos.

(C) Decay of Long-Lived Neutral Particles:

In the neutrino production target, there could be new neutral particles produced which might live long enough to reach the detector. Their decay products could be detected and separated from ν interactions by spacing the detector modules with an air gap of ~ 0.5 meters. The appearance of event vertices in the air gap should indicate clearly the existence of such particles because there is no background⁽²⁸⁾.

There could also be neutral heavy leptons, coupled weakly to ν_μ and decaying into muon pairs. The presence of such particles signifies an underlying structure a little more complicated than that implicit in the standard model. Neutrino experiments to date placed a lower mass limit of $\sim 3-4$ GeV for such fermions. The Tevatron offers the prospect of searching for these leptons with heavier masses. From a theoretical point of view, a non-zero neutrino mass is in all likelihood accompanied by the presence of neutral heavy leptons; so that this study nicely complements the proposed experiment on neutrino oscillations.

Experimentally, the best means of determining the signal for neutral heavy lepton production is by studying the characteristic energy-independent invariant dimuon mass distribution⁽²⁹⁾, especially for those dimuon events with a small energy asymmetry. At the higher energies available at the Tevatron, one could expect a detectable signal for the production of heavy leptons with masses up to about 8-9 GeV⁽²⁹⁾.

III. Experimental Apparatus

In order to study the aforementioned subjects on $\bar{\nu}_\mu e^-$ elastic scattering, neutrino oscillation and particle decays, the main detector should be a long, low effective density, fine-grained calorimeter of the type employed by us in E-253 for the measurement of $\nu_\mu e$ scattering cross section. This calorimeter measures the directions and energies of electrons, muons, and hadrons and identifies them by their interaction characteristics when they do not spatially overlap. Good angular resolution is of prime importance in indentifying the $\bar{\nu}_\mu e^-$ events. In order to deal with ν_τ search and $\bar{\nu}_e e^-$ scattering in beam dump experiments, two important related subjects to be discussed later, it is also most desirable to have the capability of measuring the direction and energy of each individual hadron produced in neutrino interactions if possible.

Following the non-magnetic calorimeter is a simple and standard magnetic spectrometer, made of toroidal magnets and drift-chambers, to measure directly the neutrino flux spectrum. By monitoring reactions such as

$$\nu_\mu(\bar{\nu}_\mu) + N \rightarrow \mu^-(\mu^+) + \text{Hadrons}, \quad (15)$$

or

$$\nu_\mu + n \rightarrow \mu^- + p, \quad (16)$$

and through Monte Carlo calculations, normalizations, acceptances, and biases can be determined.

(A) The Non-Magnetic Detector

The arrangement of a non-magnetic calorimeter is shown in Figure 3. There are 200 modules; 3m x 3m in cross section and 480 tons in total weight. Each module consists of one MWPC and one 1 r.l. thick aluminum plate (~9 cm, including the aluminum walls of the MWPC).

The aluminum plates serve as both the target for interactions and the radiator for the detection. Aluminum is presently being chosen because it contains a larger number of atomic electrons per radiation length as compared to other dense materials such as iron, etc. If iron plates are required for the sake of economy, the counting rates for $\bar{\nu}_\mu e^-$ scattering will then be reduced by a factor of two. Water radiator and target is another possibility but suffers from a reduction in inter-modular gap spacing which is important for new particle searches.

(1) The MWPC

The constructions of the MWPC⁽³⁰⁾ is shown in Figure 4a. The cathode planes are made of thick aluminum jig plates with copper-clad G-10 plates epoxied onto them. On the copper-clad G-10 plates, zigzag delay-lines are milled with a spacing of 2 mm. Delay-lines on the two cathode planes of one MWPC are arranged along orthogonal directions to measure both x- and y-positions of traversing particles in terms of time intervals.

This delay-line configuration offers a number of advantages other than being economic. For electromagnetic showers, there are too many particles involved in each chamber. It would be a difficult task in trying to digitize every one of

them. By capacitive action, this group of particles will induce a localized cluster of charges on the cathode planes. Afterwards, the induced pulse train will propagate along the long transmission line to the tap points, then be fed into the time-to-digital converters (TDC's). In order to minimize attenuations and dispersions along the delay-line, on each cathode plane we will break the delay-line into 20 pieces. Each piece of the delay-line will be digitized at one end (the other end can also be connected to a TDC if economy allows). This arrangement will eliminate the left-right ambiguities, and also limit the maximum transit time to $\sim 1 \mu\text{sec}$.

The anode wires will be connected into a hodoscope configuration, 10 cm wide for each element. The signal from each element will be fed into an analogue-to-digital converter (ADC) to measure the energy deposition. Also, these anode signals will be used to form the experimental trigger. Since the beam pulse length should be of the order of 1 second, faster timing achievable with scintillators is unnecessary because of the very low triggering rates expected.

(2) The CCD Digitizer

We have successfully developed a new type of TDC's using charge-coupled devices (CCD's). These CCD digitizers will be used on the cathode plane delay-lines. The principle of this device is illustrated in Figure 4b. The CCD is continuously clocked at 50 MHz . The incoming pulse from a given cathode tap is thus quantized into 20 nsec intervals. Charges contained in

each interval will be loaded into successive CCD buckets. For each clock pulse, the charges in each bucket will shift one bucket position. When it reaches the end, a fast ADC will start to act, digitizing the charges stored in each bucket successively. By the mean time, a scanner will keep track of the CCD bucket number. In essence, the CCD digitizer works like a superscope because it retains the complete information of the profiles of the pulses on the delay-line. The charge information will provide measurements of energy depositions. The CCD bucket numbers will yield the track position information.

It should be noted that the track positions can be measured very accurately by the CCD digitizers. Since the pulse profile (or the charge distribution along the transverse direction) is known, we can weigh the position measurements by the corresponding charges to obtain the centroid positions properly. This will be particularly helpful for measuring electromagnetic showers. Also, we do not need tilted wire planes to resolve the combinatorial ambiguities. The absolute position of a particle (or the centroid of an electromagnetic shower) is given simply by the propagation time along the delay-line.

(3) The Planned Test

We are currently in the process of converting the existing E-253 electronics into CCD digitizers. The task involves re-

placing all the amplifiers and TDC's. There are 49 MWPC's, 1m x 1m in size. Altogether, there are 490 channels of CCD digitizers.

It is anticipated that the electronics can be finished sometime during the spring of 1980. We will then make a realistic test run in the Wonder Building to learn the performances of these devices. Additional testing in various test beams will also be performed to measure energy and angular resolutions for various particles and to develop pneumonics for identifying particles.

(4) The Resolutions

In E-253 at Fermilab, the TDC's only measured the "leading" and the "trailing" edges of an electron induced shower. Shower centroids were assumed to be the midpoint of the two edges. The angular resolution achieved in this manner for that experiment was ± 5 mr. With this resolution, the $\nu_{\mu} e^{-}$ elastic scattering events were clearly separated from the copious π^0 background. Figure 5 shows the angular distribution of the E-253 results⁽¹⁶⁾. Figure 6 shows the corresponding transverse momentum distribution. The $\nu_{\mu} e^{-}$ signal to background was clearly capable of separation.

By converting the CCD digitizers mode, we anticipate improving the angular resolution to approximately ± 1 mr. The energy resolution for electron detection should remain approximately the same, $\sigma(E_e)/E_e \approx (20/\sqrt{E_e})\%$; and for hadrons,

$$\sigma(E_h)/E_h \approx (100/\sqrt{E_h})\%.$$

If the tracks are not overlapping, we can follow each individual particle to obtain its energy by adding up the energy depositions measured by the CCD digitizers. The capability of measuring both the energy and angle of each particle in a multiple-track event is of utmost importance in some experiments, e.g., ν_τ search, and the (x,y) distributions of neutral current interactions. As far as we know, these difficult tasks have not been done yet mainly because of inadequate spatial and localized energy resolutions. The approach being adopted for the proposed detector cannot solve all these problems, but certainly shows promise for alleviating part of them.

(B) The Magnetic Muon Detector

A simple magnetic spectrometer, located behind the calorimeter, is required to detect the outgoing muons. Among many purposes, it is essential for determining the neutrino flux which we will explain in a later section. The magnetic muon detector is shown in Figure 7. It consists of two segments of toroidal magnets, each followed by a set of drift chambers. Each toroid has a modest size of 4 m in diameter and 1 m in depth. We could use those toroids already in existence. If the calorimeter of this proposal could be located in front of a magnetic spectrometer facility, we envisage then that there will be no necessity for us to build another muon detector.

(C) The Neutrino Beam

The neutrino spectra, using various focussing devices, as calculated by S. Mori⁽³¹⁾, are shown in Figure 8.

For the $\bar{\nu}_{\mu} e^{-}$ elastic scattering and the neutrino oscillation experiments, we propose using the sign-selected single-horn focussed beam because the wrong-signed neutrino backgrounds can be suppressed.

For the long-lived particle decay experiment, we can run in any one of the following three modes: single-horn focussing, quadrupole-triplet focussing, and bare target. The experiment can be done in a parasitic mode.

(D) Equipment calibration

A hadron beam of rather weak intensity is needed for equipment calibration in the experimental hall. Specifically, the energy resolution and calibration for hadrons have to be measured carefully. This is particularly necessary if we want to know the energy of each individual hadron utilizing the CCD digitizing technique. Since the hadron beam always contain a few percent of electrons, we can utilize them to calibrate the calorimeter for electron detections. Questions on pion-electron separation, angular resolution, etc., can all be answered with the test beam.

(E) Beam Normalization

We have already mentioned that the main systematic error of experiments on neutrino interactions is from the uncertainty in our knowledge about the neutrino flux. With the combination of a fine-grained calori-

meter and a magnetic muon spectrometer, the energy distribution of the neutrino intensity can be measured directly. The method is to use a restricted central fiducial volume of the apparatus and measure the charged current interactions $\bar{\nu}_{\mu} + N \rightarrow \mu^{\pm} + \text{hadrons}$. In these reactions, the sign and the momentum of the outgoing muon are measured by the magnetic spectrometer, while the hadronic energy is determined by the calorimeter. The sum yields the incoming neutrino energy. Therefore, the intensities for both ν_{μ} and $\bar{\nu}_{\mu}$ can be separately determined.

The experimental determination of the ν_e and $\bar{\nu}_e$ components of the flux is not as easy. Unlike the $\bar{\nu}_{\mu}$ case, we cannot simply rely upon the reactions



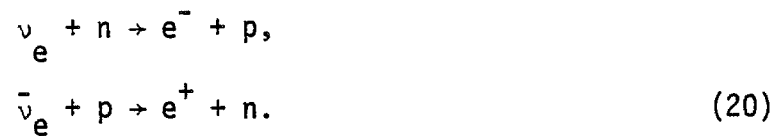
and



because (1) we cannot tell the sign of the electron charge, (2) there are single π^0 productions in the neutral current interactions of ν_{μ} and $\bar{\nu}_{\mu}$, and (3) there are $\bar{\nu}_e e^{-}$ elastic scatterings. The problem, however, is not nearly as formidable as it appears. The beam composition is anticipated to be approximately 90% ν_{μ} , 10% $\bar{\nu}_{\mu}$, and $\lesssim 1-2\%$ ν_e and $\bar{\nu}_e$. Once the spectra of ν_{μ} and $\bar{\nu}_{\mu}$ are known, we can compare the distribution for the reactions:



with those for the sum of the following two reactions:



The shape of the distributions has be similar and the normalization constant has to be fixed by a Monte Carlo beam calculation. There are π^0 contributions to reaction (20), mainly from the productions by $\bar{\nu}_\mu$. Their rates can be calculated and subtracted from the measurements.

IV. Counting Rates and Backgrounds

Before proceeding to discuss the details about the counting rates, backgrounds, etc., for $\nu_{\mu} e^{-}$ and $\bar{\nu}_{\mu} e^{-}$ elastic scattering, we like to make a brief and general remark on this subject. In the past, we were deeply worried, and being repeatedly and correctly asked, about the problem of backgrounds for doing experiment on such rare processes. The questions were centered at π^0 , quasi-elastic scattering and charged current interactions of $(\bar{\nu}_{\mu}^e) e^{-}$. In Experiment E-253 at Fermilab, $\nu_{\mu} e^{-}$ elastic scattering was measured with an instrumentation resolution of $\Delta\theta \approx \pm 5$ mr. As illustrated in Figures 5 and 6, by applying the forward angular cut first and then examining the transverse momentum distribution, a signal-to-noise ratio of approximately 10:1 was achieved. Based on this empirical fact and the anticipated improved angular resolution of $\Delta\theta \approx \pm 1$ mr, a signal-to-noise ratio of about or better than 20:1 is a reasonable expectation for the proposed $(\bar{\nu}_{\mu}^e) e^{-}$ elastic scattering experiment at the Tevatron.

(A) Counting Rate for $\nu_{\mu} e^{-}$ and $\bar{\nu}_{\mu} e^{-}$ Elastic Scattering

For 3×10^{18} protons of 1 TeV incident upon the neutrino production target, single-horn focussing, and the proposed detector of 3 m x 3 m x (200 layers) x (9 cm Al/layer), we estimate that the total number of events for the reactions, $\nu_{\mu} + e^{-} \rightarrow \nu_{\mu} + e^{-}$ and $\bar{\nu}_{\mu} + e^{-} \rightarrow \bar{\nu}_{\mu} + e^{-}$, are approximately 1,000 and 200, respectively. The assumed ν_{μ} and $\bar{\nu}_{\mu}$ fluxes are those given by Mori⁽³¹⁾. The fiducial volume is approximately 2.8 m x 2.8 m x (190 layers). The cross sections used are given by

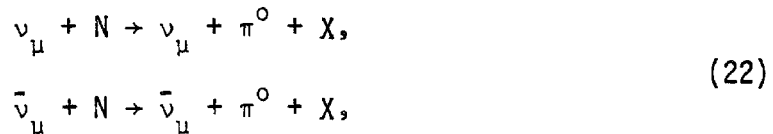
$$\sigma(E) = \frac{G_V^2 m_e E}{2\pi} [(g_V \pm g_A)^2 + \frac{1}{3} (g_V \mp g_A)^2] \quad (21)$$

where E is the energy of the incident ν_μ or $\bar{\nu}_\mu$; the upper signs inside the brackets are for ν_μ , and the lower signs for $\bar{\nu}_\mu$; the coupling constants are set to $g_V = 0$ and $g_A = -1/2$, corresponding to $\sin^2\theta_W = 1/4$ in the W-S model.

In the $g_V - g_A$ plane, the ellipses corresponding to the statistics due to 1,000 $\nu_\mu e$ events and 200 $\bar{\nu}_\mu e$ events are shown in Figure 9. The prediction of W-S, $g_A = -1/2$, is also shown. It can be seen that the value of $\sin^2\theta_W$ can be measured to the accuracy of ± 0.01 , quite comparable to the present precision of $(\bar{\nu})N$ interactions and eD scattering experiments. Since there are no theoretical complications due to uncertainty of strong interaction effects, this proposed experiment should be able to settle the question on the exact value of $\sin^2\theta_W$, if the W-S model is correct. Also, we emphasize once again, it also provide a model independent determination of g_V and g_A .

(B) Background for $\nu_\mu e^-$ and $\bar{\nu}_\mu e^-$ Elastic Scattering

The background for $\nu_\mu e^-$ and $\bar{\nu}_\mu e^-$ elastic scattering are from the following processes:



and

$$\begin{aligned} \nu_e + n &\rightarrow e^- + p, \\ \bar{\nu}_e + p &\rightarrow e^+ + n. \end{aligned} \tag{23}$$

The kinematics for the neutrino-electron elastic scattering is such that its characteristic angular width is given by $\theta_e \approx \sqrt{m_e/E_\nu}$, which is much narrower than that for the π^0 , $\theta_{\pi^0} \approx \sqrt{M_N/E_\nu}$; where M_N is the nucleon mass. Therefore, the π^0 background can be separated very easily from the $(\bar{\nu}_\mu^-) e^-$ elastic scattering events by their angular distributions of the outgoing electromagnetic showers. This is illustrated by Figure 5, which is the result of Experiment E-253 measured at Fermilab.

The angular distribution of e^- (or e^+) from the quasi-elastic scattering of $(\bar{\nu}_e^-)$ is sharper than that described by the characteristic angle, $\theta \approx \sqrt{M_N/E_\nu}$, because of the elastic nucleon form factors⁽³²⁾. Since the cross section is fairly large, $\sim 10^{-38} \text{ cm}^2$, a few percent of $(\bar{\nu}_e^-)$ contamination can, in principle, make an appreciable contribution to the forward peak corresponding to $(\bar{\nu}_\mu^-) e^-$ elastic scattering. In reality, we do not have great difficulty in separating these quasi-elastic events from the $(\bar{\nu}_\mu^-) e^-$ events. The technique is to examine the transverse momentum distribution of those events in the forward peak. The $(\bar{\nu}_\mu^-) e^-$ events all have small p_T ($\leq 300 \text{ MeV}/c$) and their distribution is sharply peaked at $p_T \approx 100 \text{ MeV}/c$. On the other hand, quasi-elastic scattering of $(\bar{\nu}_e^-)$ gives higher energy to the outgoing electron (positron) which leads to higher values of p_T and a broader p_T distribution, centered at $p_T \approx 500 \text{ MeV}/c$. As illustrated in Figure 6, which is the result measured with $E_p = 350 \text{ GeV}$ and $\Delta\theta \approx \pm 5 \text{ mr}$, the background events (including π^0 's) can be easily subtracted. With the better angular resolution which we anticipate for this proposed

experiment, of $\Delta\theta \approx \pm 1$ mr, both the angular and the p_T distributions are expected to be improved. Therefore, by the very straightforward double selection of small θ and p_T , the background problem can be satisfactorily resolved.

(C) Neutrino Oscillations

For 3×10^{18} protons at 1 TeV and with single horn focussing, approximately 7 million charged current interactions of ν_μ in the proposed detector will be detected. It is a reasonable assumption that the ν_e flux is $\approx 2\%$ of the ν_μ flux. Then we will anticipate $\approx 140,000$ events due to the charged current interactions of ν_e . If there are neutrino oscillations, $\nu_\mu \rightleftharpoons \nu_e$, the number of ν_e induced charged current interactions may be appreciably enhanced. As the calorimeter is particularly suitable for the detection of electrons, we can perform a meaningful search of the neutrino oscillations with better reliability.

The distance from the neutrino source to the detector is approximately 800 m, the experimental sensitivity is approximately given by

$$\Delta m^2 \approx \frac{4 E_\nu}{\lambda} = \frac{4 E_\nu (2 \times 10^{-14})}{(8 \times 10^4) (10^{-18})} \approx E_\nu \quad (\text{eV})^2$$

where E_ν is the neutrino energy in GeV. From the known production mechanism and the decay processes, we should be able to calculate approximately the ν_e flux for the case of no neutrino oscillations. If the detector, located at a distance of $\lambda \approx 800$ m downstream, sees a rate of ν_e charged current interactions several times larger than that anticipated, then the neutrino oscillation would be a suspect.

Since the proposed detector has a length of $\Delta l \approx 100$ m, we will measure the reaction, $\nu_e + N \rightarrow e^- + \text{hadrons}$, and analyze the results as a function of the longitudinal distance along the detector and the neutrino energy to see the finer details of the oscillation. We anticipate to narrow down the neutrino mass difference, $(\Delta m^2)^{1/2}$, to a few electron volts.

(D) Neutral Particle Decays

The possibility on the existence of new long-lived particles is totally speculative. There is no meaningful way available for us to estimate the counting rates. From the experimental point of view, it is going to be a very clean search. We will look for those events whose vertices fall between the detector modules. Since the background has to be production from air target by secondary beams, it will be totally negligible. The sources of these long-lived particles are not known. They could come from the proton dump, or the muon and neutrino interactions in the shielding berm. We should be able to observe the decay vertices if the lifetime is nearby $\sim 10^{-6}$ sec.

We propose to conduct this search on a parasitic mode.

V. Other Possibilities

Although we do not presently propose doing more than what has been already discussed and proposed, we would like to point out that this proposed calorimeter has the potential of being adaptable to other possible experiments because of its inherent excellent capability in electron detection and good spatial and energy resolutions. Specifically we believe that the apparatus can be easily adapted to the following possibilities:

(1) $\bar{\nu}_e e^-$ Elastic Scattering

In the past, there had been designs for possible ν_e and $\bar{\nu}_e$ beam based the decay processes $K_L^0 \rightarrow \pi^- e^+ \nu_e$ and $K_L^0 \rightarrow \pi^+ e^- \bar{\nu}_e$. The beam intensities are relatively low⁽³³⁾. It was pointed out by Albright and Shrock that the best way to produce copious ν_e and $\bar{\nu}_e$ beam is from the decay of the D meson in a high energy proton beam dump⁽³⁴⁾. The anticipated fluxes are shown in Figure 10. Because the beam intensity decreases rapidly with angle, we use only a 2 mr cone to estimate the counting rates.

For the elastic scattering processes:

$$\begin{aligned} \nu_e + e^- &\rightarrow \nu_e + e^- \\ \bar{\nu}_e + e^- &\rightarrow \bar{\nu}_e + e^- \end{aligned}$$

the coupling constants are given by the W-S model as $g_A = 1/2$ and $g_V = 1$ for $\sin^2 \theta_w = 1/4$. The ratios of the total cross sections are given by

$$\sigma(\nu_\mu e^-) : \sigma(\bar{\nu}_\mu e^-) : \sigma(\nu_e e^-) : \sigma(\bar{\nu}_e e^-) = 1 : 1 : 7 : 3 \quad (24)$$

With 3×10^{18} protons of 1 TeV on a beam dump, we anticipate that approximately 140 $\nu_e e^-$ events, 60 $\bar{\nu}_e e^-$ events, and 90 background events from the quasi-elastic scattering of ν_e and $\bar{\nu}_e$ will be observed.

The major difficulty of this experiment is the flux normalization. Since we do not yet have an exact knowledge of the D production mechanism (e.g. the A-dependence, etc.), there is no easy way to normalize the cross section. Also, we cannot separate the $\nu_e e^-$ events from the $\bar{\nu}_e e^-$ events. The $\bar{\nu}_e N$ quasi-elastic scattering events can be subtracted out from the P_T -distribution.

(2) Search of ν_τ

It is generally believed that there are three generations of leptons and quarks. The members so far which have escaped detection are the t-quark and the ν_τ . It was pointed out by Albright and Shrock⁽³⁴⁾ that the best way to produce a ν_τ beam is from the F decays in a high energy beam dump. The reactions initiated by an incident $\bar{\nu}_\tau$ are the following:

$$\bar{\nu}_\tau + N \rightarrow \bar{\nu}_\tau + \text{hadrons}$$

and

$$\bar{\nu}_\tau + N \rightarrow \begin{cases} \tau^\pm + \text{hadrons} \\ \bar{\nu}_\tau + e^\pm + \bar{\nu}_e \\ \bar{\nu}_\tau + \mu^\pm + \bar{\nu}_\mu \end{cases} \quad (25)$$

The cross section of the above reaction is approximately 1.1×10^{-39} cm^2 , and is independent of energy. Their contaminations to the quasi-elastic scattering can be calculated from the $\nu_\mu(\bar{\nu}_\mu)$ flux and subtracted.

(c) Consistency Check

A consistency check can be made by observing the equality:

$$\begin{aligned} &\text{Total "apparent" NC events} \\ &= (\text{CC} + \text{NC})_{\nu_e} + (\text{CC} + \text{NC})_{\bar{\nu}_e} \\ &\quad + R_{\nu} * (\text{CC})_{\nu_\mu} + R_{\bar{\nu}} * (\text{CC})_{\bar{\nu}_\mu}, \end{aligned}$$

where $R_{\nu} \equiv (\text{NC}/\text{CC})_{\nu_\mu}$ and $R_{\bar{\nu}} \equiv (\text{NC}/\text{CC})_{\bar{\nu}_\mu}$ are the known ratios. The CC events due to ν_μ and $\bar{\nu}_\mu$ can be measured by counting the events with μ^- and μ^+ respectively. In the above expression, we still do not know exactly the R's for ν_e and $\bar{\nu}_e$. Because of μ -e universality, we may assume that the CC and NC cross sections of $(\bar{\nu}_e)$ are the same as that for $(\bar{\nu}_\mu)$.

(d) Check against the Hadronic Distribution

The measured flux can also be checked against the hadronic energy spectrum of the charged current events. In E-253, the neutrino spectrum could not be directly measured because of the lack of a magnet. We adjusted the calculated neutrino spectrum until the Monte Carloed hadronic distribution of the charged current events agreed with the measured hadronic energy spectrum. It turned out later that the neutrino spectrum we used agreed quite well with that measured by G. Snow et al on the $\nu_\mu D$ interactions in the 15' bubble chamber.³⁷

VI. Program of Test

For a massive neutrino calorimeter as we are proposing, test and calibration of the apparatus are not small undertakings. We have to debug the hardware and the software. And we have to equalize the gain of each module, and to know the calibration constants and resolution functions. Since we apparently cannot move the detector around easily, we need to be able to test at the experimental location. This entails the following procedures:

(1) Hadron and Electron Beam

A hadron beam should be available to the apparatus. Its small electron component is equally useful. The calorimeter responds differently to the hadrons and the electrons. We have to calibrate the apparatus with both beams.

(2) Cosmic Ray Test

Once a fraction of the detector modules is equalized in gain (e.g. 20 to 30 modules), we can equalize the gains of the whole detector assembly using cosmic rays. By our experience with E-253, we can set the high voltages to ± 2 volts for the MWPC's, and ± 1 volt for the photo-multipliers. The total running period with cosmic rays was about two months.

(3) Muon Test

Timing of fast electronics and chamber alignment can be done with stray muons without any special requirements.

VII. Proposal and Request

We propose to build a non-magnetic calorimeter, as described above, to study some specific aspects of neutrino physics at Fermilab. Also, we will build the drift chambers for the magnetic muon detector if necessary.

We request the laboratory to provide us with the following items:

1. The laboratory space to house the detector together with the necessary utilities. An overhead crane may be required to handle the equipment.
2. Fast electronics from PREP. This will not include the CCD digitizers. (See Appendix 1)
3. A hadron beam for testing the detector.
4. Toroid magnets for muon measurements. This may not be necessary if the proposed detector can be located in front of a magnetic detector facility.
5. 200 aluminum plates, 3 m x 3 m x 7 cm, to be used as target/radiators or equivalent.

We anticipate finishing the construction of 200 MWPC's, together with amplifiers and CCD digitizers, within two years starting from the date on which funding commences. Most of the equipment can be installed and tested during this construction period.

We further request:

1. Three months testing time with the hadron and electron beam.
2. 3×10^{18} protons at 1 TeV on the neutrino production target and

with single-horn focussing to measure the cross section for $\bar{\nu}_{\mu} + e^{-} \rightarrow \bar{\nu}_{\mu} + e^{-}$. We anticipate obtaining about ~200 events.

3. 3×10^{18} protons at 1 TeV on the neutrino production target and with single-horn focussing to measure the cross section for $\nu_{\mu} + e^{-} \rightarrow \nu_{\mu} + e^{-}$. We anticipate obtaining ~1,000 events.
4. Parasitic running time for neutrino oscillations and search for long-lived neutral particle decays.

Appendix 1

Cost Estimate

In this appendix, we only include the cost estimate for the non-magnetic detector proper. Laboratory space, hadron beam line, utilities, magnetic toroids, etc., are excluded at this time.

1. Construction of 200 3 m x 3 m MWPC's, labor and material included @ \$12,000/chamber.	\$2,400,000
2. Electronics for 200 MWPC's included all CCD digitizers, ADC's, and amplifiers.	\$ 600,000
3. 200 aluminum plates 3 m x 3 m x 7 cm each, total weight ~380 tons.	\$ 700,000
4. Cables, H.V. and L.V. power supplies for chambers, gas manifold, tools, misc.	\$ 500,000
5. Contingency (10%)	<u>\$ 400,000</u>
Total	\$4,600,000

Appendix 2

Manpower, Resources and Support

(1) Manpower

There are presently five senior physicists who will lead the proposed experiment and the construction of the facility. We will recruit about six post-doctorals and four graduate students to participate in this undertaking. Also, we are inviting physicists from other institutions to participate. Eventually we hope to increment the number of physicists to the level of about twenty.

The senior engineer of this collaboration is T. A. Nunamaker. He will supervise constructions of the equipment, as well as the necessary R & D.

(2) Resources and Support

In this collaboration, the Fermilab members are supported by DOE; V.P.I. members, by a research grant from the National Science Foundation; members from the Institute of High Energy Physics, by the PRC Government; and a member by N.S.F.

We are inviting other institutions to participate this collaboration. Negotiations by our collaborators from P.R.C. with their Government is also underway for equipment support. The projected cost of the detector can be shared by the participating institutions. Since it can be distributed over a period of 2 1/2 years, it should not appear as an unusual burden as far as funding of neutrino experiments is concerned.

The chamber construction will need a rather large working space and staging area. We plan to negotiate the use of the User's Support Center of Argonne National Laboratory.

The only unambiguous way to identify the ν_τ induced reaction is to examine the decay mode of $\tau^\pm \rightarrow \bar{\nu}_\tau + \mu^\pm + \bar{\nu}_\mu$, and to construct the transverse-momentum vectors in a plane perpendicular to the incident $\bar{\nu}_\tau$ as shown in Figure 11. The azimuthal-angle and the missing momentum distributions are also shown. In order to perform this task, it is clear that we have to be able to measure the momenta of the muon and the hadrons. Apparently, this proposed detector can do a fairly good, if not complete, job on this interesting subject.

One of the reasons for limiting our program is that the latter two possibilities are beam dump experiments and consequently require different beam lines and locations from those of our primary areas of interest.

References

1. F. J. Hasert et al., Phys. Lett. 46B, 121 (1973); and 138 (1973).
2. J. Blietschau et al., Nucl. Phys. B114, 189 (1976).
3. A. Para, summary talk on "Recent Measurements of Nucleon Structure Functions from Neutrino Scattering", Proc. of 1979 Int. Symposium on Lepton and Photon Interactions at High Energies, Fermilab, 1979.
4. K. Winter, summary talk on "Review of Experimental Measurements of Neutral Current Weak Interactions", Proc. of 1979 Int. Symposium on Lepton and Photon Interactions at High Energies, Fermilab, 1979.
5. S. Weinberg, Phys. Rev. Lett. 19, 1264 (1967); 27, 1688 (1971);
A. Salam, Elementary Particle Theory, ed., N. Svartholm (Almqvist and Wiksells, Stockholm, 1968), p. 367.
6. M. K. Gaillard, summary talk "Gauge Theories and Weak Interactions",
Proc. of 1979 Int. Symposium on Lepton and Photon Interactions of High Energies, Fermilab, 1979.
7. G. 't Hooft, Phys. Lett. 37B, 195 (1971).
8. R. E. Marshak and R. N. Mohapatra, Festschrift for Maurice Goldhaber, New York Academy of Sciences (to be published, 1980), VPI & SU preprint (1979); and preprint VPI-HEP-80/1 (1980). Riazuddin and Fayyazuddin, Trieste preprint IC/79/154 (1979).
9. Y. Ne'eman, Phys. Lett. 81B, 190 (1979); J. G. Taylor, Phys. Lett. 83B, 331 (1979).
10. H. Georgi, H. R. Quinn and S. Weinberg, Phys. Rev. Lett. 33, 451 (1974); J. Ellis, CERN Report Ref. TH. 2723-CERN (1979).
11. J. Blietschau et al., Phys. Lett. 73B, 232 (1978).
12. H. Faissner et al., Phys. Rev. Lett. 41, 213 (1978).
13. A. M. Cnops et al., Phys. Rev. Lett. 41, 357 (1978).

14. P. Alibrán et al., Phys. Lett. 74B, 422 (1978).
15. M. Jonker et al., Neutrino 1979 Conference, Bergen, Norway, June 18-22, 1979.
16. R. H. Heisterberg et al., Phys. Rev. Lett. 44, 1980; contributed paper to 1979 Int. Symposium on Lepton and Photon Interactions at High Energies, Fermilab, August, 1979.
17. J. Blietschau et al., Nucl. Phys. B114, 189 (1976).
18. H. Faissner et al., Phys. Rev. Lett. 41, 213 (1978).
19. F. Reines et al., Phys. Rev. Lett. 37, 315 (1976). The event number is obtained from multiplying 7.1 events/day, from 1.5 to 4.5 MeV, by the number of operating days. The background in this experiment was ~85%.
20. P. Q. Hung and J. J. Sakurai, UCLA Report UCLA 79/TEP/9.
21. C. Prescott et al., Phys. Lett. 77B, 347 (1978); 84B, 524 (1979).
22. M. Holder et al., Phys. Lett. 72B, 254 (1977).
23. M. Veltman, Nucl. Phys. B123, 89 (1977); M. S. Chanowitz, M. A. Furman and I. Hinchliffe, Phys. Lett. 78B, 285 (1978); N. Byers et al., Physica 96A, 163 (1979).
24. P. Langacker et al., Neutrino 1979 Conference, Bergen, Norway, June 18-22, 1979.
25. R. N. Mohapatra and G. Senjanović, Phys. Rev. Lett. 44, 912 (1980).
26. B. Pontecorvo, Zh. Eksp. Teor. Fiz. 33, 549 (1957); 34, 247 (1958); 53, 1717 (1967); A. K. Mann and H. Primakoff, Phys. Rev. 15D, 655 (1977).
27. S. Eliezer and A. Swift, Nucl. Phys. B105, 45 (1976). S. M. Bilenky and B. Pontecorvo, Phys. Report, Vol. 41C, No. 4 (1978). A. De Rújula, et al, CERN Report Ref. TH.2788-CERN(1979).
28. J. D. Bjorken, private communication.

29. L. N. Chang, E. Derman and J. Ng, Phys. Rev. Lett. 35, 6 (1975).
30. T. A. Nunamaker et al., preprint VPI-HEP-80/3, to be published in Nucl. Instr. and Meth., 1980.
31. S. Mori, Fermilab Report TM-837 (1979).
32. R. E. Marshak et al., Theory of Weak Interactions in Particle Physics, John Wiley & Sons, Inc., New York (1968), p. 322.
33. S. Mori, Fermilab Report TM-769 (1978).
34. C. H. Albright and R. Shrock, Phys. Rev. 20D, 2177 (1979). At the XVth Rencontre de Moriond (March 9-21, 1980, Savoie, France), the CDHS collaboration presented new results on their beam dump experiment: $\nu_e/\nu_\mu \approx 0.62 \pm 0.13$ and $\bar{\nu}_\mu/\nu_\mu \approx 0.17 \pm 0.20$. If the model of this reference is correct, these ratios should all be unity.

Figure Captions

- Fig. 1 Determination of the ν_e coupling constants. The factorization constraint due to Sakurai is also shown.
- Fig. 2 Loop corrections to the intermediate boson propagators.
- Fig. 3 Schematic arrangement of the non-magnetic calorimeter. The dimension is 3 m x 3 m x 200 modules.
- Fig. 4a Schematic of the MWPC.
- Fig. 4b Schematic illustration of the CCD digitization. The ADC digitizes the charge in each CCD bucket, and the scanner records the CCD bucket number. The CCD is clocked at 50 MHz.
- Fig. 5 The angular distribution of the reaction, $\nu_\mu + e^- \rightarrow \nu_\mu + e^-$, measured in E-253 at Fermilab. There are 46 events in the angular range $0 \leq \theta \leq 10$ mr.
- Fig. 6 The transverse momentum distribution of the events shown in Fig. 5 and within the angular range of $0 \leq \theta \leq 10$ mr. The "background" events have $E\theta^2 \geq 3$ MeV.
- Fig. 7 Schematic of the magnetic muon spectrometer.
- Fig. 8 Neutrino Spectra at the Tevatron.
- Fig. 9 Determination of ν_e coupling constants with 1,000 $\nu_\mu e^-$ and 200 $\bar{\nu}_\mu e^-$ elastic scattering events, respectively.
- Fig. 10 Neutrino fluxes from a 1 TeV proton beam dump, calculated by C. Albright and S. Mori. See footnote of Ref. 34.
- Fig. 11 Distributions in (a) azimuthal angle of the transverse momentum vectors. H denotes the hadron vector; μ , the muon vector; and m , the transverse momentum vector of the two

missing neutrinos; ϕ , the angle between any two of the three vectors, and (b) missing momentum perpendicular to the beam direction and normal to the apparent production plane shown as solid curves for the chain reaction $\nu_\tau + N \rightarrow \tau^- + X$, $\tau^- \rightarrow \nu_\tau + \mu^- + \bar{\nu}_\mu$ with cuts $E_\mu > 4$ GeV, $E_H \geq 5$ GeV. The dashed curves refer to the corresponding $\bar{\nu}_\tau$ reaction.

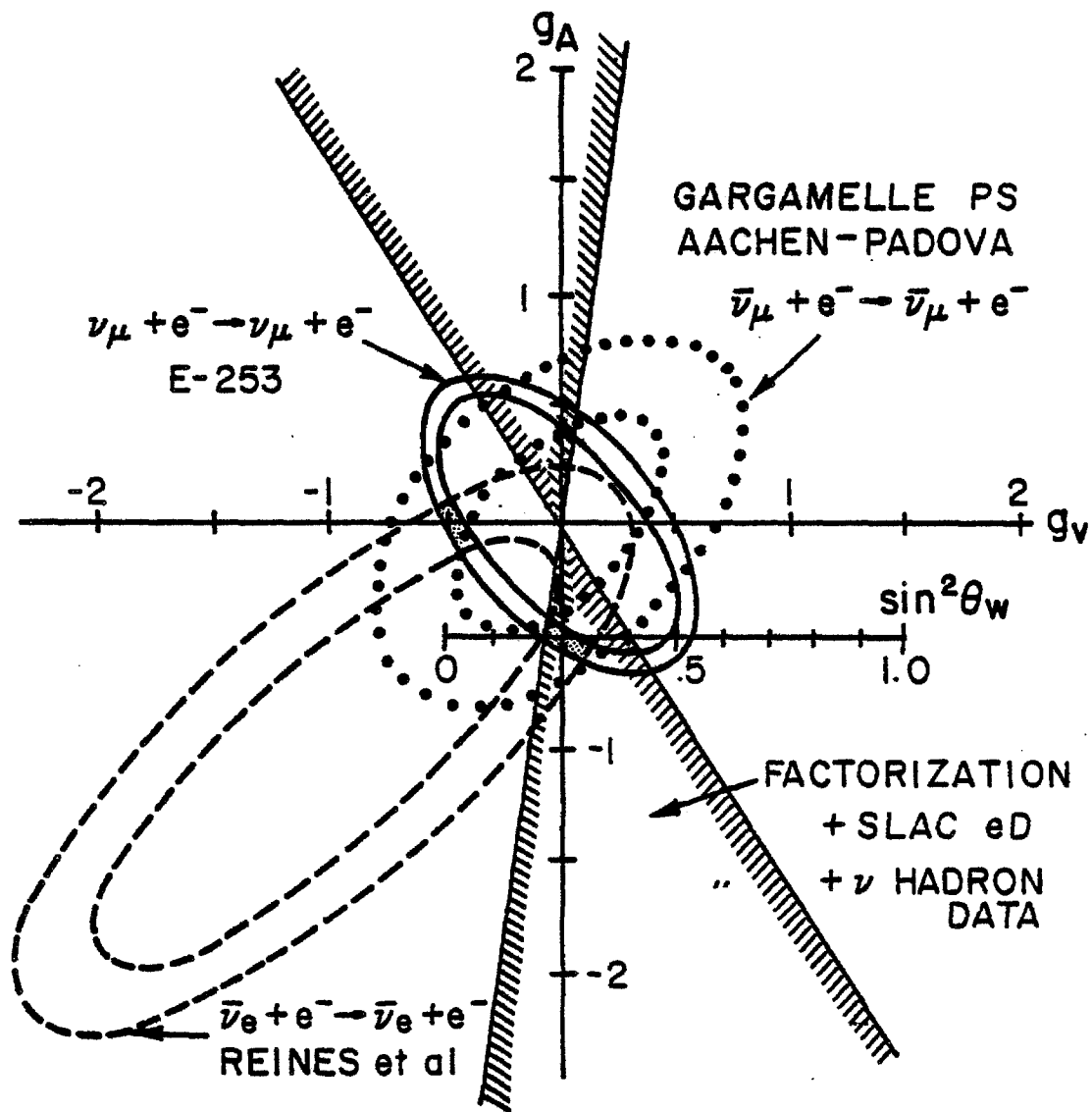


FIG. 1

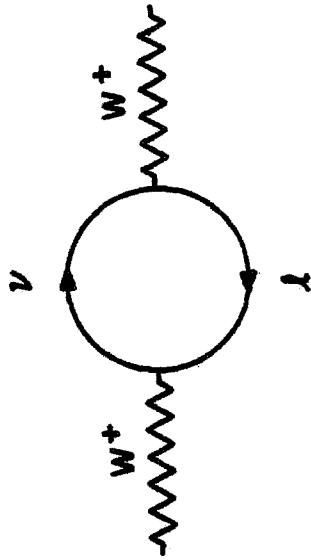
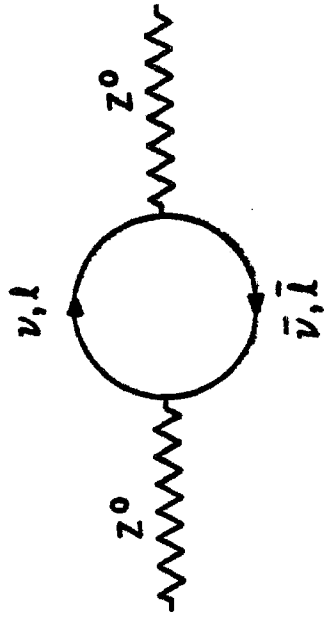


FIG. 2

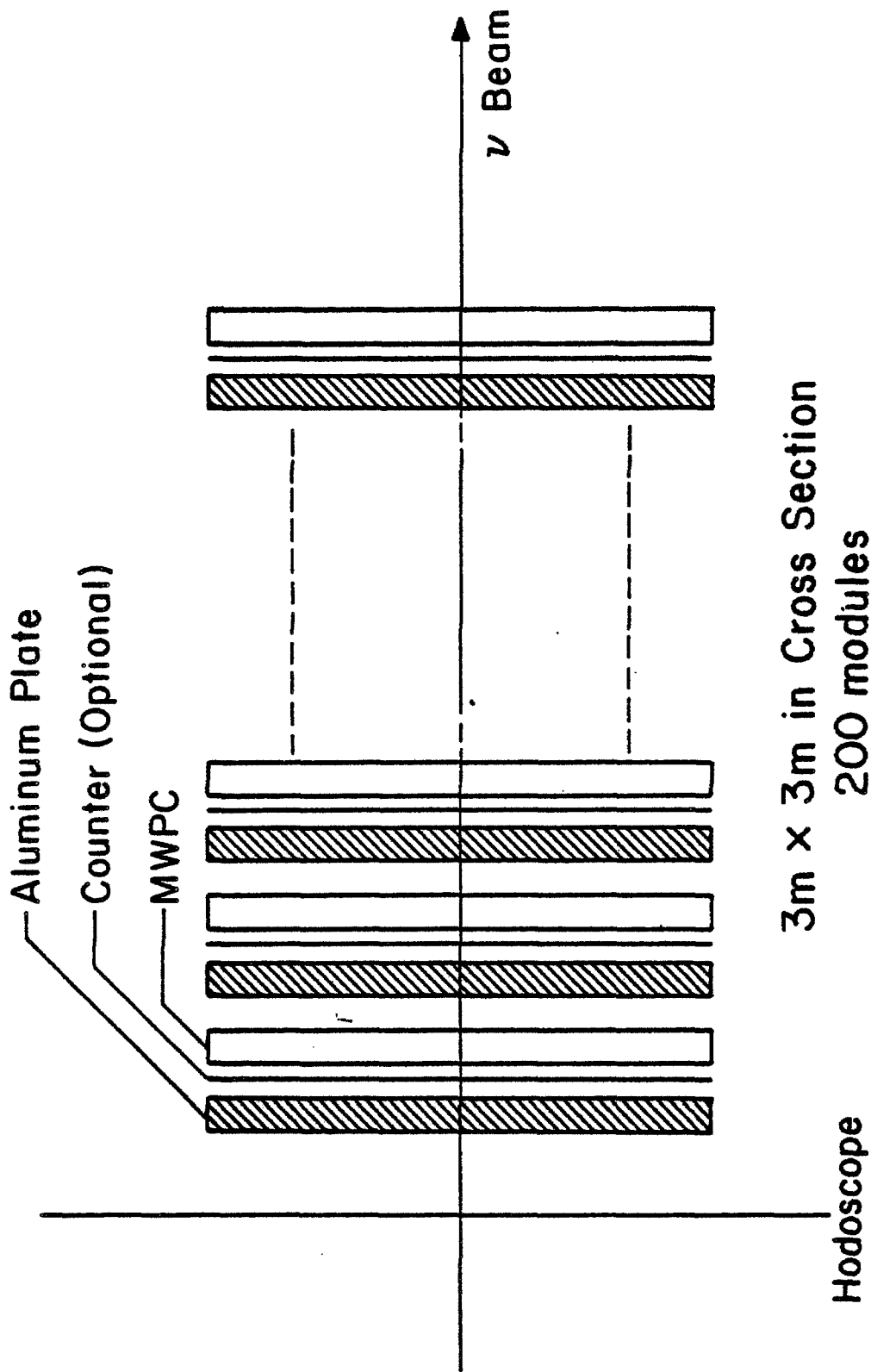


FIG. 3

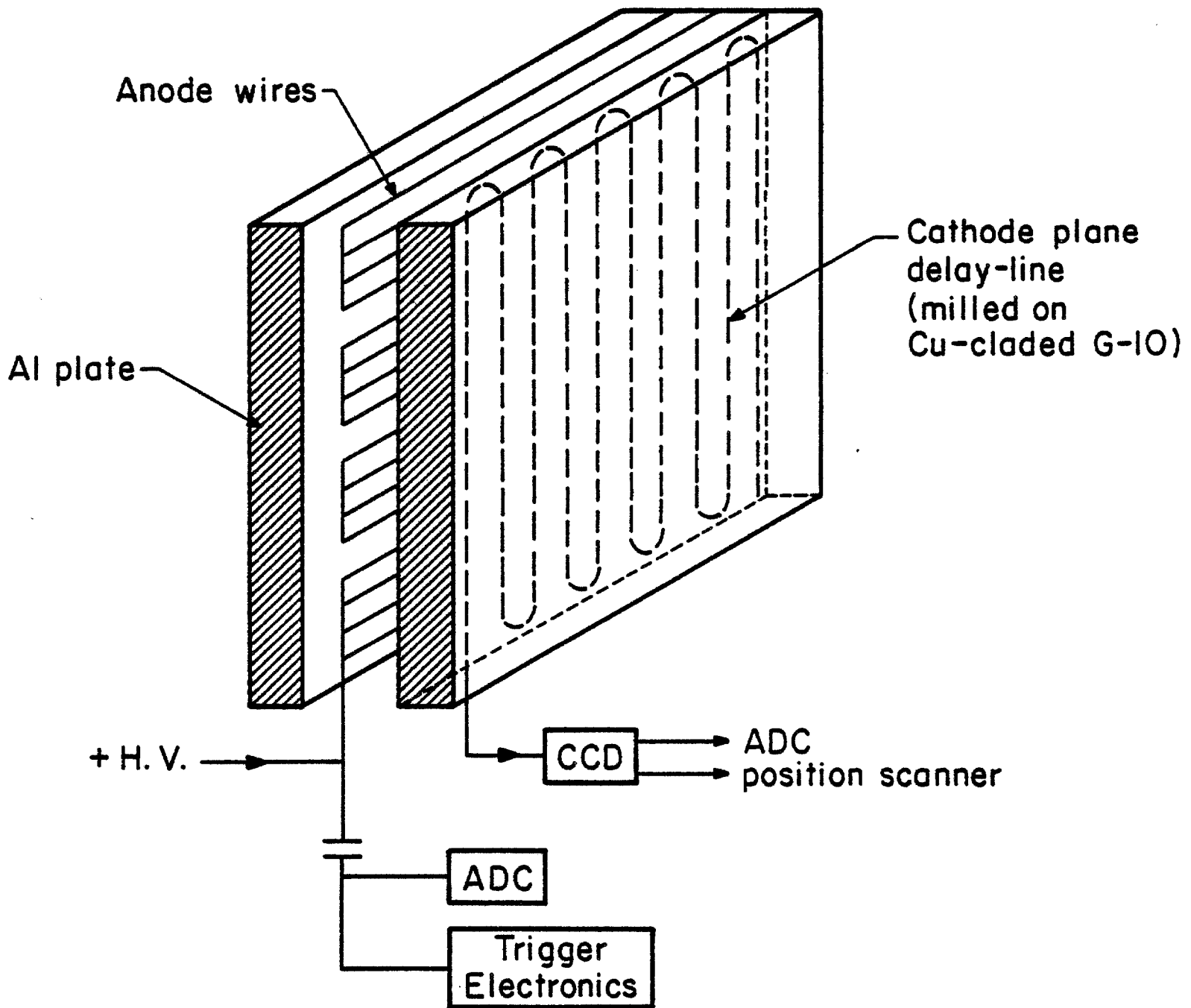


FIG. 4a

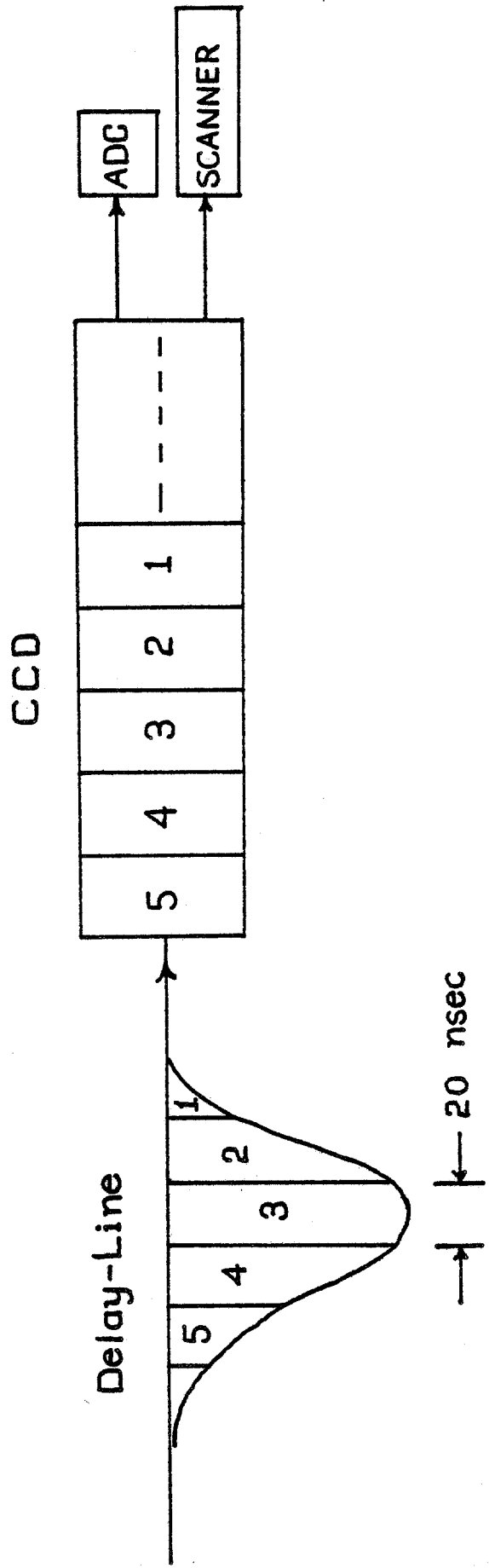


FIG. 4b

56 P/P

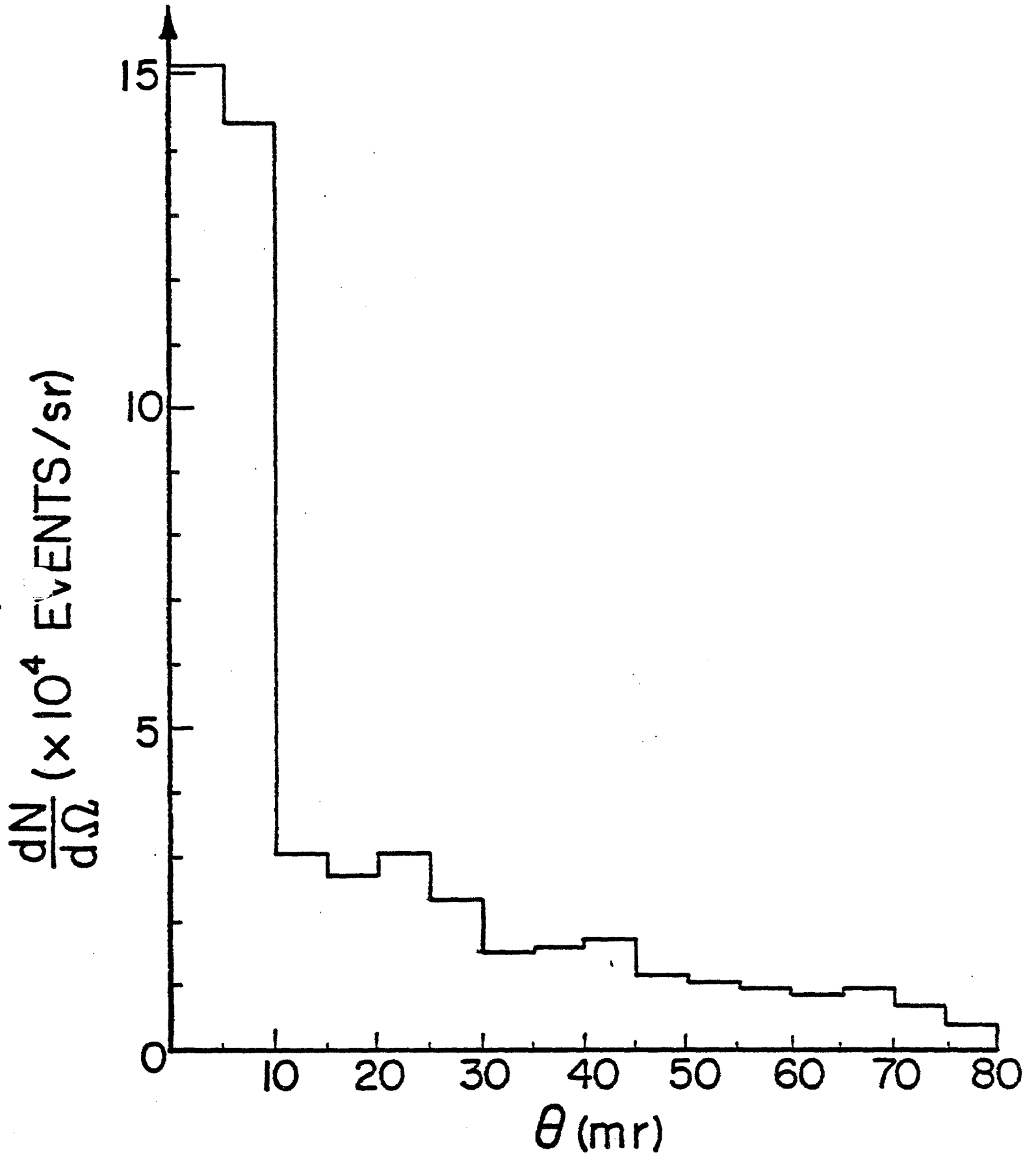


FIG. 5

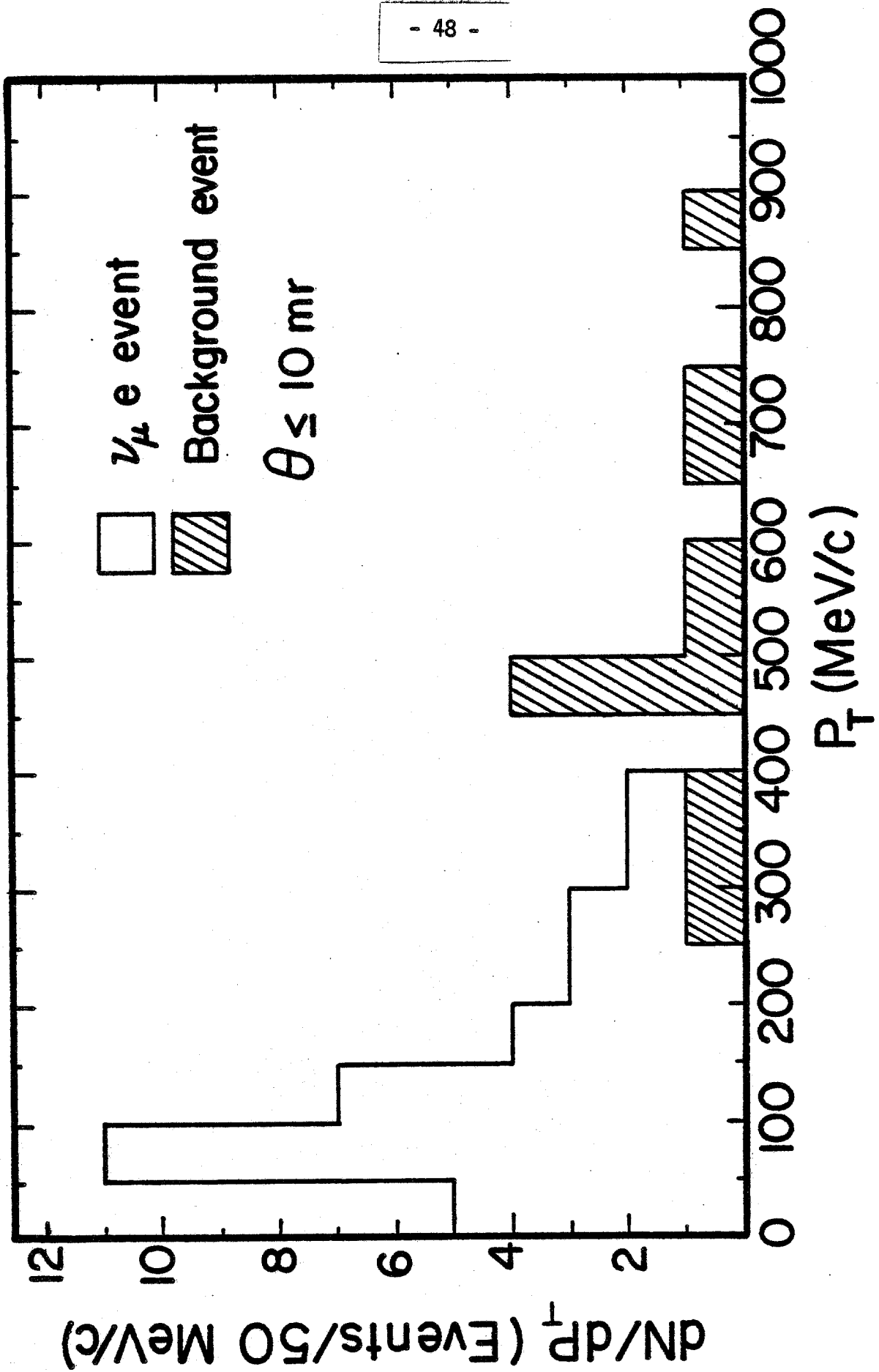


FIG. 6

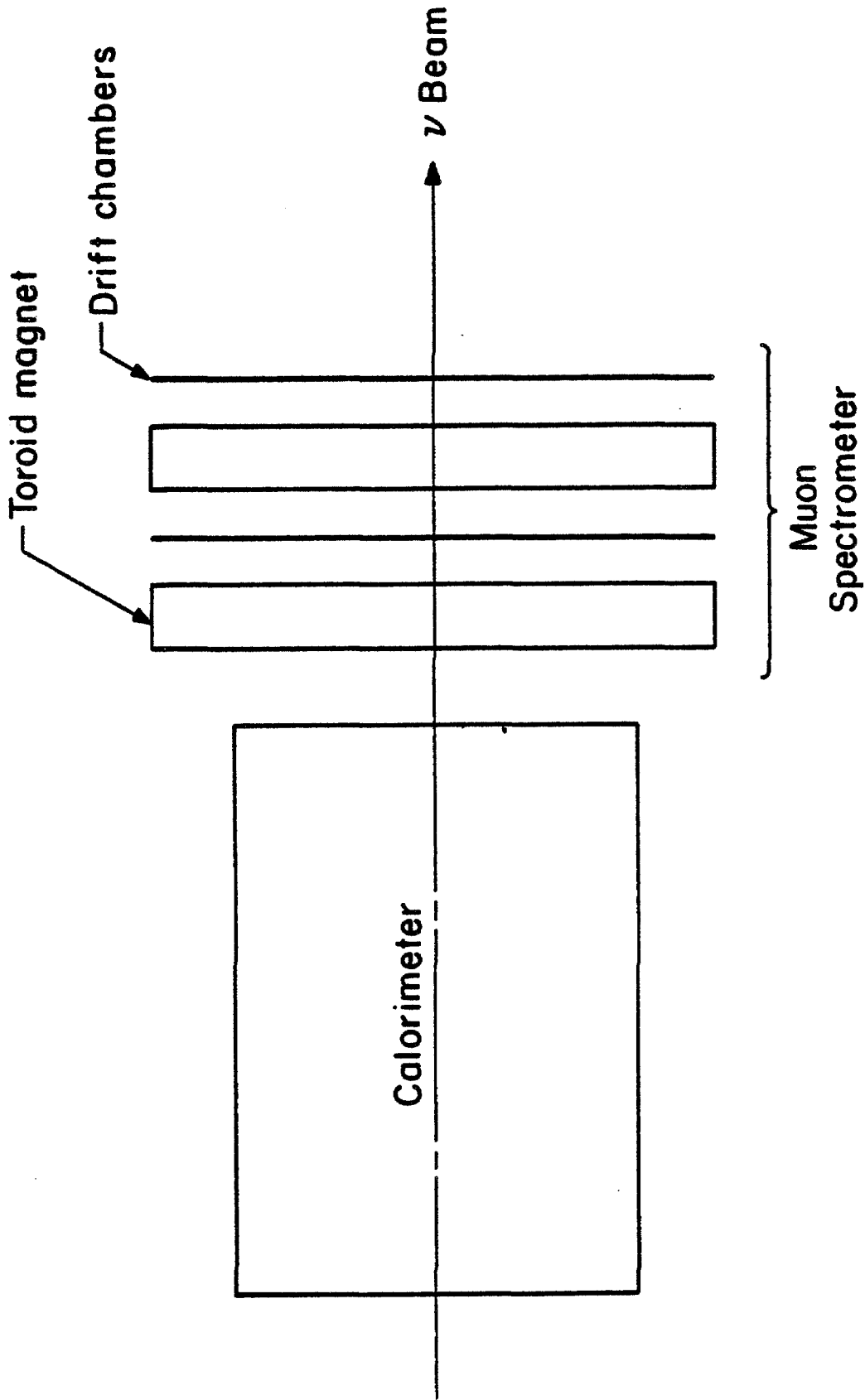
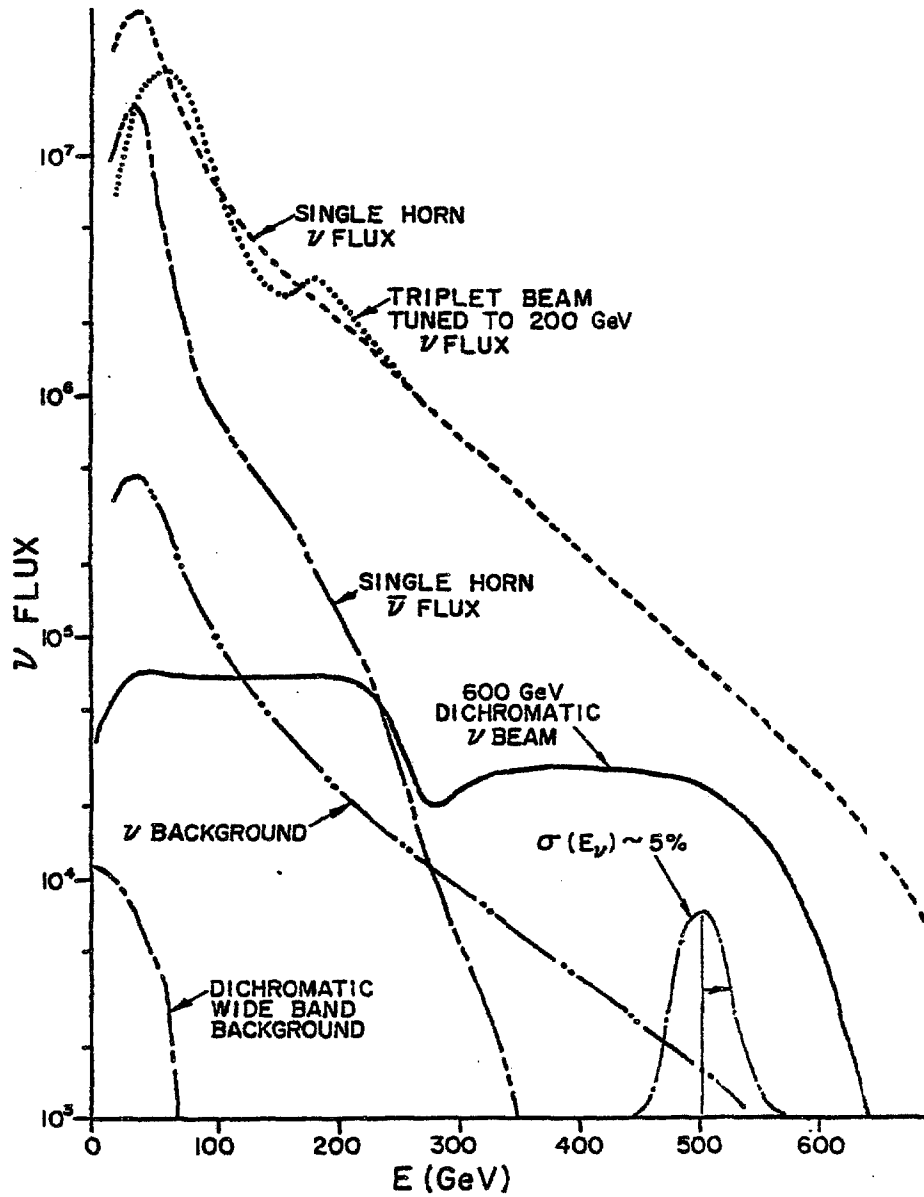


FIG. 7



Tevatron Neutrino Fluxes
($\nu/m^2/GeV/10^{13}$ p's)
1-TeV Protons Incident on $1m^2$ Detector at 1400m Distance

FIG. 8

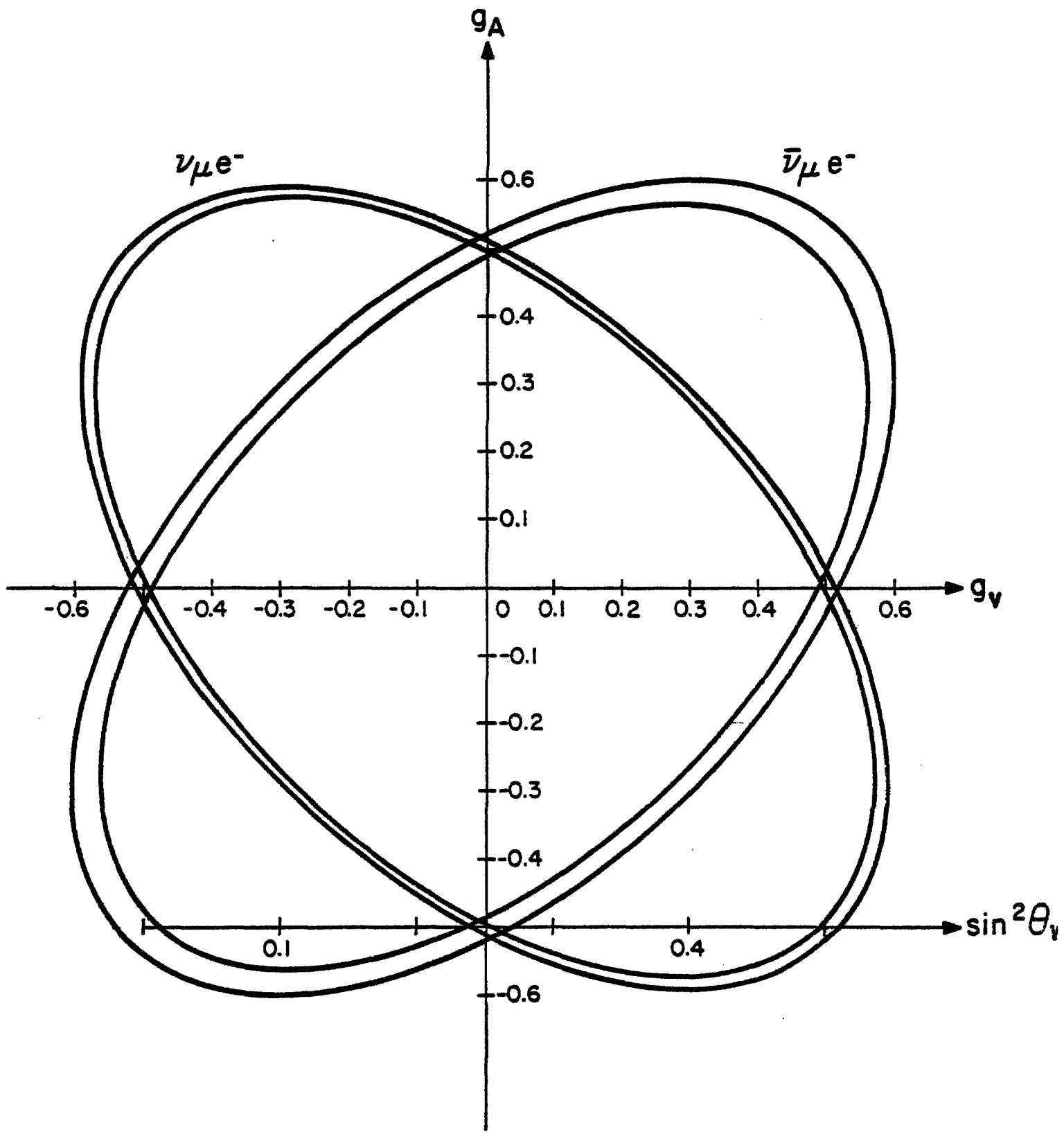


FIG. 9

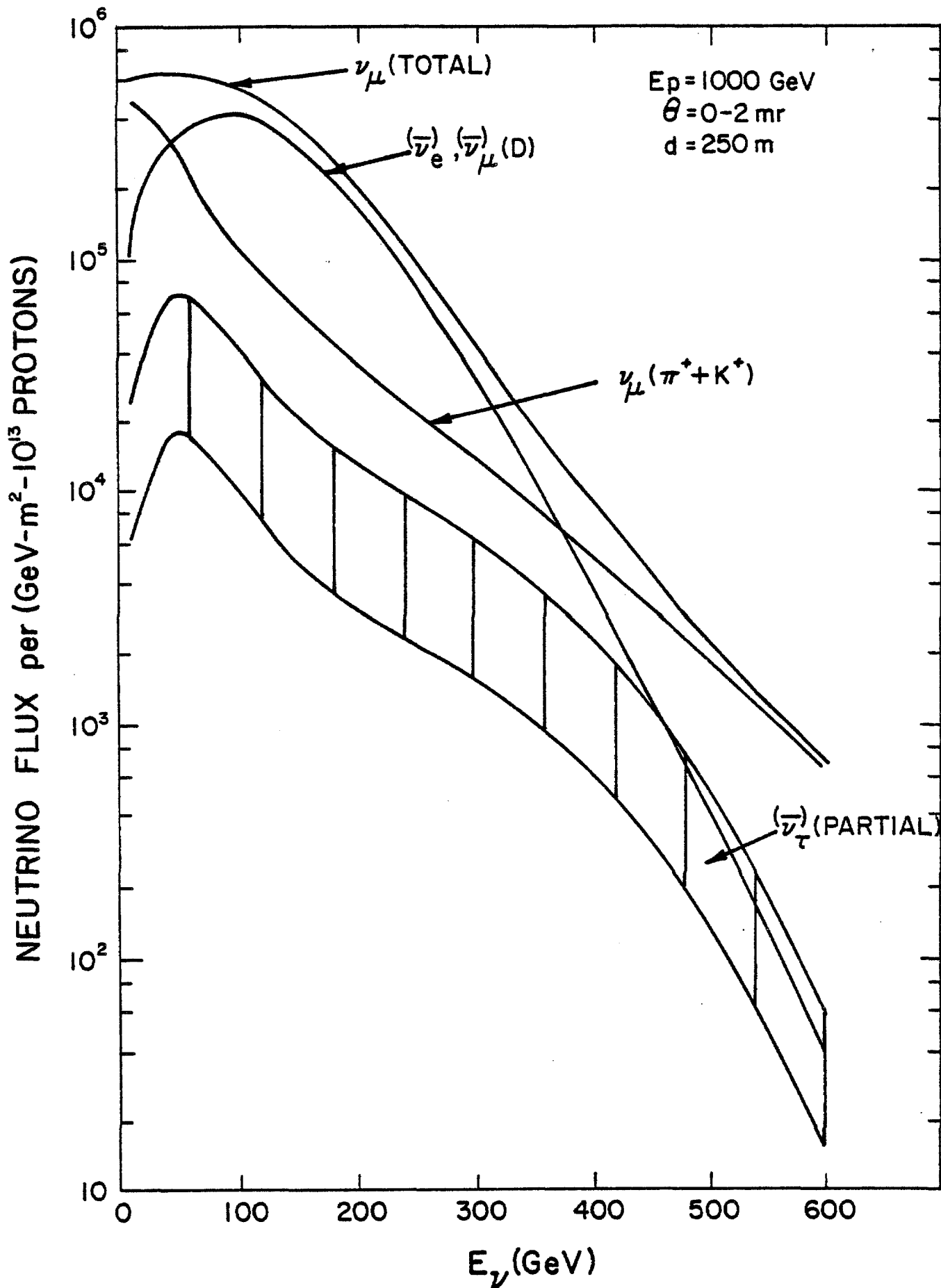


FIG. 10

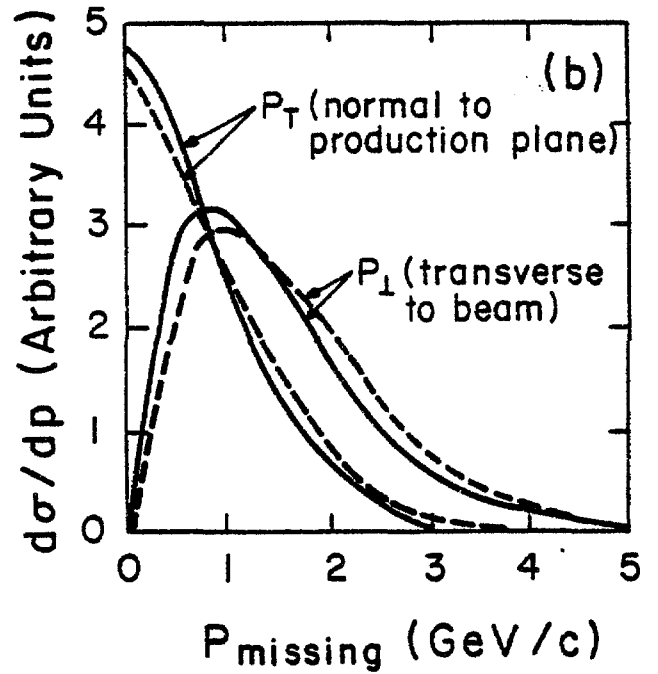
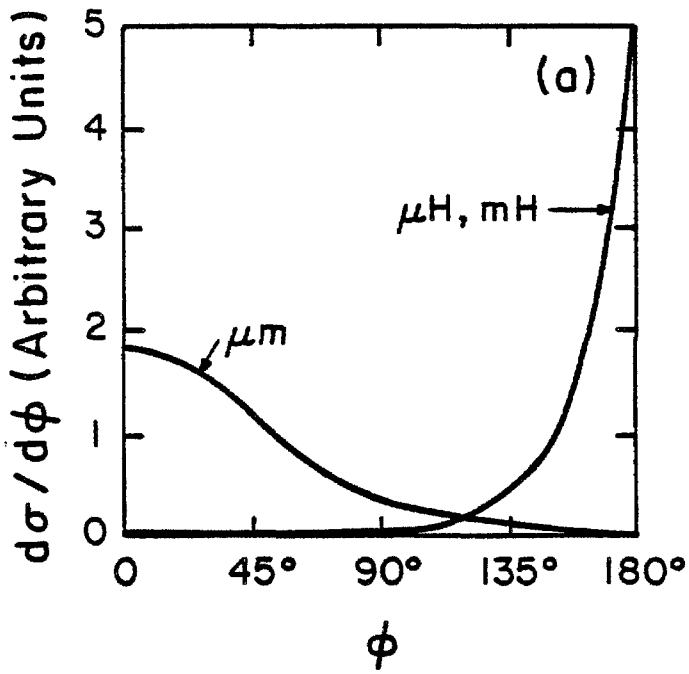
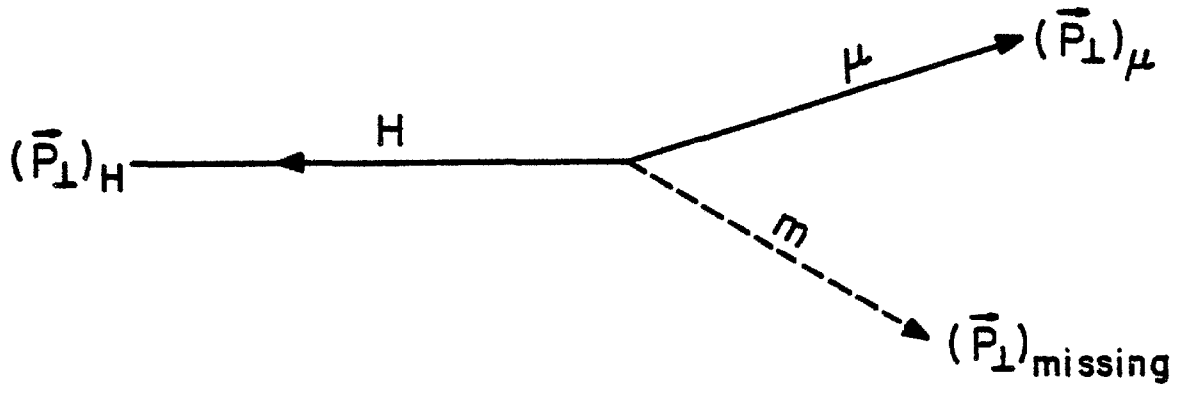


FIG. 11

Addendum and Revision of P635I. Introduction

In 1980, the authors of proposal P-635 outlined a program of investigation in three important areas. They were the following:

1. Determination of the leptonic weak coupling constants, g_V and g_A , through measurements of $\nu_\mu e \rightarrow \nu_\mu e$ and $\bar{\nu}_\mu e \rightarrow \bar{\nu}_\mu e$ scattering cross sections.
2. Search for neutrinos oscillations.
3. Search for decays of long-lived neutral particles, such as axions.

These areas of investigation remain as topical today as they were when originally proposed.

The Fermilab Program Advisory Committee in its 1980 Summer Meeting deferred action on the proposal, awaiting further developments on the part of the proponents. During the ensuing period, the authors have been actively developing the technical features as well as refining the physics goals of the proposed experiments. This addendum and revision updates the original proposal and will, hopefully, permit a reconsideration of the proposal by the Program Advisory Committee in its 1982 Summer Meeting.

II. Progress from 1980-1982

P-635 was a proposal in which the difficult but fundamental physics was proposed to be done by a powerful technique we had spent years in its development and improvement. Based upon excellent results obtained with delay line proportional chambers used in experiment E-253 in which the cross section for $\nu_\mu e \rightarrow \nu_\mu e$ was measured to the best accuracy to date, the authors proposed a detector which was 40 times larger than previously used. Furthermore, the proposed readout system for the chambers employed, as of that date, an untested new method for reading out these chambers. The new chambers were to be 3m x 3m in cross sectional area (compared to 1m x 1m used in E253) and were to employ a CCD (Charge Coupled Device) digitizing system. Understandably, some hesitation developed on the part of the PAC.

To proceed to demonstrate the feasibility and desirability of what was proposed, the authors initiated a step-by-step program of research and development which permitted an orderly, cost-effective, and measured approach as well as the investigation of interesting physics.

Since the summer of 1981, the group has been conducting a search for axion-like objects at SLAC. The apparatus used at SLAC has been the reconfigured 1m x 1m chambers of E253 outfitted with the new CCD readout system. In January, 1982, the experiment had a two-week long data-taking run in which one third of the requested beam was dumped onto the production target. Approximately 5600 triggers were recorded with 9.5 Coulombs of 20 GeV electrons. Almost all of that data has already been scanned and measured.

The run at SLAC fully demonstrated the success of the CCD readout system. Electromagnetic showers, hadron showers, and muon or hadron tracks were observed with high resolution and reliability as had been anticipated. Details of the readout system are included in Appendix I.

As a result of the success of the January run, the SLAC management has specified that a six week dedicated run be provided to the group to acquire the remaining data of the experiment. A decision was made to replace the 48 1m x 1m chambers with between 8 and 10 of the 3m x 3m chambers outfitted with the now demonstrated CCD readout system. The 3m x 3m chambers have been built and are now awaiting the fabrication of new amplifiers and CCD digitizers. The authors are confident that this system will become operative by the late summer of 1982.

The importance of these developments to P-635 is that by October, 1982, the group will have in hand the equipment to start the search for axion-like objects at Fermilab upon the completion of E-137 at SLAC. Possibly in as short a time as three months but certainly within six months, we would be capable of setting up an experiment at Fermilab with equipment of demonstrated capability. Questions of technical feasibility do not need to be conjectured or debated but can be answered by

data from conducted experiments.

III. The Modified Experimental Proposal

We have re-examined the physics goals of P635 and have come to the conclusion that a stage-by-stage approach, in which a "final" detector may evolve, would be the most logical and reasonable, consistent with the funding constraints. The modified experimental proposal is described as following:

(1) Search for Axion-like Objects

Initially, we like to set up a very modest apparatus to search for the axion-like objects. It is the natural extension to higher bombarding energies of the search experiment, E-137, at SLAC. The dominant decay mode we will look for at Fermilab is the process $X^0 \rightarrow \mu^+ \mu^-$, where X^0 represents the new neutral particles. At SLAC, we are searching for the decay mode $X^0 \rightarrow \gamma\gamma$. This two-photon mode can also be automatically searched for on this proposed detector at Fermilab.

The detector is to be located approximately 600 meters downstream from the new Tevatron beam dump. It consists of sixteen 3m x 3m MWPC's interlaced with steel plates (1 r.l. thick each) and plastic scintillation counters, a 3m x 3m x 3m solid iron magnet. The 3m x 3m MWPC's have delay lines along the x- and the y-directions on the cathode planes. The signals are readout with CCD digitizers which can measure both the pulse heights and positions of particle tracks. The anode wires of each 3m x 3m chamber are connected into 8 groups and they can be used as "hodoscopes" for pulse-height measurements and triggering purposes. These 16 chambers are currently under construction. Eight of them are already finished and they will be used at SLAC in E-137 for the scheduled running in the Fall of 1982. We anticipate that the construction of the remaining chambers will be completed before the end of 1982. The details of the detector is shown in Figure 1.

Since most of the experimental apparatus, including an on-line computer system, is in existence, this axion search experiment should not seriously tax the Laboratory resources. The Laboratory would still be asked to provide us a building with utilities, the solid iron magnet, and the necessary fast electronics including NIM and CAMAC power crates.

The building housing the detector could be one of the size of the present Wonder Building. We ask that the building be approximately as long as the Wonder Building to allow for the inclusion of additional detector modules which would be required when attention turns later to neutrino experiments.

(2) The Neutrino Experiment

While the "axion" search experiment is being set up or operative, we will continue to construct more 3m x 3m chambers at a rate commensurate with our funding levels. With a total number of 50 chambers, we can conduct an outstanding $\nu_{\mu}e$ and $\bar{\nu}_{\mu}e$ scattering experiment in the future. These chambers can be added gradually to the front end of the apparatus provided that the housing has approximately the same size as the present Wonder Building. This detector, made of 50 3m x 3m modules, has about ten times the fiducial tonage of E-253. When coupled with the higher energy of the Tevatron operation, it is possible to acquire $\nu_{\mu}e$ and $\bar{\nu}_{\mu}e$ elastic scattering events in the 10^3 range. The 3m x 3m MWPC's with CCD readout possess the salient features of good angular resolution, fast speed, and multiple-track/shower capability. Also, it can identify electromagnetic showers, hadronic showers, and minimum ionizing particles. It is particularly suitable for the measurement of energy flow and for use in experiments such as the neutrino-electron scattering. The directions of electromagnetic showers or muons can be determined to approximately ± 2 mr by using chambers within the first five radiation lengths from the vertex.

We are persuaded that this option in the future is a sound one, both in terms of physics and economics. As it turned out, progress made in $\nu_{\mu}e$ and $\bar{\nu}_{\mu}e$ scattering during the past years has been much

slower than generally expected. It is quite clear that these processes are the best for the determination of $\sin^2\theta_w$ or alternatively g_V and g_A , the exact values of which are still an important physics issue. As pointed out by Veltman, if the experiment can be carried out with sufficient precision, then the radiative corrections can yield good physics on heavy quarks. For some time, it was anticipated that the measurement of forward-backward asymmetry in the pure leptonic process $e^+e^- \rightarrow \mu^+\mu^-$ should give a good determination of $\sin^2\theta_w$. Thus far, the storage ring results need much more improved precision; this leaves the neutrino-electron scattering as a very competitive alternative.

IV. Physics Goals of the "Axion-like" Particle Search at Fermilab

The physics space we can explore at Fermilab is estimated by Bjorken as the following:

Suppose the best object for a search is an X^0 coupled to quarks and leptons with mass greater than 200 MeV, then $X^0 \rightarrow \mu^+\mu^-$ is the dominant decay mode. Assume that X^0 is produced like pions with

$$\frac{X}{\pi} = 10^{-3} \left(\frac{1 \text{ GeV}}{F_X} \right)^2,$$

the decay width is

$$\Gamma(X^0 \rightarrow \mu^+\mu^-) = \frac{M_X M_\mu^2}{8\pi F_X^2},$$

where F_X is the decay coupling constant. Using these two expressions together with the experimental geography, we can estimate the counting rate as a function of M_X and F_X .

Since the Tevatron beam dump is approximately 300 m from Lab C of Neutrino Area, it is logical to locate the experiment ~300 m downstream from Lab C. Because the new Muon Lab is adjacent, the utilities can be conveniently brought over from there. For a small detector, the rate is

proportional to $\lambda/(\lambda + 300 \text{ m})^2$ for this geography, where λ is the decay path available behind Lab C. For the 3m x 3m detector we are proposing, the angle it subtended is $\theta = \pm 1.5 \text{ m}/600 \text{ m} = \pm 2.5 \text{ mr}$; for $E_x \geq 100 \text{ GeV}$ this gives $P_{\perp}^{\text{max}} \geq 250 \text{ MeV}$. With an $X^0 \rightarrow \mu^+ \mu^-$ originating at 200 m from the detector, the separation of the two muons at the detector is approximately $(5 \text{ m}) \cdot (M_x/1 \text{ GeV}) \cdot (100 \text{ GeV}/E_x)$. This is adequate for $M_x = 200 \sim 300 \text{ MeV}$, but deteriorates as the mass increases.

The rate is estimated by taking for the pion yield

$$\frac{\pi (E > 100 \text{ GeV}; P_{\perp} < 200 \text{ MeV})}{\text{Proton on Target (POT)}} \approx 1,$$

which gives

$$\frac{X}{\text{POT}} \approx 10^{-3} \left(\frac{1 \text{ GeV}}{F_x} \right)^2$$

Since

$$\frac{\gamma c \tau}{500 \text{ m}} = 10^{-17} \frac{E_x M_p F_x^2}{M_{\mu}^2 M_x^2},$$

therefore

$$\frac{\text{Detected } X}{\text{POT}} = 10^{10} \left(\frac{100 \text{ GeV}}{E_x} \right) \left(\frac{M_x}{1 \text{ GeV}} \right)^2 \left(\frac{1 \text{ GeV}}{F_x} \right)^4.$$

If we ask for 10^{-17} or more detected X^0 per POT, then

$$F_x \leq (5000 \text{ TeV}) \left(\frac{M_x}{1 \text{ GeV}} \right)^{\frac{1}{2}} \left(\frac{100 \text{ GeV}}{E_x} \right)^{\frac{1}{2}}.$$

The condition that X^0 reaches the decay region

$$\frac{\gamma c \tau}{500 \text{ m}} \geq 1$$

translate into

$$F_x \geq (300 \text{ TeV}) \left(\frac{M_x}{1 \text{ GeV}} \right) \left(\frac{100 \text{ GeV}}{E_x} \right)^{1/2} .$$

The region in the M_x - F_x space which this experiment can explore is shown in Figure 2. Just for comparison, the region, which E-137 can explore at SLAC by detecting $X^0 \rightarrow \gamma\gamma$, is shown in Figure 3. It should be emphasized that the decay constant, F_x , which E-137 can reach at SLAC is about 10^3 GeV; while at Fermilab, this proposed experiment can reach approximately 10^7 GeV.

There are three main sources of backgrounds; namely, (1) neutrino interactions between the Tevatron beam dump and Lab C, (2) neutrino interactions in the useful decay volume between Lab C and the proposed detector, and (3) the "sky-shine" produced by the deep-inelastic scattering of all the "spoiled" muons.

The neutrino interactions between the Tevatron beam dump and Lab C should not worry us because there will be over 100' of sweep magnets behind the beam dump to sweep out the charged particles from reaching the 15' bubble chamber. It is designed such that only less than $\sim 10 \mu\text{'s}/10^{13}$ protons can enter the 15' bubble chamber. Additional sweeping power provided by the magnets of Lab E, the 15' bubble chamber, and Lab C, should have our proposed detector fully protected. The backgrounds due to the sky-shine of the "spoiled" muons have to have very large transverse momenta ($\geq 5 \text{ GeV}/c$) in order to reach the proposed detector. Their effects are inconsequential because of the approximate $e^{-5P_{\perp}}$ dependence. Since there are approximately 2,700 kg of air in the useful decay volume, neutrino interactions can produce up to 10^4 background events per 10^{18} POT (~ 1 event/10 pulses). The majority of these backgrounds can be eliminated from triggering the apparatus by demanding that at least two charged particles are required, among other things, in the experimental trigger. This condition can be easily satisfied by the utilization of matrix logics

in conjunction with two 2-dimensional hodoscopes as shown in Figure 1. In the data analysis, the remaining backgrounds can be eliminated by utilizing cuts in the following facilities:

1. Dimuon identification,
2. Coplanarity,
3. Symmetry in momentum of the dimuon,
4. No accompanying particles,
5. Invariant mass and total energy.

V. The Request

We request the Laboratory to allow us to set up an experiment in the Neutrino Area to search for new, long-lived, and neutral particles, such as "axions", etc. We ask the Laboratory to provide us a detector housing ~ 300 m downstream from Lab C, a 3m x 3m x 3m solid iron magnet, and fast electronics.

Initially, we request to run the experiment with $10^{18} \sim 10^{19}$ protons on target at the new Tevatron beam dump. In due course, we propose to enlarge the detector to 50 modules which will enable us to do a future neutrino-electron scattering experiment.

Appendix I

Delay-Line Chambers and CCD Digitizers

In this appendix, the essential features of the delay-line chambers and the CCD digitizers are briefly described.

1. The Delay-Line Chambers

On the cathode planes of the MWPC's used in E-253 at Fermilab and E-137 at SLAC there are delay-lines along both the x- and y-direction. They are continuous zig-zag conducting strips machine-milled on copper-clad G-10 plates. Typically, they behave like transmission lines of impedance ~ 100 ohms. When a particle passes through the chamber, a positive signal will be induced on the delay-line due to capacitive coupling. The signal will then propagate along the delay-line at a speed of ~ 5 nsec/m. By measuring the propagation time, one can obtain the track position.

The transverse spacing of the delay-line is 2 mm. For the 1m x 1m chamber we used in E-253, the delay-line was continuous over the entire cathode plane. Readout ports were tapped at 5 equi-distance points. This arrangement is required to take care of the attenuation and provides redundancy; but it introduces left-right ambiguities (although self-resolved) for the three ports in the middle. For the 3m x 3m MWPC's, the delay-line on each cathode plane is cut into 24 separate sections. One end of each section is properly terminated. The other end is connected to an amplifier, then fed to a CCD digitizer. This arrangement simplifies the data-reduction algorithm because the signals will all propagate along the same direction.

For the eight 3m x 3m chambers already built, the mechanical construction is very similar to that of the 1m x 1m chambers used in E-253 at Fermilab. The G-10 delay-line boards were glued onto 1/4" thick aluminum plates. Two of such plates are bolted together to form the

cathode planes of one chamber. In order to prevent the aluminum plates from buckling, aluminum "spiders" are welded to each plate to provide the necessary mechanical strength. This scheme is adequate but it makes the chambers rather heavy, weighing approximately 1,500 lbs. each. For the new 3m x 3m chambers under construction, the aluminum plates and the reinforcement spiders are replaced with "Hexcel" like boards. They are not only lighter, but also stronger. Each 3m x 3m chamber will only weigh approximately 350 lbs., and most of the weight comes from the G-10 delay-line boards.

2. The CCD Digitizer

The operation of the CCD digitizer is shown schematically as Figure 4.

The signals from a cathode-plane delay line are first amplified by an amplifier located on the chamber. The output is fed to a CCD digitizer (in a CAMAC crate) through a long coaxial cable. The CCD is continuously clocked by a 50 MHz oscillator. Upon occurrence of each clock pulse, a 20 nsec slice of the input signal is loaded into a CCD bucket. The charges stored in the CCD buckets are shifted forward in sequence very much like a shift-register, except that it is operated in the analogue mode. Immediately after the occurrence of the master experimental trigger, the signal is "frozen" in the CCD. Then an ADC (analogue-to-digital converter) will sequentially digitize the charges in each CCD bucket and store the results in the RAM (random access memory) of the module, waiting to be read into the on-line computer via the CAMAC data highway. This simple scheme offers an elegant method in measuring both the pulse heights and track positions simultaneously. The CCD bucket number represents the track position in quantum of 20 nsec, and the charges in CCD buckets provide direct information on pulse-height distributions. Since the master experimental trigger can happen within one clock pulse of 20 nsec, its timing is also separately digitized to the accuracy of 1/125-th of one CCD bucket width (20 nsec) to provide the vernier corrections. By mapping the particle position and dE/dx information into the CCD bucket space in this manner, the original pulse profiles are thus retained in the on-line computer for later detailed analysis. Physical effects, such as delay-line attenuations, dispersions, energy calibrations, propagation

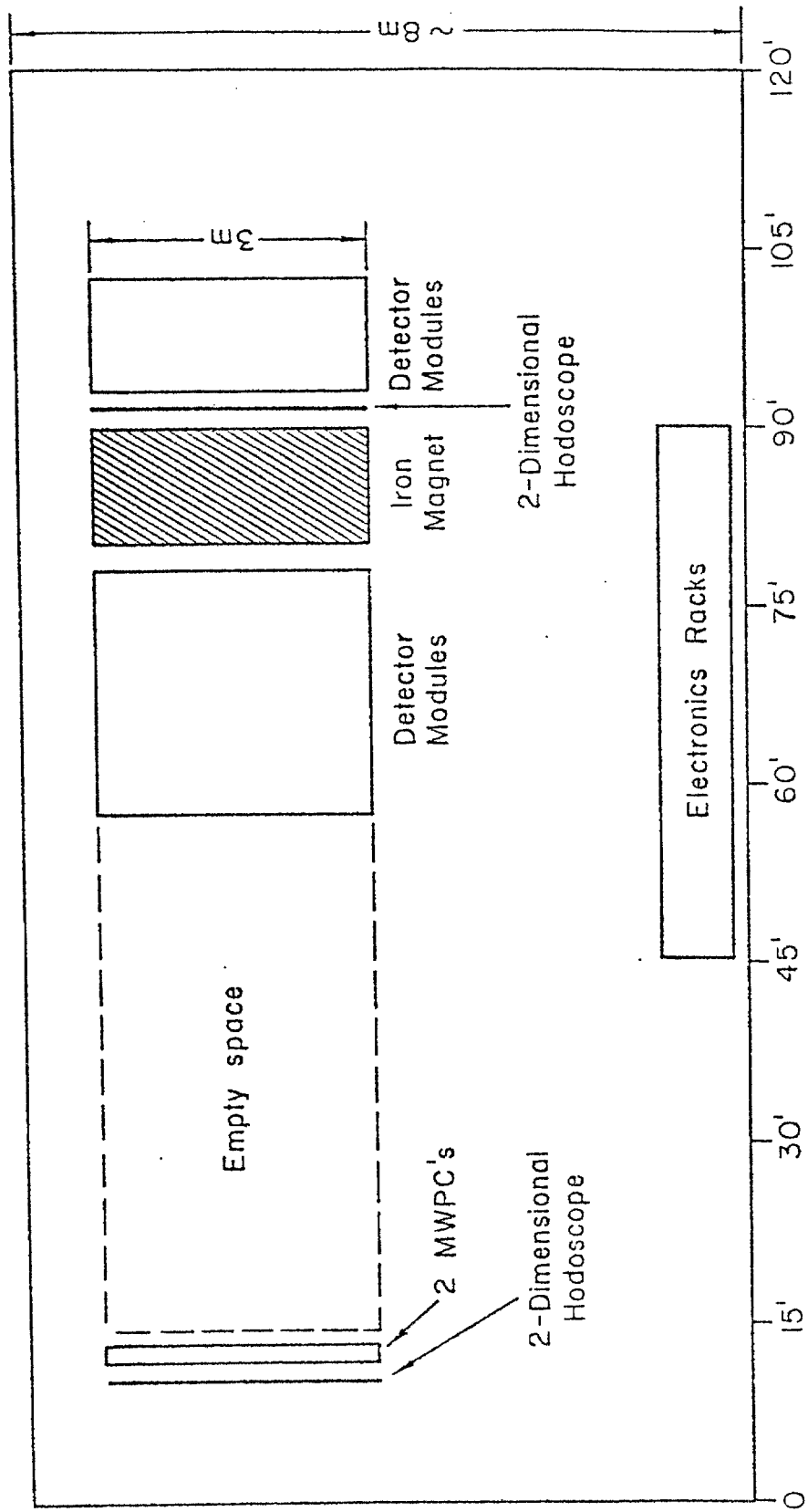
velocities, etc., can all be taken into account precisely in the final data-reduction stage.

Figure 5 illustrates one example of the CCD information from one of the 1m x 1m cathode planes. Pulse trains from the 5 readout ports of a continuous delay-line are shown. Each bucket represents ~ 8 mm in real space. Since we can determine the centroid of each pulse to the accuracy of a fraction of a bucket, by using 5 chambers at a spacing of 15" apart from each other, the direction of the track can be determined to the accuracy of $\sim \pm 2$ mr.

As described previously, on each cathode plane of the 3m x 3m chamber, the delay-line is divided into 24 sections. Only one end of each section is connected to a CCD digitizer, the other end is terminated (in principle, a second CCD digitizer can also be used, instead of the termination, to provide redundancy if finance permits). Since all the detected signals are traveling along the same direction, there is no ambiguity in sorting out their spatial positions. The pattern recognition is helped enormously by the pulse height information, which is not available in the conventional wire chambers. Due to the use of the delay-lines, the multiple-track events can be handled naturally because they appear as pulse trains. Once the straight-line tracks are determined, one can see the longitudinal distribution of pulse heights along the track direction, as well as the distributions transverse to the track direction at each chamber. This information is particularly useful in particle identifications, e.g., the π/e separations, etc.. If the tracks of a multi-particle event do not overlap one can follow each individual track to determine its energy by adding up the pulse-heights along the track. In this manner, the CCD digitizer has opened up a revolutionary possibility which permits the simultaneous measurement of energy and direction of each individual track of a multi-particle event by a non-magnetic detector. This novel approach has gained attention lately. At SLAC, the design of a future SLC calorimeter has considered the use of CCD's along, more or less, the same line as described here.

Figure Captions

- Figure 1 Schematic layout of the experimental apparatus.
- Figure 2 The region in the F_x - M_x space which this proposed experiment can explore with the decay mode $X^0 \rightarrow \mu^+ \mu^-$.
- Figure 3 The region in the F_x - M_x space which E-137 can explore at SLAC with the decay mode $X^0 \rightarrow \gamma\gamma$.
- Figure 4 Schematics of the CCD digitizer.
- Figure 5 An example of the CCD data from one cathode plane of a 1m x 1m MWPC. They are readout from 5 equi-distance tap points of a continuous delay-line. The signals are the redundant measurements of a single shower.



Schematic Arrangement of the Experiment

Fig. 1

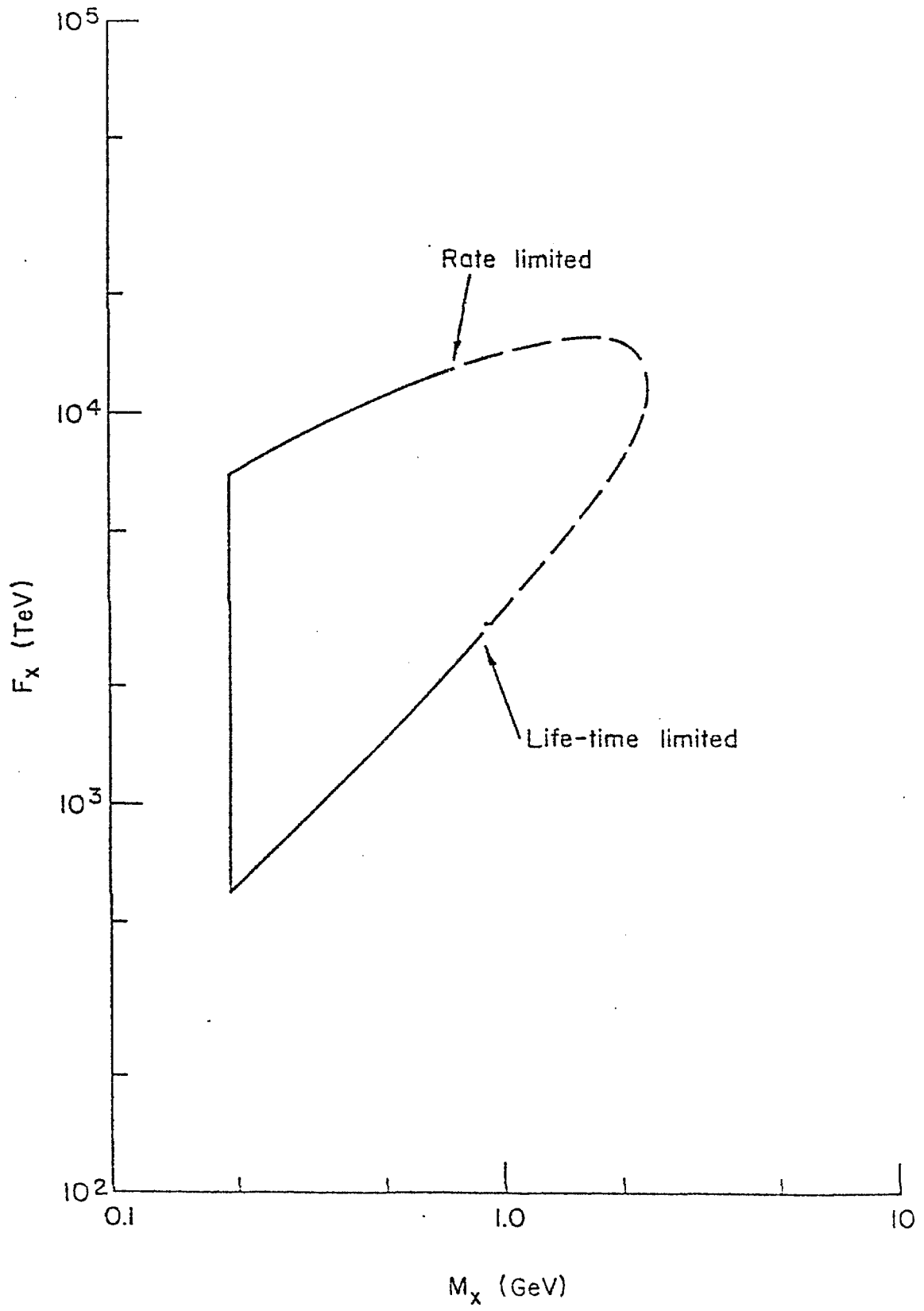


Fig. 2

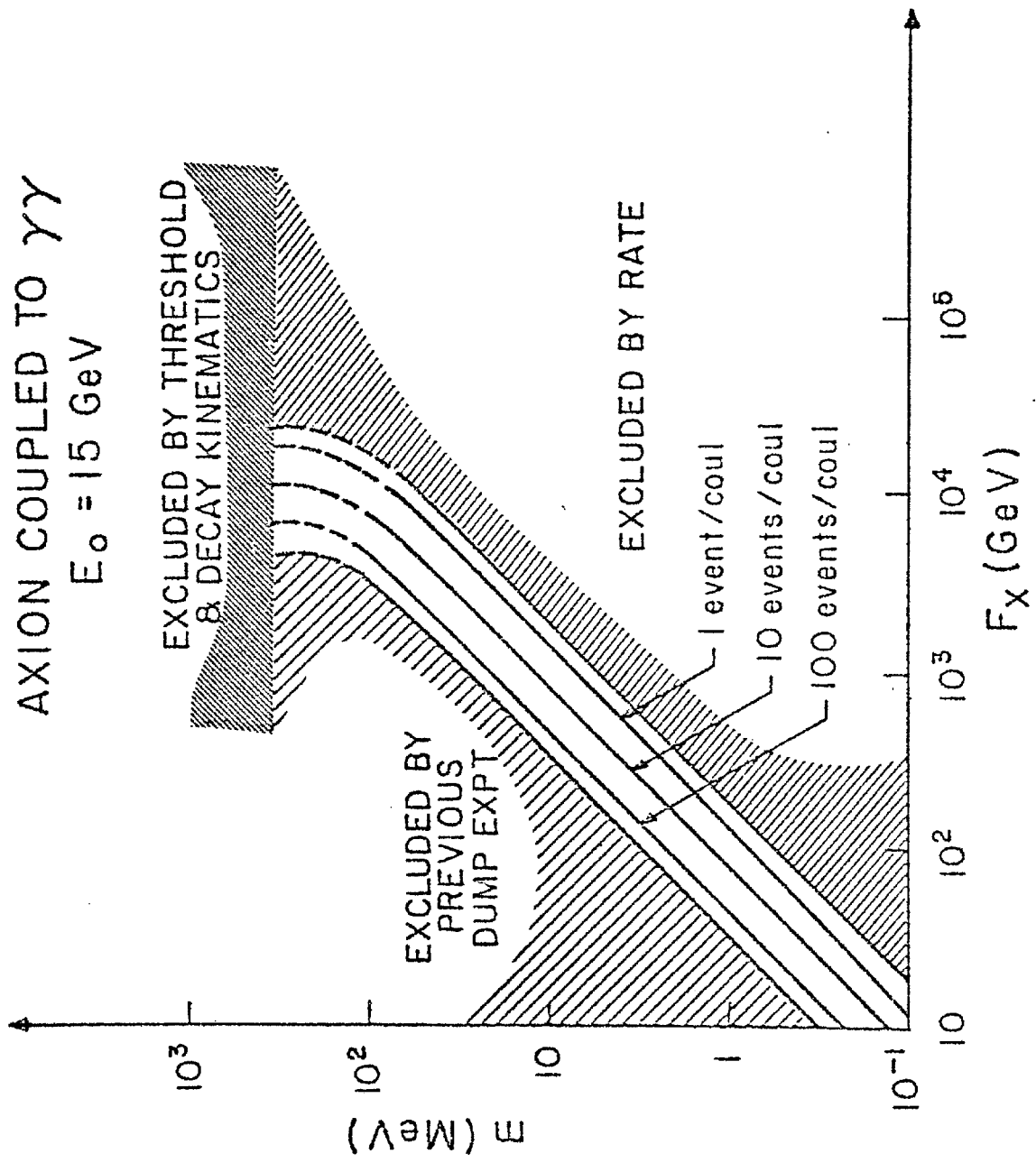
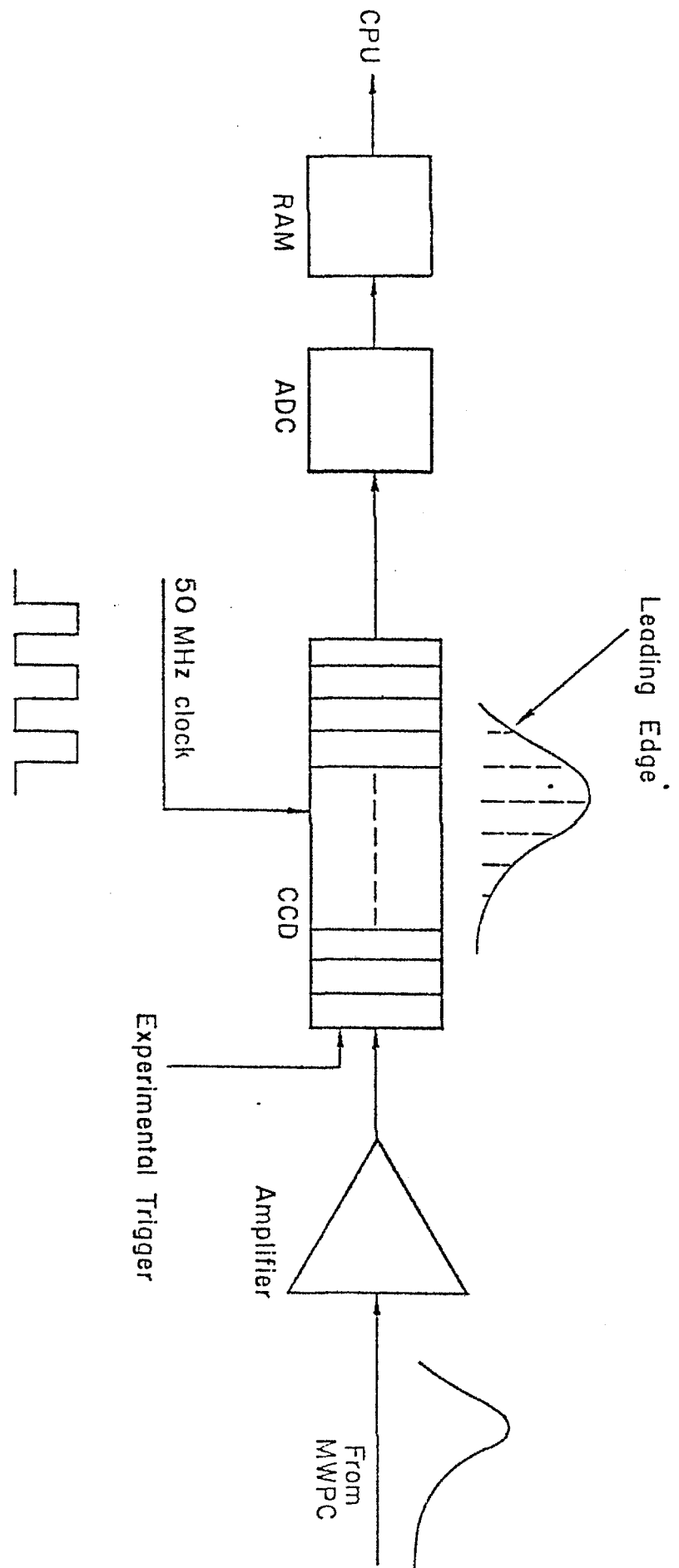


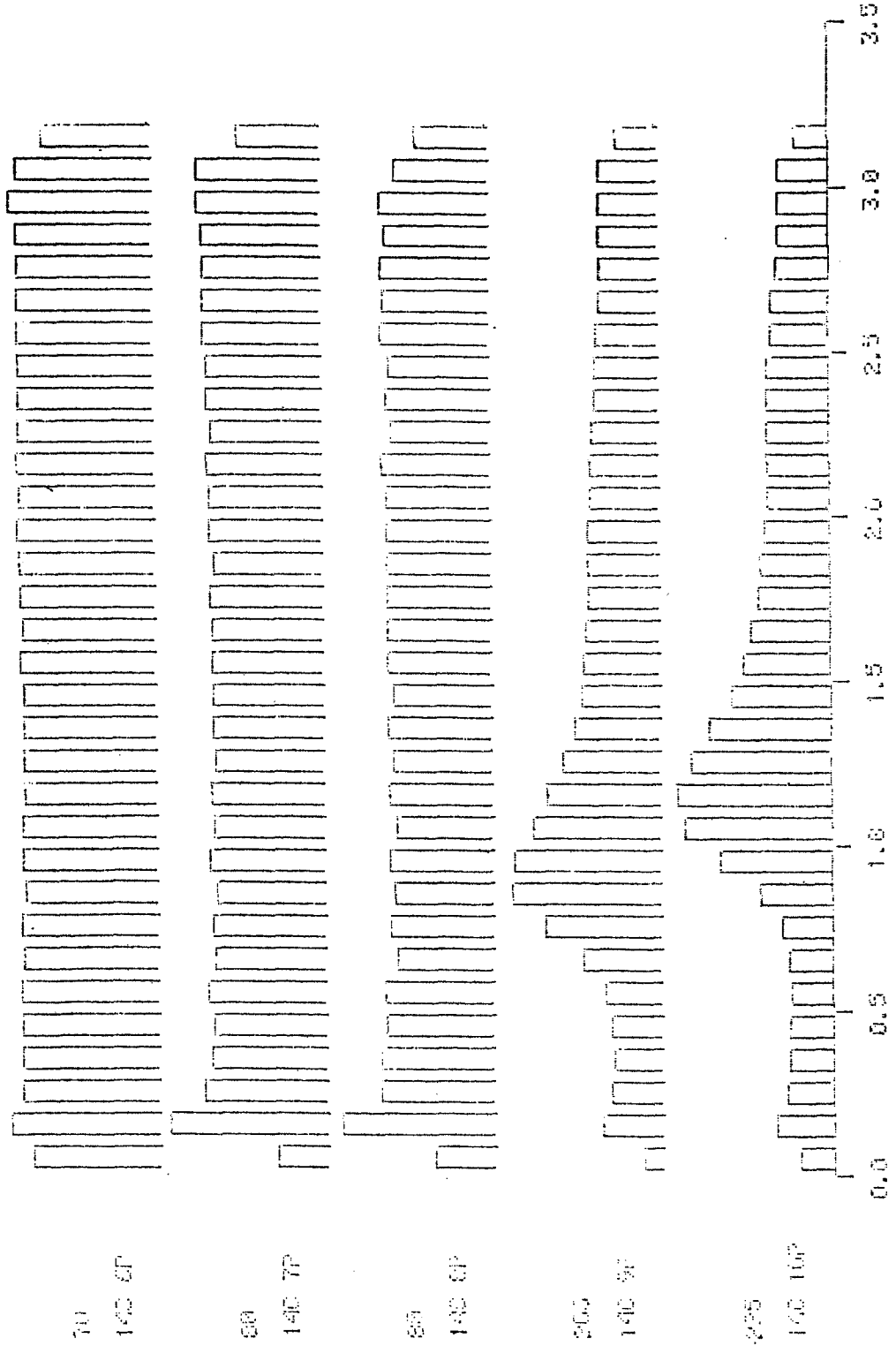
Fig. 3



Schematics of CCD Digitizer

FIG. 4

1981 01 01 1981 01 01 1981 01 01 1981 01 01 1981 01 01



BUCKET (101)

Appendix 2

Estimate of Sky-shine Background for P-635

The background for P-635 due to deep-inelastic scattering of the "spoiled" muons, analytically estimated by Bjorken, is described below:

The mechanism considered is limited to production of secondary hadrons in air by the intense muon beam which is diverted skyward by the dump magnets. According to the simulations carried out by the dump designers (M. Peters, private communication with Bjorken), there is very little muon intensity for angles less than a critical value, the vertical component of which is $\theta_{\min} \simeq 25$ mrad. The total differential muon intensity, $dN/d\sigma$ rises rapidly at this critical value, and soon saturates at approximately $(1 \sim 3) \times 10^6$ μ 's/mrad (these values are integrated over a fairly large swath of horizontal angles; θ is the vertical angle.)

The trigger will be assumed to be:

- (1) Two muons (or equivalent) traversing the apparatus with vertical angle less than 50 mrad. This implies that they penetrate the 3m of the solid-iron magnet, i.e., have incident energy in excess of 4 \sim 5 GeV. A concurrent trigger is:
- (2) Large energy deposition in the Fe-scintillator calorimeter. We shall find a rather steeply falling hadron energy spectrum, implying a relatively easy (and quite adjustable) trigger rate.

We assume all muons in the primary skyshine beam to be of sufficient energy to produce the hadrons of interest (which typically have energies in the range of 5 \sim 20 GeV). The standard deep inelastic scattering cross section is approximated by the following expressions:

$$\frac{d\sigma}{dq^2 dv} \simeq \frac{\alpha}{2\pi} \cdot \frac{1}{q^2} \cdot \frac{1}{v} \sigma_{\gamma}$$

and

$$\sigma_{\nu N} \approx \frac{\alpha}{2\pi} \cdot \ln \left(\frac{m_p}{m_\mu} \right)^2 \cdot \ln \frac{v_{\max}}{v_{\min}} \cdot \sigma_\gamma.$$

Take

$$\frac{v_{\max}}{v_{\min}} \approx \frac{100 \text{ GeV}}{5 \text{ GeV}} = 20,$$

$$\sigma_\gamma \approx 100 \text{ } \mu\text{b},$$

then

$$\sigma_{\mu N} \approx 1.5 \times 10^{-30} \text{ cm}^2.$$

This energy independent cross section, $\sigma(\mu+N \rightarrow \mu + \text{hadrons}) \approx 1.5 \times 10^{-30} \text{ cm}^2$, leads to $\sim 10^{-7}$ interactions per muon per meter of air traversed. The secondary pion spectrum (charged only) is taken to be

$$\frac{E}{\sigma} \frac{d\sigma}{d^3p} = \frac{b^2}{2\pi} \left(\frac{dN_\pi}{dy} \right) e^{-bp_\perp},$$

where $b \approx 5 \text{ GeV}^{-1}$, $dN_\pi/dy \approx 2$ and y is the rapidity. The geometry for the calculation is shown in Figure, 1. A muon produced at e_1 in the dump interacts in the air and produces a hadron at production angle $\theta_1 + \theta_2$, which reaches the P-635 detector and is seen with vertical angle θ_2 . The dump-to-detector distance, L , is $\sim 600\text{m}$; and the detector area, A , is $\sim 9 \text{ m}^2$. We require $\theta_1 \geq 25 \text{ mrad}$, and $\theta_2 \leq 50 \text{ mrad}$. We also temporarily ignore decay in flight of the pions (or hadrons) and comment on that later. The differential flux at the detector is

$$dN = \int ds \, d\theta_1 \left(\frac{dN}{ds \, d\theta_1} \right) \left(\frac{E}{\sigma} \frac{d\sigma}{d^3p} \right) p \, dp \, \Delta\Omega.$$

From the geometry,

$$s = \frac{L\theta_2}{\theta_1 + \theta_2},$$

$$ds = \frac{L\theta_1 d\theta_2}{(\theta_1 + \theta_2)^2},$$

$$\Delta\Omega = \frac{A}{(L-s)^2} = \frac{A}{L^2} \frac{(\theta_1 + \theta_2)^2}{\theta_1^2},$$

we will have

$$\frac{dN}{dp} = \frac{A}{L} \frac{b^2}{2\pi} \left(\frac{dN_\pi}{dy} \right) \int_{\theta_{\min}}^{\infty} \frac{d\theta_1}{\theta_1} \int_0^{\theta_{\max}} d\theta_2 e^{-bp(\theta_1 + \theta_2)} \frac{dN}{ds d\theta_1}$$

We overestimate the flux if θ_1^{-1} is replaced by θ_{\min}^{-1} . It is worth making that approximation in order to easily do the subsequent integrals. We end up with

$$p \frac{dN}{dp} < \frac{A}{2\pi L \theta_{\min}} \left(\frac{dN_\pi}{dy} \right) e^{-bp\theta_{\min}} (1 - e^{-bp\theta_{\max}}) \frac{dN}{ds d\theta_{\min}}.$$

Putting in our numbers gives

$$\frac{dN}{dp} \sim \frac{40}{p} e^{-\frac{p}{8\text{GeV}}} \left(1 - e^{-\frac{p}{4\text{GeV}}} \right).$$

The result is plotted in Figure 2. In that plot is also shown a simple estimate of flux due to π decay. Integration over momentum gives the final results:

$$\frac{\text{Single muons } (E > 4.5 \text{ GeV}; \theta < 50 \text{ mrad})}{10^{13} \text{ POT}} \lesssim 13.$$

Furthermore, the single muons will be out of time, in as much as the detector live-time (controlled by the delay-line and CCD readout) is $\lesssim 1 \mu\text{sec}$ out of a spill time of $\gtrsim 1 \text{ msec}$.

The pair rate should be easily much less than unity. This is estimated by expressing the solid angle subtended by the detector as

$$\Delta\Omega = \frac{A}{(L-S)^2} \equiv (\theta_1 + \theta_2)^2 \Delta y \Delta\phi.$$

Hence,

$$\Delta y \Delta\phi = \frac{A}{L_{\theta_1}^2} \leq \frac{A}{L_{\theta_{\min}}^2} \simeq 0.04.$$

The probability of a second accompanying track (ignoring correlations in production) in a given interaction is

$$P \simeq \frac{dN}{dy d\phi} (\Delta y \Delta\phi) \simeq \frac{2}{2\pi} \times 0.04 = 0.013.$$

From Figure 2, at least half of these particles are below energy threshold, so that:

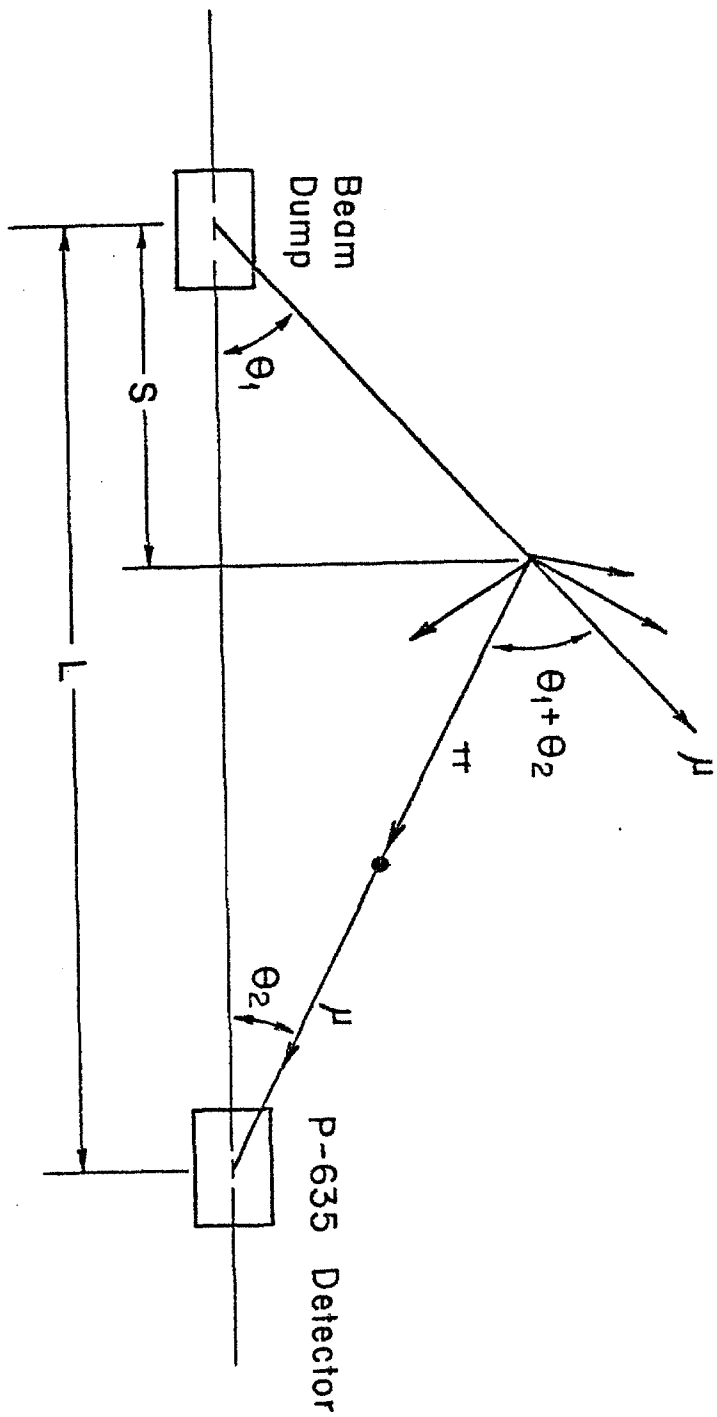
$$\frac{2 \text{ track}}{1 \text{ track}} < 6 \times 10^{-3},$$

and the 2-track triggers per spill is less than $\sim 8 \times 10^{-2}$ (approximately 1 trigger every 10 pulses).

Figure Captions

Figure 1: Geometry for the muon sky-shine calculation

Figure 2: Muon spectrum at the P-635 detector due to muon sky-shine



$L \approx 600 \text{ m}$
 $\theta_1 \approx \theta_{\min} = 25 \text{ mrad}$
 $\theta_2 \leq \theta_{\max} = 50 \text{ mrad}$

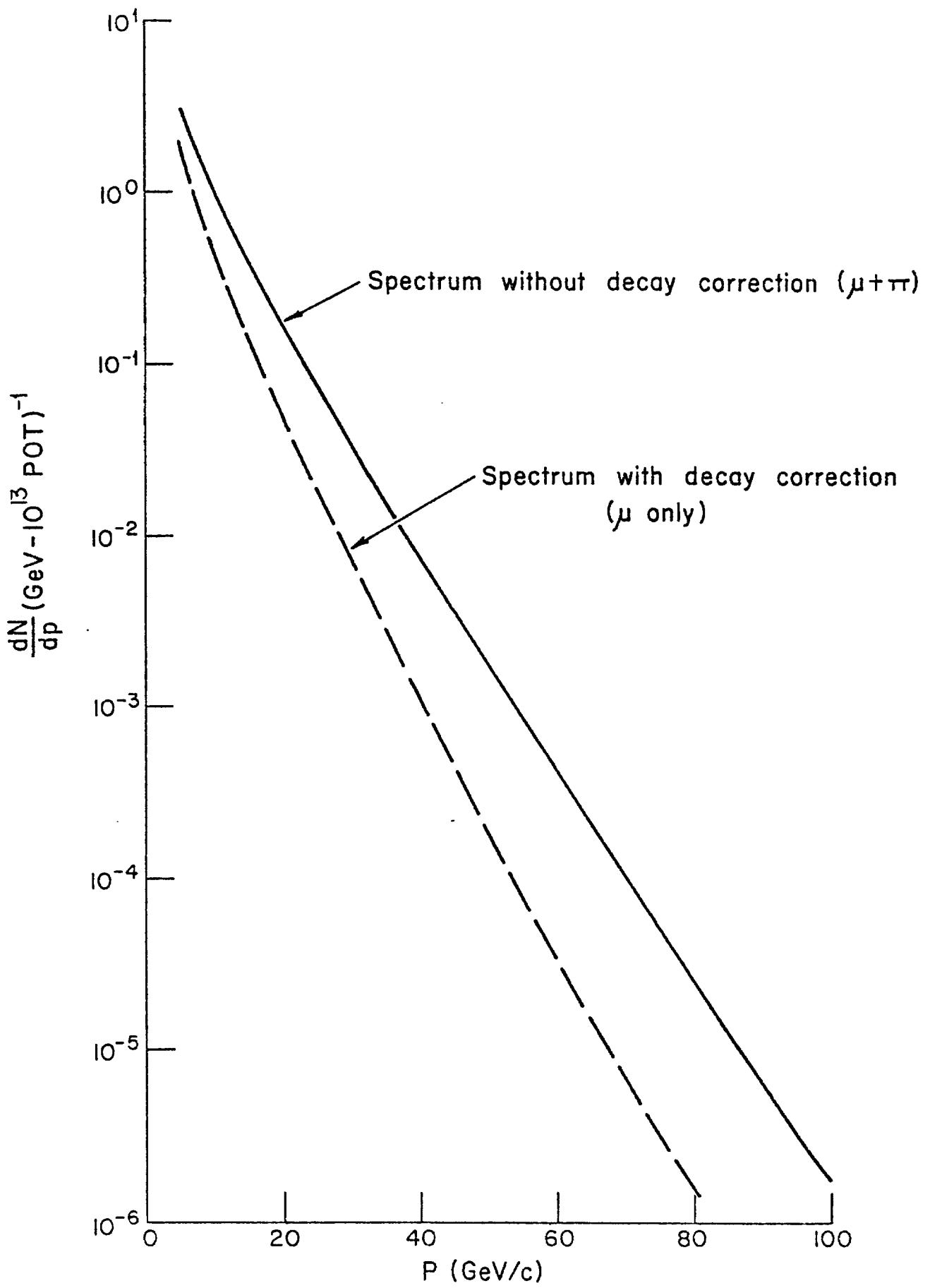


Fig. 2

Proposal to Search for
Axion-Like Particles and to Measure
 $\nu_{\mu}e$ and $\bar{\nu}_{\mu}e$ Elastic Scattering
at
The Tevatron of Fermilab*

* First submitted 1980
Revised March, 1983

Table of Contents

- I. Introduction
- II. Search for Axion-Like Particles
 - A. Pseudo-Nambu-Goldstone Bosons: Axion-Like Entities
 - B. Characterization of Axion-Like Entities
 - C. Decay of X
 - D. Phenomenology
- III. Neutrino-Electron Elastic Scattering
- IV. Experimental Proposal on the Search for Axion-Like Objects
 - (1) The Experimental Arrangement
 - (2) The Physics Goal
 - (3) Backgrounds for the Axion Search Experiment
 - (4) The Vertex and Mass Resolution of the Magnetic Muon Spectrometer
- V. Experimental Proposal on Neutrino Electron Scattering
 - (1) The Non-Magnetic Detector
 - (2) The Counting Rate and Statistics
 - (3) Separation of Signal Form Background
 - (4) Beam Normalization and Systematic Errors
 - (5) Equipment Calibration
 - (6) The Magnetic Muon Detector
- VI. Other Experimental Possibilities
- VII. Proposal and Request
 - Appendix 1: Estimate of Sky-Shine Background for P-635
 - Appendix 2: Delay-Line Readout Chambers and CCD Digitizers
 - Appendix 3: Cost Estimate
 - Reference and Footnotes
 - Figures 1-20

I. Introduction

Since the submission of Proposal P-635, the scope of the proposal had been modified by us. Also, it was deferred twice by the Physics Advisory Committee. In the meantime, a fraction of the apparatus we propose to use in P-635 was built and was already used in the axion search experiment at SLAC (E-137). We feel that it is time for us to recapitulate the proposal, in order to express clearly what we wish to do at the Tevatron of Fermilab as well as the way we plan to do it.

The proposal consists of two parts. They are:

- (1) The search for metastable, neutral, "axion-like" particles which decay in flight into muon pairs; and
- (2) The elastic $\nu_{\mu}e$ and $\bar{\nu}_{\mu}e$ scattering.

II. Search for Axion-Like Particles

The existing list of elementary particles, while large and well-organized, may not be complete. It is without question important to search for unexpected particles in as many ways as practical. This is done as a matter of course at new machines. Particles carrying electroweak charge are produced reasonably copiously in e^+e^- colliders, and the frontier is mainly one of pushing to higher and higher mass scales. Particles carrying no electroweak charge but carrying color may be produced reasonably copiously in hadron machines and colliders, and occasionally in e^+e^- machines as well (e.g. gluons or gluinos). The systematic search is more difficult but reasonably accessible. Again the frontier probably lies toward higher mass.

The proposed P-635 experiment addresses yet another class of possible particles: those that carry no net quantum numbers and couple

at best very weakly to ordinary quarks, leptons, and gauge-fields. Theory suggests that it is possible that there exist such particles with low mass, (say, from the sub-MeV range to the sub-GeV range). Because of the low mass and very weak coupling to matter, fixed target, high luminosity experiments become an especially appropriate search technique. We propose to search for metastable, low mass particles produced in the Fermilab beam dump, which decay in flight upstream of the detector into leptons and/or photons.

Several classes of such particles might be entertained (exotic gauge bosons, photinos, familons,...). For definiteness, we discuss in this proposal only one class, that of axion-like pseudo-Nambu-Goldstone bosons.^{1,2} However, it is likely that if a positive result of the search were found, it would not correspond to the scenario we describe. The scope of theoretical speculation evolves rapidly. For example when the pioneering beam dump experiment at SLAC was proposed by M. Schwartz et al.³, it could only point to one tangible object of search: prompt decay neutrinos from pair-production of a conjectured (τ -like!) "heavy" lepton. That experiment turned out to be most useful in limiting properties of the PQWW (Peccei-Quinn-Wilczek-Weinberg⁴) axion, invented only after the completion of the experiment.⁵ Likewise the SLAC E-137 experiment⁶, which focuses on the axion search, turns out to be sensitive to photino⁷ production as well. It is therefore quite possible that the focus of P-635 will likewise change as theory evolves.

A. Pseudo-Nambu-Goldstone Bosons: Axion-Like Entities

In the standard model, gauge coupling constants are free parameters. If they are set to zero, one is left with free (transverse) gauge quanta, along with a "Higgs sector" of scalar bosons which interact with each other and (regrettably) very weakly with quarks and leptons. Among those Higgs bosons are massless Nambu-Goldstone bosons. These comprise, in the original coupled theory, the longitudinal components of the gauge bosons. Here they are better characterized as the inevitable "collective modes" accompanying the spontaneous symmetry breakdown of the Higgs sector.

In typical theories, the number of such spinless, massless Nambu-Goldstone bosons is matched to the number of massive gauge bosons. In $SU(2) \times U(1)$, there are 3, in $SU(5)$ there are 15, etc. But it is possible that there exist some extra massless - or nearly massless - bosons produced by the spontaneous symmetry breakdown and which do not become the longitudinal components of gauge bosons. The most well known example is the PQWW axion, invented to provide an explanation of the absence of CP violation in QCD. While the PQWW axion is by now ruled out experimentally, other axion-like bosons have been suggested. (ETC axions, Majorons, familons, etc.). Inasmuch as this is a generic class of particles (like quarks, leptons, gauge-bosons), it seems appropriate to mount searches for them in as general a way as possible, with the search - in the absence of compelling arguments to the contrary - decoupled from specific theoretical models. This is especially important in this case because the theory of the Higgs sector is in very unsatisfactory condition.

B. Characterization of Axion-Like Entities

Central to the notion of pseudo-Nambu-Goldstone-boson is the existence of a conserved or almost-conserved current associated with the spontaneous broken symmetry. The axion-like object X couples to the divergence of the current. An important parameter is the decay constant F_X , defined as

$$\sqrt{2E_X} \langle 0 | J_\mu | X \rangle = F_X q_\mu.$$

This parameter reflects the mass scale for the dynamics of spontaneous symmetry breaking. For example

$F_X \sim 100 \text{ MeV}$	$X = \text{pion}$
$\sim 250 \text{ GeV}$	$X = \text{electroweak axion}$
$\sim 10\text{-}100 \text{ TeV}$	$X = \text{ETC axion}$
$\sim 10^{15} \text{ GeV}$	$X = \text{Majoron}$

In typical theories, this parameter also characterizes the coupling to fermions. We assume, to avoid questions of flavor-changing currents, that the current couples with equal strength to all fermions of a given electric charge and that it is self-conjugate. Then the coupling of X to fermions is diagonal and of strength

$$g_{Xff} \cong \frac{m_f}{F_X}.$$

The above relation is not necessarily a strict logical consequence of all spontaneous symmetry breaking schemes, but is reasonable and will be assumed in what follows.

Also assumed in what follows is that X couples to all quarks and leptons, and has nonvanishing coupling to $\gamma\gamma$. This then provides a characterization sufficiently complete to define a phenomenology. In particular the axion-like entity (pseudo-Nambu-Goldstone-boson) X is

characterized in terms of mass m_X and decay constant F_X . We may now ask which values of these parameters are empirically allowed and which are forbidden. We emphasize that this characterization does not apply to all axion models, but ought to be sufficiently generic that it provides a rough guide for comparing the sensitivity of different experiments.

C. Decays of X

For the X as we have defined, there is a fairly definite decay systematics. If $m_X < 1$ MeV, $X \rightarrow \gamma\gamma$ with relatively long lifetime:

$$\frac{\Gamma(X \rightarrow \gamma\gamma)}{\Gamma(\pi^0 \rightarrow \gamma\gamma)} \approx \left(\frac{F_\pi}{F_X}\right)^2 \left(\frac{m_X}{m_\pi}\right)^3.$$

For $1 \text{ MeV} < m_X < 200 \text{ MeV}$, the X decays predominantly into e^+e^- :

$$\Gamma(X \rightarrow e^+e^-) = \frac{1}{8\pi} \frac{m_e^2}{F_X^2} m_X:$$

For $1\text{-}2 \text{ GeV} > m_X > 200 \text{ MeV}$, the X decays predominantly into $\mu^+\mu^-$. This is the mass region which P-635 addresses; thus a dimuon search seems especially promising. (However, $\gamma\gamma$, e^+e^- , $\mu^\pm e^\mp$, ... are available to the experiment as well.) For $m_X \gg 1\text{-}2 \text{ GeV}$, the X will decay predominantly into pairs of hadron jets, with dileptonic signatures becoming of lesser importance.

It may be noticed that decay rates are all proportional to F_X^{-2} . This is also true of production cross-sections. Hence the sensitivity of most laboratory tests tend to behave as F_X^{-4} .

D. Phenomenology

A large variety of constraints exist for axion parameters. Astrophysics restrain them in a variety of ways; the line of argument parallels those used for massive neutrinos. For example,

- a) if $\tau_X > 10^9$ yrs and $m_X > 100$ eV, then X contributes too much mass and closes the universe;
- b) if $\tau_X \geq 10^4$ sec, then the 3° black-body spectrum is distorted;
- c) if $\tau_X \approx 10^{\pm 3}$ sec and $m_X > 10$ MeV, then phenomenology of supernova collapse is unacceptable;
- d) if $m_X < 200$ keV, $F_X < 10^9$ GeV, then red giants burn out;
- e) if $F_X > 10^{12}$ GeV, long wavelength coherent quantum fluctuations of the Higgs condensate has enough energy to close the universe.

Another class of limits come from previous beam dump experiments, in particular experiments at LAMPF, BNL, CERN, and SLAC. Most of them are sensitive to $X \rightarrow \gamma\gamma$ and/or $X \rightarrow e^+e^-$ if $m_X < 200$ MeV⁸.

Another class of tests come from reactor experiments. In addition, decays such as $K \rightarrow \pi X$ ⁹, $\psi \rightarrow \gamma X$ ¹⁰, $T \rightarrow \gamma X$ ¹¹ (and eventually $Z \rightarrow \gamma X$) provide useful limits. We do not go into details, but sketch in Figs. 1 and 2 the regions of parameter space excluded¹².

The PQWW axion lies in densely explored territory and has been decisively excluded by searches in ψ and T decays. The territory to be explored in P-635 is shown in Fig. 2. There is no known theoretical motivation for existence of an axion-like entity in this region of parameter space. However, it should be noted that the value of the decay constant to which the experiment is sensitive is very large, $\sim 10^3$ - 10^4 TeV. This corresponds to an

intrinsic mass or energy scale beyond almost all experiments to date (excluding proton decay), and sensitivity to dynamics at a distance scale of $\sim 10^{-20}$ cm.

The available range of parameter space for the proposed measurement will be described in more detail in Section IV.

At SLAC, we recently performed an electron beam dump experiment (E-137) to look for possible low mass (1-200 MeV), metastable, neutral particles made by highly collimated production mechanism. The axion-like entity best searched for at SLAC would be a boson which did not couple to quarks or leptons. If this is the case, we may expect such a particle to be photo-produced and to decay into two photons. Three different production mechanisms as shown in Fig. 3, quite unique at SLAC, are

- (1) Production of boson X^0 via Primakoff process, followed by its decay into two photons.
- (2) Production of a boson X^0 via bremsstrahlung from an electron.
- (3) Production of a lepton (or boson) via annihilation of a positron (produced in the electron-initiated cascade) with an atomic electron.

The data taking of E-137 at SLAC was complete in December, 1982. The experiment received 29.9 Coulombs of 20 GeV electrons. We anticipate to finish the data analysis within the next few months. Preliminary analysis of the data taken in January, 1982, with 9.5 Coulombs of 20 GeV electrons, indicates no axion signal.

As we discussed above, if the axion-like object, X^0 , is coupled to quarks and leptons, then it can be best searched for at the Tevatron beam dump. The X^0 can be produced in hadron-hadron collisions via mixing with pseudoscalar mesons, as shown in Fig. 4. Also, if its mass is greater than 200 MeV, then $X^0 \rightarrow \mu^+ \mu^-$ is the dominant decay mode. This particular mode is what we are mainly interested in pursuing at Fermilab.

III. Neutrino-Electron Elastic Scattering

There are two parameters, ρ and $\sin^2\theta_w$, in the neutral current of GWS theory, as expressed by

$$J_\mu^{\text{NC}} = \rho(I_\mu^3 - \sin^2\theta_w J_\mu^{\text{EM}}),$$

where ρ is the ratio of neutral to charged current; I_μ^3 , the third isospin component of weak current; $\sin^2\theta_w$, the mixing parameter; J_μ^{EM} , the electromagnetic current. The value of $(\rho-1)$ can provide a test of the doublet structure for the Higgs field assumed in the theory. Also, within the context of the $SU(2)_L \times U(1)$ model, the radiative corrections¹³ due to the self-energy loop can also render the value of ρ differ from unity:

$$\rho = 1 + G_F^2 m_f^2 / (8\sqrt{2} \pi^2) + (\text{logarithmic terms}),$$

where m_f is the mass of the fermion which circulates in the vacuum polarization loop; G_F is the Fermi coupling constant. A good determination of ρ could provide an upper bound of the heaviest quark mass allowed.

The parameters of the electroweak theory have been determined in five different kinds of experiments. They are:

- (1) Deep inelastic $\nu_\mu N$ and $\bar{\nu}_\mu N$ scattering;
- (2) Elastic $\nu_\mu p$ and $\bar{\nu}_\mu P$ scattering;
- (3) Elastic $\nu_\mu e$, $\bar{\nu}_\mu e$, $\nu_e e$ and $\bar{\nu}_e e$ scattering;
- (4) Scattering of polarized electrons and muons off unpolarized targets; and
- (5) Forward-backward lepton asymmetry in high energy e^+e^- collisions.

The properties and the results of these experiments are briefly summarized¹⁴ as follows:

(1) The processes $\nu_\mu(\bar{\nu}_\mu) + N \rightarrow \nu_\mu(\bar{\nu}_\mu) + X$:

The value of $\sin^2\theta_w$ can be extracted from the deep inelastic neutrino scattering data using the Paschos-Wolfenstein relation¹⁵

$$\frac{\sigma_{\nu}^{NC} - \sigma_{\bar{\nu}}^{NC}}{\sigma_{\nu}^{CC} - \sigma_{\bar{\nu}}^{CC}} = \frac{1}{2}(1 - 2 \sin^2\theta_w) \rho^2.$$

The recent experimental results are

$$\sin^2\theta_w = 0.228 \pm 0.018 \text{ (CDHS)}^{16},$$

$$\sin^2\theta_w = 0.230 \pm 0.23 \text{ (CHARM)}^{17}.$$

If the GWS theory is taken for granted, the parameters ρ and $\sin^2\theta_w$ are determined as¹⁷

$$\rho = 1.027 \pm 0.23 ,$$

$$\sin^2\theta_w = 0.247 \pm 0.038 .$$

One should bear it in mind that the experimental results in the νq sector are subject to uncertainties in the knowledge of detailed quark distribution functions, QCD corrections and radiative corrections.

(2) The process $\nu_\mu(\bar{\nu}_\mu) + p \rightarrow \nu_\mu(\bar{\nu}_\mu) + p$:

The differential cross section $d\sigma_{\nu,\bar{\nu}}/dq^2$ can be expressed in terms of the parameter $\sin^2\theta_w$, in addition to the elastic electromagnetic form factors of the neutron and proton, and a less accurately known axial form factor of the nucleon. The most accurate experimental data were obtained at BNL.¹⁸ In that experiment, 212 events were seen for $\nu_\mu p$ elastic scattering and 110 events for $\bar{\nu}_\mu p$ elastic scattering

in the interval $0.4 < q^2 < 0.9 \text{ (GeV/c)}^2$. The best description of the data is obtained with

$$\sin^2 \theta_w = 0.28 \pm 0.03.$$

(3) The leptonic processes $\nu(\bar{\nu}) + e \rightarrow \nu(\bar{\nu}) + e$:

The cross sections for $\nu_\mu(\bar{\nu}_\mu)e$ elastic scattering are given, respectively, by

$$\sigma(\nu_\mu e \rightarrow \nu_\mu e) = \frac{G_F^2}{2\pi} m_e E_\nu [(g_V + g_A)^2 + \frac{1}{3}(g_V - g_A)^2],$$

$$\sigma(\bar{\nu}_\mu e \rightarrow \bar{\nu}_\mu e) = \frac{G_F^2}{2\pi} m_e E_\nu [\frac{1}{3}(g_V + g_A)^2 + (g_V - g_A)^2].$$

In the standard electroweak theory of GWS, the leptonic coupling constraints, g_V and g_A , are given as

$$g_V = -\frac{1}{2} + 2\sin^2 \theta_w,$$

$$g_A = -\frac{1}{2}.$$

For the processes of $\nu_e(\bar{\nu}_e) + e \rightarrow \nu_e(\bar{\nu}_e) + e$, the values of g_V and g_A are both increased by unity.

The experimental data on the process $\nu_\mu + e \rightarrow \nu_\mu + e$ is summarized in Table 1 below::

Table 1

Group	Number of Candidates	Background	σ/E_{ν} ($10^{-42} \text{ cm}^2/\text{GeV}$)
GGM PS ¹⁹	1	0.3 ± 0.1	<3.0
Serpukhov ²⁰	1	0.2	<3.8
Aachen-Padova ²¹	11	3	1.1 ± 0.6
BNL-Columbia ²²	8	0.5 ± 0.5	1.8 ± 0.8
GGM SPS ²³	9	0.5 ± 0.2	$2.4^{+1.2}_{-0.9}$
E-253 FNAL ²⁴	34	12	1.4 ± 0.3
CHARM ²⁵	11	4.5 ± 1.4	2.6 ± 1.6

The $\nu_{\mu}e$ result of E-253 yields $\sin^2\theta_w = 0.25^{+0.07}_{-0.05}$.

The experimental data on the process $\bar{\nu}_{\mu} + e \rightarrow \bar{\nu}_{\mu} + e$ is summarized in Table 2 below:

Table 2

Group	Number of Candidates	Background	σ/E_{ν} ($10^{-42} \text{ cm}^2/\text{GeV}$)
GGM PS ²⁶	3	0.4 ± 0.1	$1.0^{+2.1}_{-0.9}$
BEBC ²⁷	1	0.5 ± 0.2	<3.4
15' FNAL ²⁸	0	0.2 ± 0.2	<2.1
GGM SPS ²⁹	0	<0.2	<2.7
Aachen-Padova ²¹	8	1.7	2.2 ± 1.0
CHARM ³⁰	72 ± 12	$\sim 50\%$	1.7 ± 0.33

The $\bar{\nu}_{\mu}e$ result of the CHARM collaboration gives $\sin^2\theta_w = 0.29 \pm 0.05$.

The process, $\bar{\nu}_e + e \rightarrow \bar{\nu}_e + e$, was done on a nuclear reactor. After subtracting a serious background of $\sim 85\%$, 460 events were obtained. The cross section was found to be³¹

$$\sigma(\bar{\nu}_e e \rightarrow \bar{\nu}_e e) = (0.85 \pm 0.25) \sigma_{V-A}, (1.5 \leq E' \leq 3.0 \text{ MeV}),$$

$$\sigma(\bar{\nu}_e e \rightarrow \bar{\nu}_e e) = (1.70 \pm 0.44) \sigma_{V-A}, (3.0 \leq E' \leq 4.5 \text{ MeV}),$$

where σ_{V-A} is the cross section calculated with the V-A theory; E' , the recoil electron energy. This cross section gives the following result:

$$\sin^2 \theta_w = 0.29 \pm 0.05.$$

There is no result on the process $\nu_e + e \rightarrow \nu_e + e$.

(4) Scattering of longitudinally polarized electrons by nucleons:

When scattering longitudinally polarized electrons from a nucleon target, the interference between the weak neutral current and the electromagnetic current will produce a parity-violating asymmetry between electrons of different helicities. The experiment at SLAC on polarized electron scattering from deuterium gives³²

$$\sin^2 \theta_w = 0.224 \pm 0.020.$$

Recently, a CERN experiment on polarized muon scattering from C^{12} gives³³

$$\sin^2 \theta_w = 0.21 \pm 0.09.$$

(5) The process $e^+e^- \rightarrow \ell^+\ell^-$:

In high energy e^+e^- collisions, the forward-backward lepton asymmetries in the process, $e^+ + e^- \rightarrow \ell^+ + \ell^-$ ($\ell = e, \mu, \tau$), can be

expressed as

$$A_{\mu\mu} = 4g_A^2 \frac{G_F s}{\sqrt{2} 8\pi\alpha} \rho \left(\frac{m_Z^2}{s - m_Z^2} \right) \frac{6 \cos^2 \theta_0}{3 + \cos^2 \theta_0}$$

for the muon pair case, where s is the C.M. energy squared; m_Z , the Z^0 mass; θ_0 , the minimum angle of measurement.

The experimental data from PEP and PETRA are summarized in Table 3 below;^{34,35}

TABLE 3

Group	$A_{\mu\mu}$ %	$\sin^2 \theta_w$ ($\mu\mu$)	$\sin^2 \theta_w$ ($ee, \mu\mu, \tau\tau$)
MAC	-4.4 ± 2.4	—	0.25 ± 0.16
Mark II	-9.6 ± 4.5	—	—
CELLO	-6.4 ± 6.4	0.22 ± 0.12	0.21 ± 0.12
JADE	-10.8 ± 2.2	0.25 ± 0.15	0.25 ± 0.15
Mark J	-10.4 ± 2.1	0.25 ± 0.11	0.26 ± 0.09
PLUTO	—	—	0.23 ± 0.17
TASSO	-10.4 ± 2.3	0.25 ± 0.10	0.27 ± 0.07

The combined result is $\sin^2 \theta_w = 0.25 \pm 0.07$.³⁴

From the brief review of the experimental situation as described above, it can be seen clearly that much more work has to be done in order to better determine the value of $\sin^2 \theta_w$.

The purely leptonic processes of $\nu_\mu e$ and $\bar{\nu}_\mu e$ elastic scattering at high energies are most attractive for the determination of $\sin^2\theta_w$, or alternatively g_V and g_A , because they are completely free from the complicated hadronic degrees of freedom. As emphasized by Veltman, the radiative corrections to νe scattering can yield good physics on heavy quarks if sufficient precision can be obtained. It requires $\sim 10^4$ or more events. Such a goal is beyond the grasp of this proposal by a factor of ≥ 10 with our modest detector made of only 50 modules. We feel that eventually this goal can be achieved in the future by expanding the detector and/or by running the experiment longer.

Recently, the discovery of W boson was announced at CERN in experiments using $270 \times 270 \text{ GeV}^2$ $p\bar{p}$ collisions. The mass of the W boson was reported to be $\sim 81 \text{ GeV}$. Since the masses of the intermediate vector bosons are given by

$$m_W = \frac{37.3}{\sin\theta_w} ,$$

$$m_Z = \frac{37.3}{\sin\theta_w \cos\theta_w} ,$$

the value of $\sin^2\theta_w$ can be determined at $q^2 = m_W^2$. This will make the $\nu_\mu (\bar{\nu}_\mu) e$ scattering even more interesting, because in these experiments the value of $\sin^2\theta_w$ is determined at $q^2 \leq 0$. It will allow a test of the detailed predictions on $\sin^2\theta_w$ from SU(5) by Marciano and Sirlin.³⁶

IV. The Experimental Proposal on the Search for Axion-Like Objects

(1) The Experimental Arrangement

Initially, we propose to set up a modest apparatus to search for the axion-like objects. It is the natural extension to higher bombarding energies of the search experiment, E-137, at SLAC. The dominant decay mode we will look for at Fermilab is the process $X^0 \rightarrow \mu^- \mu^+$, where X^0 represents the new neutral particles. At SLAC, we are searching for the decay mode $X^0 \rightarrow \gamma\gamma$. This two-photon mode can also be automatically searched for on this proposed detector at Fermilab, along with other possibilities such as e^+e^- , or $e^\pm \mu^\mp$.

The detector is to be located approximately 600 meters downstream from the new Tevatron beam dump. It consists of twenty-two 3m x 3m MWPC's interlaced with steel or aluminum plates (1 r.l. thick each) and plastic scintillation counters, a 3m x 3m x 3m solid iron magnet. The 3m x 3m MWPC's have delay lines along the x- and the y-directions on the cathode planes. The signals are read out with CCD digitizers which can measure both the pulse heights and positions of particle tracks. The anode wires of each 3m x 3m chamber are connected into 8 groups and they can be used as "hodoscopes" for pulse-height measurements and triggering purposes. These 22 chambers are currently under construction. Thirteen chambers were already finished and eight of them were used at SLAC in E-137 in the data-taking during the fall of 1982. We anticipate that the construction of the remaining chambers will be completed before the end of 1983. The detailed schematic arrangement of the detector is shown in Fig. 5.

Two 2-dimensional scintillation hodoscopes are used to select the dimuon signature of the decay process $X^0 \rightarrow \mu^+ \mu^-$. One hodoscope is located at the front end of the apparatus, and the second one is behind the iron magnet. The experimental apparatus is triggered by the traversing of at least two charged particles through these two hodoscopes. This requirement will enable us also to reject most of the background due to the sky-shine which is caused by the deep inelastic scattering of "spoiled" muons in air. The muon pair will be measured by eight 3m x 3m MWPC's at the front end of the apparatus, and eight more chambers before the iron magnet. These two groups of chambers are separated by a distance of $\sim 50'$, and they can determine the muon direction to the accuracy of ± 0.13 mr. After the iron magnet, the muons are measured by six chambers for the determination of their momenta.

In order to pick up the signals from the decay processes, $X^0 \rightarrow e^+ e^-$, $X^0 \rightarrow \gamma\gamma$, and $X^0 \rightarrow \mu^\pm e^\mp$, we have to utilize the "total energy" trigger. Each module of the detector in front of the iron magnet consists of one chamber, one layer of scintillation counter and 1 r.l. thick radiator. If there are electrons or photons entering the detector from the decay region, a characteristic energy deposit in the first several modules (e.g. 5~6 modules) will signal its occurrence. Since the beam spill is only ~ 1 msec/pulse, we do not anticipate any problem due to background caused by cosmic rays. Showers due to skyshines could cause "total energy" triggers. This type of background trigger can be killed easily by increasing the energy threshold because its rate decreases steeply with energy.

In the decay processes of $X^0 \rightarrow \mu^+ \mu^-$, $e^+ e^-$, $\gamma\gamma$, $\mu^\pm e^\mp$, the muon momentum will be measured by the magnetic spectrometer; the energy flow of the electron or photon will be measured by the detector modules at the front end of the apparatus.

(2) The Physics Goals

The parameter space we can explore at Fermilab on the search for axion-like objects is estimated as follows:

Supposing the best object for a search is an X^0 coupled to quarks and leptons with mass greater than 200 MeV, then $X^0 \rightarrow \mu^+ \mu^-$ is the dominant decay mode. Assuming that X^0 is produced like pions with

$$\frac{\Gamma}{\pi} \approx 10^{-3} \left(\frac{1 \text{ GeV}}{F_X} \right)^2,$$

the decay width is

$$\Gamma(X^0 \rightarrow \mu^+ \mu^-) = \frac{M_X M_\mu^2}{8\pi F_X^2},$$

where F_X is the decay coupling constant. Using these two expressions together with the experimental geography, we can estimate the counting rate as a function of M_X and F_X .

Since the Tevatron beam dump is approximately 300 m from Lab C of Neutrino Area, it is logical to locate the experiment ~300 m downstream from Lab C. Because the new Muon Lab is adjacent, the utilities can be conveniently brought over from there. For a small detector, the rate is proportional to $\ell/(\ell + 300 \text{ m})^2$ for this geography, where ℓ is the decay path available behind Lab C. For the 3m x 3m detector we are proposing, the angle it subtended is

$\theta = \pm 1.5 \text{ m}/600 \text{ m} \approx \pm 2.5 \text{ mr}$; for $E_x \geq 100 \text{ GeV}$ this gives $P_{\perp}^{\text{max}} \geq 250 \text{ MeV}$.
 With an $X^0 \rightarrow \mu^+ \mu^-$ originating at 200 m from the detector, the separation of the two muons at the detector is approximately (5 m) \cdot
 $(M_x/1 \text{ GeV}) (100 \text{ GeV}/E_x)$. This is adequate for $M_x \approx 200 \sim 300 \text{ MeV}$, but deteriorates as the mass increases.

The rate is estimated by taking for the pion yield

$$\frac{\pi (E > 100 \text{ GeV}; P_{\perp} < 200 \text{ MeV})}{\text{Proton on Target (POT)}} \approx 1,$$

which gives

$$\frac{X}{\text{POT}} \approx 10^{-3} \left(\frac{1 \text{ GeV}}{F_x} \right)^2.$$

Since

$$\frac{\gamma_{\text{CT}}}{500 \text{ m}} = 10^{-17} \left(\frac{E_x M_x F_x}{M_{\mu}^2 M_x^2} \right)^2,$$

therefore

$$\frac{\text{Detected } X}{\text{POT}} = 10^{10} \left(\frac{100 \text{ GeV}}{E_x} \right) \left(\frac{M_x}{1 \text{ GeV}} \right)^2 \left(\frac{1 \text{ GeV}}{F_x} \right)^4.$$

If we ask for 10^{-17} or more detected X^0 per POT, then

$$F_x \leq (5000 \text{ TeV}) \left(\frac{M_x}{1 \text{ GeV}} \right)^{\frac{1}{2}} \left(\frac{100 \text{ GeV}}{E_x} \right)^{\frac{1}{4}}.$$

The condition that X^0 reaches the decay region

$$\frac{\gamma_{\text{CT}}}{500 \text{ m}} \geq 1$$

translates into

$$F_x \gtrsim (300 \text{ TeV}) \left(\frac{M_x}{1 \text{ GeV}} \right) \left(\frac{100 \text{ GeV}}{E_x} \right)^{\frac{1}{2}}$$

The region in the M_x - F_x space which this experiment can explore is shown in Fig. 6. It should be emphasized that the decay constant, F_x , which most previous reactor and beam dump experiments have reached is about 10^3 GeV; while at Fermilab, this proposed experiment can reach approximately 10^7 GeV.

(3) Backgrounds for the Axion Search Experiment

There are three main sources of backgrounds; namely, (a) neutrino interactions between the Tevatron beam dump and Lab C, (b) neutrino interactions with air in the useful decay volume between Lab C and the proposed detector, and (c) the "sky-shine" produced by the deep-inelastic scattering of the "spoiled" muons. Their details are discussed as the following:

(a) Background from Neutrino Interactions between the Tevatron Beam Dump and Lab C:

The neutrino interactions between the Tevatron beam dump and Lab C should not worry us because there will be over 100' of sweeping magnets behind the beam dump to prevent the charged particles from reaching the 15' bubble chamber. It is designed such that only less than $\sim 10 \mu\text{'s}/10^{13}$ protons can enter the 15' bubble chamber. Additional sweeping power provided by the magnets of Lab E, the 15' bubble chamber and Lab C, should have our proposed detector fully protected.

(b) Background from Muon Sky-shine:

The deep inelastic scattering of "spoiled" muons (which emerge from the beam dump) in air constitutes the most serious background for the axion search experiment. The muon pair signals can be faked by the inelastically scattered muon, plus one or two muons from the decays of the muonproduced pions. This background rate has been analytically estimated. Its full detail is described in Appendix 1.

It turns out that the majority of the sky-shine backgrounds can be eliminated from triggering the apparatus by demanding that at least two charged particles are required in the experimental trigger. This condition can easily be satisfied by the utilization of matrix trigger logic together with two 2-dimensional hodoscopes, as shown in Fig. 5. In this manner, the trigger rate due to sky-shine can be reduced to approximately 0.1 events/pulse. Their total triggering rate will be $\sim 10^4$ events for a 3×10^{18} POT.

In the off-line data analysis, the sky-shine backgrounds can be eliminated by the following requirements:

1. Dimuon identification,
2. Coplanarity of the diumuon and the neutrino beam line,
3. Symmetry of the dimuon in momentum: They should have approximately the same momentum if from X^0 decay,
4. No accompanying particles,
5. Values of invariant mass and total energy.

(c) Background from Neutrino Interactions with Air in the Decay Region:

The neutrino flux from the beam dump is approximately a

factor of 10^3 smaller than that of the conventional neutrino beam using the single-horn trainload. Therefore, the background due to neutrino interactions in the 300 m air space (≈ 3 fiducial tons) is totally negligible. Figs. 7a through 7c show the neutrino spectra from the beam dump, calculated by A. Malensek, using 104 cm of cu, 72 cm of tungsten, and 200 cm of Be as target, respectively. These fluxes can only give a total of ~ 100 charged current neutrino interactions with 300 m of air in the decay region for 3×10^{18} POT. Since the dimuon rate is less than 1% of the charged current event rate, its contribution to the background is negligible. Di-hadrons or one muon plus one hadron can cause a possible background trigger. Such events can be filtered out in the off-line analysis.

(4) The Vertex and Mass Resolution of the Muon Spectrometer

In order to eliminate the backgrounds caused by large angle sky-shines in the off-line data analysis, it is desirable that the decay vertex of X^0 be fairly well located along the neutrino beam line, and that the invariant mass resolution of the muon pair be reasonably small. For the proposed experimental configuration, as shown in Fig. 5, the resolutions are discussed below:

(a) The Vertex Resolution

The spatial resolution of the MWPC's is 2 mm along the transverse direction. The muons are measured by two groups of chambers in front of the iron magnet. They are separated by a distance of $\sim 50'$. The angular resolution for the muon measurement before the iron magnet is $\Delta\theta \approx \pm 0.13$ mr.

The worst possible uncertainty in the vertex determination

along the longitudinal direction happens when the axion decays at the beginning of the decay region and the two muons have small opening angle. For example, if the axion decays at a distance of 300 m from the detector and each one of the two muons makes an angle of 1 mr with respect to the axion momentum, the longitudinal uncertainty will be approximately ± 35 m. If the angle is 5 mr, then the uncertainty will be reduced to ± 7.6 m. For small distances between the decay vertex and the detector, the longitudinal uncertainty of the vertex position becomes proportionally smaller. Figs. 8a-8c illustrate the dependence of the longitudinal uncertainty as a function of the distance and angle. It can be seen that there is no serious difficulty in locating the decay vertex of the axion.

(b) The Mass Resolution

The mass resolution of the spectrometer is mainly dominated by the measurement of muon momenta behind the iron magnet. At lower muon energies, the dominant factor is the multiple Coulomb scattering of muons in traversing the 3 m thick iron magnet. At higher muon energies, the dominant factor is the angular resolution of the wire chambers behind the iron magnet. For the case of an axion decaying into two muons symmetric with respect to the axion momentum, the mass resolution can be approximated by the following expression:

$$\frac{\Delta m}{m} = \frac{5}{9} \sqrt{2} [p_{\mu}^2 + (15)^2 \times \frac{300}{1.76}]^{\frac{1}{2}} \times 10^{-3}$$

where the first term inside the bracket is due to the angular

resolution of the wire chambers behind the iron magnet, and we have used the value of $\Delta\theta \approx \pm 1$ mr; and the second term is due the multiple Coulomb scattering of muons in the 3m iron magnet. The relationship between the mass resolution and the muon momentum is shown in Fig. 9.

We like to remark here that if we just want to detect only the muons from axion decays, apparently the drift chambers should give better resolutions in vertex positions and invariant mass. However, the MWPC's with delay line readout are capable of detecting showers. Their resolutions are adequate, and they offer better capabilities in handling background events due to sky-shines. We might consider the possibility of supplementing the detector with drift chambers. We have on hands 12 planes, 2m x 2m in size. They could be stacked behind the iron magnet to improve upon the mass resolution at higher energies.

V. Experimental Proposal on Neutrino-Electron Scattering

While the "axion" search experiment is being set up or operative, we plan to continue the construction of more 3m x 3m chambers at a rate commensurate with our funding level. With a total number of 50 chambers, we can conduct a good $\nu_\mu e$ and $\bar{\nu}_\mu e$ scattering experiment. These chambers can be gradually added to the front end of the axion search apparatus provided that the experimental enclosure has approximately the same size as the present Wonder Building. Details of the experimental proposal are discussed below:

(1) The Non-Magnetic Detector

The main detector for measuring the $\nu_\mu (\bar{\nu}_\mu) e$ elastic scattering is a fine grained non-magnetic calorimeter. Its arrangement is shown schematically in Fig. 10. There are 50 modules, 3m x 3m in transverse dimensions. Each module consists of one MWPC, one 1 r.l. thick aluminum plate and one layer of plastic scintillation counters.

The aluminum plates serve as both the electron target and the radiator for measuring the recoil electrons. Aluminum is chosen because it contains more atomic electrons per radiation length as compared to heavier metals such as steel. If iron plates are used instead, the counting rate will be reduced by a factor of ~ 1.8 . In view of this significant difference, we are thinking seriously about the use of aluminum, or its equivalent, e.g., prefabricated concrete slabs, as radiator.

The 3m x 3m MWPC's have zigzag delay-lines on the cathode planes along orthogonal directions. After particles pass through the chamber,

the induced signals on the delay lines will be digitized by CCD (charged coupled devices) digitizers. The pulse profiles and track positions are retained in the computer for later analysis. Details on the design, construction and operation of the chamber, as well as the data analysis technique, are described in Appendix 2. We like to state here that we have devoted the last ten years in developing, using, and improving this device for this specific purpose. It is most suitable for the measurement of electromagnetic energy flows in condensed media. In addition to good angular resolution and multiple track capability, it can also identify electromagnetic showers, hadrons, and minimum ionizing particles. The angular resolution is estimated to be $\sim \pm 1$ mr by using chambers within the first five radiation lengths from the vertex.

The plastic scintillators are used to trigger the experiment and to measure the energy. Its fast timing is particularly invaluable in helping the pattern recognition and masking out the out-of-time tracks. We plan to use the more economic NE114 plastic scintillators. If the economy does not permit, we will install at least part of them. In each 3m x 3m MWPC, the anode wires are ganged into 8 groups. They can be used as "hodoscopes" for triggering the experiment and measuring the energy. The defect is that they are not as fast as the plastic scintillators.

The experimental trigger is formed by demanding a large energy deposit in any group of 5-6 consecutive detector modules. The triggering threshold can be set at a level which corresponds to the electron energy of 1-2 GeV. Signals from all the groups are then ORed together to give the master trigger. This trigger can preferentially pick up the electromagnetic showers, and it was used in E-253 satisfactorily.

(2) The Counting Rate and Statistics

Using 50 detector modules and the single-horn neutrino beam, the $\nu_\mu e$ elastic scattering rate is approximately 300 events for 3×10^{18} POT if r.l. thick aluminum radiators are used. The neutrino spectrum we used is calculated by A. Malensek as shown in Fig. 11. This event number can yield an accuracy of ± 0.02 on $\sin^2 \theta_w$ when combined with the condition $g_A = -1/2$ of the GWS model.

For 3×10^{18} POT, we can only anticipate to obtain $\sim 70 \bar{\nu}_\mu e$ elastic scattering events. This number is difficult to improve unless running the experiment longer or building more detector modules.

For 3×10^{18} POT, the total number of charged current events is $\sim 1.4 \times 10^6$ in 3×10^5 accelerator pulses. In the actual experiment, these charged current events can be reduced to about 1 \sim 2 triggers per pulse. In order to reduce the on-line computer dead time, we have to run the CCD digitizers at the mode of accepting two to five triggers per 1 msec fast pulse. The on-line dead-time losses and those at the analysis level should then be less than a few per cent. Another 10 \sim 20% of the running time will be devoted to the beam measurement. It is reasonable to anticipate approximately 20% or less overall losses. In the old E-253 at Fermilab, we could take only 1 trigger/pulse and the on-line dead-time loss was $\sim 40\%$. Additional few per cent of running time was used for equipment tuning, and there was almost no losses at the off-line analysis stage.

(3) Separation of Signal from Background

It has been well understood that the signal-to-noise ratio for measuring ν_e elastic scattering events is almost purely related to the angular resolution of the equipment. Just for the purpose of comparison, the old E-253 at Fermilab achieved a signal-to-background ratio of 3:1. It was done with an angular resolution of $\approx \pm 5$ mr. Among other sins, we used TDC's to measure only the edges of the electron shower and then assumed the shower centroid to be their average.

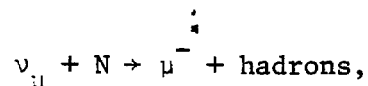
After learning all the lessons, we have put all the necessary improvements into the 3m x 3m chamber. The most noteworthy part is on the adoption of CCD digitizers. It measures the transverse charge distributions by retaining the original pulse profiles, which will in turn allow a better determination of the centroid positions of the electromagnetic showers. Fig. 12 shows a calculation of the P_T -distributions of the processes, $\nu_\mu + e \rightarrow \nu_\mu + e$ and $\nu_e + n \rightarrow p + e$, after an angular cut of $\theta_e \lesssim 10$ mr. It can be seen that a background contamination at $\sim 10\%$ level is a good estimation.

(4) Beam Normalization and Systematic Errors

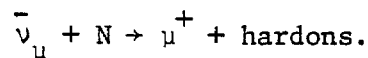
The main source of systematic errors for neutrino experiments comes from the uncertainty in our knowledge about the neutrino flux. We propose to handle the problem as the following:

(a) The ν_μ and $\bar{\nu}_\mu$ Flux

The ν_μ and $\bar{\nu}_\mu$ flux can be determined directly by the charged current (CC) events of the following two reactions:



and



The sign and the momentum of the outgoing muon are measured by a magnetic muon spectrometer which we will describe later. The hadronic energy is measured by the non-magnetic calorimeter. Their sum gives the energy of the incoming neutrino. Therefore, the energy distribution of the ν_μ or $\bar{\nu}_\mu$ beam can be directly measured.

Also, we will separately monitor the two-body reactions:

$$\nu_\mu + n \rightarrow \mu^- + p,$$

and

$$\bar{\nu}_\mu + p \rightarrow \mu^+ + n.$$

They will furnish another independent check.

(b) The ν_e and $\bar{\nu}_e$ Flux

In this case, the flux spectra can only be determined from the two-body reactions:

$$\nu_e + n \rightarrow e^- + p,$$

and

$$\bar{\nu}_e + p \rightarrow e^+ + n.$$

Since we do not know the signs of the electron charges, we can only measure their sum to obtain the visible energy spectrum and the angular distribution. Also, we have to take into account the π^0 contaminations from the processes

$$\nu_\mu(\bar{\nu}_\mu) + N \rightarrow \nu_\mu(\bar{\nu}_\mu) + N + \pi^0.$$

The cross section of the above reaction is approximately 1.1×10^{-39} cm^2 , and is independent of energy. Their contaminations to the quasi-elastic scattering can be calculated from the ν_μ ($\bar{\nu}_\mu$) flux and subtracted.

(c) Consistency Check

A consistency check can be made by observing the equality:

$$\begin{aligned} & \text{Total "apparent" NC events} \\ &= (\text{CC} + \text{NC})_{\nu_e} + (\text{CC} + \text{NC})_{\bar{\nu}_e} \\ &+ R_{\nu} * (\text{CC})_{\nu_\mu} + R_{\bar{\nu}} * (\text{CC})_{\bar{\nu}_\mu}, \end{aligned}$$

where $R_{\nu} \equiv (\text{NC}/\text{CC})_{\nu_\mu}$ and $R_{\bar{\nu}} \equiv (\text{NC}/\text{CC})_{\bar{\nu}_\mu}$ are the known ratios. The CC events due to ν_μ and $\bar{\nu}_\mu$ can be measured by counting the events with μ^- and μ^+ respectively. In the above expression, we still do not know exactly the R's for ν_e and $\bar{\nu}_e$. Because of μ -e universality, we may assume that the CC and NC cross sections of $(\bar{\nu}_e)$ are the same as that for $(\bar{\nu}_\mu)$.

(d) Check against the Hadronic Distribution

The measured flux can also be checked against the hadronic energy spectrum of the charged current events. In E-253, the neutrino spectrum could not be directly measured because of the lack of a magnet. We adjusted the calculated neutrino spectrum until the Monte Carlo hadronic distribution of the charged current events agreed with the measured hadronic energy spectrum. It turned out later that the neutrino spectrum we used agreed quite well with that measured by G. Snow et al on the ν_μ D interactions in the 15' bubble chamber.³⁷

(e) The Systematic Error

It is quite difficult to estimate how much should be the systematic error. The major systematic error should come from the determination of neutrino fluxes. These errors can be assigned only by comparing different experimental results or by consistency checks. It is only an educated guess that the systematic error is at the level of $\sim 10\%$.

(5) Equipment Calibration

Originally, we proposed to have a hadron calibration beam going into the detector. Prompted by a serious concern about its cost, we concluded that we could calibrate the apparatus without the special beam. The scheme is described as the following:

- (a) The scintillation counters can be calibrated individually in an electron test beam of known energy. Their individual gains can be set identically by comparing the pulse height spectra of showers after a radiator.
- (b) The total energy calibration of the scintillation counters can be done also in an electron test beam with an assembly of 20 layers of scintillation counters interlaced with radiators, 1 r.l. thick each.
- (c) A fraction of the MWPC's will have their gains calibrated the same way as the scintillation counters. After the whole detector is assembled, gains of all the chambers can be set uniformly with cosmic rays. Their total energy calibration can be obtained by comparison with the scintillation counters.

(d) Some of the calibration work will be done at SLAC in 1983 up to 20 GeV. At Fermilab, we would like to calibrate a fraction of the calorimeter to higher energies at the Muon Lab. The π 's, μ 's, and a small fraction of e's, which are available at the Muon Lab, should be very adequate for us to do the calibration work.

We like to add that the afore-mentioned calibration procedure was used at Fermilab in E-253. For E-137 at SLAC, the gain of every new scintillation counter was adjusted to the same calibration mark used in E-253. It turned out that it was not a bad practice at all.

(6) The Magnetic Muon Detector

A simple magnetic spectrometer, located behind the calorimeter is required to detect the outgoing muons. Its detailed arrangement is shown in Fig. 13. For the axion search part of this proposal, the μ -pair momenta are measured by a set of 3m x 3m MWPC's with delay-line readout placed behind a solid iron magnet of dimension 3m x 3m x 3m.

For the neutrino-electron scattering part of this proposal, we can either use the 3m x 3m MWPC's or replace them with 2m x 2m drift chambers if economy does not permit. We have 12 planes of drift chambers on hand.

VI Other Experimental Possibilities

The detector we propose to build, as described above, is quite unique and specialized. We can visualize that it can serve our purpose for the search of axion-like objects and measuring elastic $(\bar{\nu}_\mu)_e$ scattering. We would like to think the facility could also fulfill the goals of the following experimental possibilities:

(1) x-distribution of Hadronic Neutral Current

In the νq sector of neutrino interactions, the y-distribution of the neutral current event is quite easy to measure (where y is defined as $y = \nu/E_\nu$, ν is the energy loss of neutrino, E_ν is the incoming neutrino energy). But the x-distribution is quite difficult to handle (where $x \equiv q^2/(2M_N \nu)$). The detector has to measure the energy flow well, also it has to be able to handle the multi-particle events. We would think that this detector can offer a good possibility to do it.

(2) $(\bar{\nu}_\mu \leftrightarrow \bar{\nu}_e)$ Oscillations:

Since the $(\bar{\nu}_e)$ component in the $(\bar{\nu}_\mu)$ beam is rather small, we would think that the search for enhancement of $(\bar{\nu}_e)$ is more sensitive than the search for the disappearance of $(\bar{\nu}_\mu)$. This subject remains interesting because the solid evidence of a finite neutrino mass is still lacking.

We like to add that we are not intending to make our proposal into a long program. We merely try to point out that the physics opportunities, other than the ones we are interested, do exist at the Tevatron with this proposed detector. If physicists are becoming interested, certainly they can do it with this apparatus or with its enlarged version.

VII. Proposal and Request

We propose to build a fine-grained calorimeter, as described above, to search for the "axion-like" objects first at the Tevatron of Fermilab. Most of the equipments necessary for performing this experiment already exists. Afterwards, we will use the full detector to perform the elastic $\nu_{\mu}e$ and $\bar{\nu}_{\mu}e$ scattering experiment.

We request the Laboratory to provide us with the following items:

1. A laboratory space, with necessary utilities, to house the detector. A simple overhead crane may be required to handle the equipment.
2. Fast electronics from PREP
3. Toroid magnet for muon measurements.
4. 45 aluminum plates (or their equivalents), 3m x 3m x 9.2 cm, to be used as target/radiator. (approximately 5 pieces exist).

For the experimental physics part, we further request:

- 1) Simultaneous running time with other beam dump experiments to search for the "axion-like" particles.
- 2) 3×10^{18} protons at 1 TeV on the neutrino production target, with single-horn focusing, to measure the cross section for $\nu_{\mu} + e^{-} \rightarrow \nu_{\mu} + e^{-}$. We expect to obtain 300 events.
- 3) 3×10^{18} protons at 1 TeV on the neutrino production target, with single-horn focusing, to measure the cross section for $\bar{\nu}_{\mu} + e^{-} \rightarrow \bar{\nu}_{\mu} + e^{-}$.
- 4) Use of a portion of the present Muon Laboratory as a staging and testing area. Also, the use of a low intensity hadron in that

area to test and calibrate the equipment. Once the equipment is set up to take data, the test beam will be needed for a period of ~2 weeks.

Our own time schedule is the following: We have almost enough equipment to set up the "axion-like" search experiment. For the ve scattering part of the proposal, we can finish the equipment construction within two years, starting from the date on which funding commences. The estimate for new equipment cost, including that for the aluminum radiators, is described in Appendix 3.

Appendix 1

Estimate of Sky-shine Background for P-635

The background for P-635 due to deep-inelastic scattering of the "spoiled" muons, analytically estimated by Bjorken, is described below:

The mechanism considered is limited to production of secondary hadrons in air by the intense muon beam which is diverted skyward by the dump magnets. According to the simulations carried out by the dump designers (M. Peters, private communication with Bjorken), there is very little muon intensity for angles less than a critical value, the vertical component of which is $\theta_{\min} \approx 25$ mrad. The total differential muon intensity, $\frac{dN}{d\theta}$, rises rapidly at this critical value, and soon saturates at approximately $(1 \sim 3) \times 10^6 \mu/s/mrad$ (these values are integrated over a fairly large swath of horizontal angles; θ is the vertical angle.)

The trigger will be assumed to be:

- (1) Two muons (or equivalent) traversing the apparatus with vertical angle less than 50 mrad. This implies that they penetrate the 3m of the solid-iron magnet, i.e., have incident energy in excess of 4 ~ 5 GeV. A concurrent trigger is:
 - (2) Large energy deposition in the Fe-scintillator calorimeter.
- We shall find a rather steeply falling hadron energy spectrum, implying a relatively easy (and quite adjustable) trigger rate.

We assume all muons in the primary skyshine beam to be of sufficient energy to produce the hadrons of interest (which typically have energies

in the range of 5 ~ 20 GeV). The standard deep inelastic scattering cross section is approximated by the following expressions:

$$\frac{d\sigma}{dq^2 dv} \approx \frac{\alpha}{2\pi} \cdot \frac{1}{q^2} \cdot \frac{1}{v} \sigma_\gamma$$

and

$$\sigma_{\mu N} \approx \frac{\alpha}{2\pi} \cdot \ln\left(\frac{m_p}{m_\mu}\right)^2 \cdot \ln\left(\frac{v_{\max}}{v_{\min}}\right) \cdot \sigma_\gamma$$

Take

$$\frac{v_{\max}}{v_{\min}} \approx \frac{100 \text{ GeV}}{5 \text{ GeV}} = 20,$$

$$\sigma_\gamma \approx 100 \text{ } \mu\text{b},$$

then

$$\sigma_{\mu N} \approx 1.5 \times 10^{-30} \text{ cm}^2.$$

This energy independent cross section, $\sigma(\mu+N \rightarrow \mu + \text{hadrons}) \approx 1.5 \times 10^{-30} \text{ cm}^2$, leads to $\sim 10^{-7}$ interactions per muon per meter of air traversed. The secondary pion spectrum (charged only) is taken to be

$$\frac{E}{\sigma} \frac{d\sigma}{d^3p} = \frac{b^2}{2\pi} \frac{dN_\pi}{dy} e^{-bp_1},$$

where $b \approx 5 \text{ GeV}^{-1}$, $dN_\pi/dy \approx 2$ and y is the rapidity. The geometry for the calculation is shown in Fig. 14. A muon produced at θ_1 in the dump interacts in the air and produces a hadron at production angle θ_1 and θ_2 , which reaches the P-635 detector and is seen with vertical angle θ_2 . The dump-to-detector distance, L , is $\sim 600\text{m}$; and the detector area, A , is $\sim 9\text{m}^2$. We require $\theta_1 \gtrsim 25 \text{ mrad}$, and $\theta_2 \lesssim 50 \text{ mrad}$. We also temporarily ignore decay in flight of the pions (or hadrons) and comment on that later. The

differential flux at the detector is

$$dN = \int ds d\theta_1 \frac{dN}{ds d\theta_1} \frac{E}{\sigma} \frac{d\sigma}{d^3p} p dp \Delta\Omega.$$

From the geometry,

$$s = \frac{L\theta_2}{\theta_1 + \theta_2},$$

$$ds = \frac{L\theta_1 d\theta_2}{(\theta_1 + \theta_2)^2},$$

$$\Delta\Omega = \frac{A}{(L-s)^2} = \frac{A}{L^2} \frac{(\theta_1 + \theta_2)^2}{\theta_1^2},$$

we will have

$$\frac{dN}{dp} = \frac{A}{L} \frac{b^2}{2\pi} \left(\frac{dN}{dy} \right) \int_{\theta_{\min}}^{\infty} \frac{d\theta_1}{\theta_1} \int_0^{\theta_{\max}} d\theta_2 e^{-bp(\theta_1 + \theta_2)} \frac{dN}{ds d\theta_1}$$

We overestimate the flux if θ_1^{-1} is replaced by θ_{\min}^{-1} . It is worth making that approximation in order to easily do the subsequent integrals.

We end up with

$$p \frac{dN}{dp} < \frac{A}{2\pi L \theta_{\min}} \left(\frac{dN}{dy} \right) e^{-bp\theta_{\min}} (1 - e^{-bp\theta_{\max}}) \frac{dN}{ds d\theta_{\min}}.$$

Putting in our numbers gives

$$\frac{dN}{dp} \approx \frac{40}{p} e^{-\frac{p}{8 \text{ GeV}}} \left(1 - e^{-\frac{p}{4 \text{ GeV}}} \right)$$

The result is plotted in Fig. 15. In that plot is also shown a simple estimate of flux due to π decay. Integration over momentum gives the final results:

$$\underline{\text{Single muons (E > 4.5 GeV; } \theta < 50 \text{ mrad)}} \lesssim 13.$$

$$10^{13} \text{ POT}$$

Furthermore, the single muons will be out of time, in as much as the detector live-time (controlled by the delay-line and CCD readout) is \lesssim 1 μ sec out of a spill time of \gtrsim 1 msec.

The pair rate should be easily much less than unity. This is estimated by expressing the solid angle subtended by the detector as

$$\Delta\Omega = \frac{A}{(L-S)^2} \equiv (\theta_1 + \theta_2)^2 \Delta y \Delta\phi.$$

Hence,

$$\Delta y \Delta\phi = \frac{A}{L^2 \theta_1^2} < \frac{A}{L^2 \theta_{\min}^2} \approx 0.04.$$

The probability of a second accompanying track (ignoring correlations in production) in a given interaction is

$$P \lesssim \frac{dN}{dy d\phi} (\Delta y \Delta\phi) \approx \frac{2}{2\pi} \times 0.04 = 0.013.$$

From Fig. 15, at least half of these particles are below energy threshold, so that:

$$\frac{2 \text{ track}}{1 \text{ track}} < 6 \times 10^{-3},$$

and the 2-track triggers per spill is less than $\sim 8 \times 10^{-2}$ (approximately 1 trigger every 10 pulses).

APPENDIX 2

Delay-Line Readout Chambers and CCD Digitizers

The detector we propose to use in P-635 for the search of axion-like objects and ν_e elastic scattering at Fermilab is quite unique and simplistic. The main components are 3m x 3m MWPC's and CCD digitizers. We first started to work on this device in 1972. During the last ten years, we have gained some experience in its construction, operation and improvement. Perhaps we can explain it better if we start from a brief review about what has been done in the past.

1. The 1m x 1m chambers³⁸

The first MWPC with delay-line readout we built was for $\nu_\mu e$ scattering at Fermilab (E-253). They are 1m x 1m in size and 49 of them were eventually constructed.

On the two cathode planes of each chamber, there are delay-lines along both x- and y- direction. The delay-lines are continuous zigzag conducting strips machine-milled on copper-clad G-10 plates. The G-10 plates are glued to aluminum plates, 1/4" in thickness. Two of such plates are bolted together to serve as the cathode planes of a chamber. All the anode wires are ganged together to be used as one single counter to measure the energy only. The chamber construction is shown schematically in Fig. 16.

The cathode plane delay-lines behave like transmission lines of ~100 ohms in impedance. When a particle passes through the chamber, the anode wires will collect a large number of electrons because of the gas amplification. Meanwhile, the delay-lines on the two cathode planes will also receive localized positive pulses, which are induced by

capacitive coupling. The signal will then propagate along the delay-line at a speed of ~ 5 nsec/m. The propagation time can be translated into the transverse track position on each cathode plane.

The transverse spacing of the delay-line is 2 mm for the 1m x 1m chamber. Also, the delay-line is continuous over the entire cathode plane. Readout ports were tapped at 5 equi-distance points. This arrangement is necessary to take care of the signal attenuations and to provide redundancy; but it also introduces left-right ambiguities (although self-resolved) for the three ports in the middle.

The gas used to operate the chambers is a mixture of 80% argon, 19.7% CO_2 and 0.3% Freon B1-13. It is rather temperature-stable and can be packed into $\sim 2,000$ psi cylinders. Its gas amplification factor is smaller than most other commonly used gases. But the strong quenching effect of this gas can prevent the unruly spread of the electromagnetic shower. Another important point is that this gas does not deposit hydro-carbon tars on the anode wires which will cause dark current in the chamber.

In E-253, the signal from each readout port went through an amplifier first, then measured by a TDC (time-to-digital converter). Therefore, only the two edges of the shower were measured. Their mean value was regarded as the centroid of the shower. In this manner, the angular resolution for electron showers was obtained as ± 5 mr. They were tested in the electron beam at Cornell in 1974, also at Fermilab in 1978.

The disadvantages of this combination, namely the 1m x 1 m chambers plus TDC's, are apparent. It cannot handle multiple particles/showers unless they occur between different tap points. Since the TDC has to be

operated at a constant threshold, attenuation and dispersion of the signal on the delay-line contribute to the uncertainty in determining the centroid position. These defects prompted us to develop the CCD digitizers.

2. The CCD Digitizer

The operation of the CCD digitizer is shown schematically as Fig. 17.

The signals from a cathode-plane delay-line are first amplified by an amplifier located on the chamber. The output is fed to a CCD digitizer through a coaxial cable. The CCD is continuously clocked by a 50 MHz₂ quartz-stabilized oscillator. Upon occurrence of each clock pulse, a 20 nsec wide slice of the input signal is loaded into one CCD bucket at the front end. The charges stored in the CCD buckets are shifted forward in sequence, one bucket every clock pulse. Immediately after the arrival of the master experimental trigger at the CCD, the input signals are "frozen" in the CCD space. An ADC (analogue-to-digital converter) will then sequentially digitize the charges in each CCD bucket, and the results are stored in the RAM (random access memory) waiting to be readout into the on-line computer.

Since the master experimental trigger can happen within the 20 nsec width of a clock pulse, its timing is separately recorded to provide the vernier corrections. A TDC, one on each CCD module, is started by the leading edge of each 20-nsec long clock pulse, and is stopped by the master experimental trigger. The time interval between these two signals is digitized and stored in the RAM. Its accuracy is 256 steps for 20 nsec.

This simple scheme offers an elegant method in measuring both the pulse heights and track positions simultaneously. It is essentially a computerized multi-beam oscilloscope. The CCD bucket number represents

the track position in quantum steps of 20 nsec, and the charges in CCD buckets provide the information on pulse height distributions.

By mapping the particle position and dE/dx information into the CCD bucket space, the original pulse profiles are retained for later analysis. Physical effects can all be taken into account in the data reduction stage. These effects include length, attenuation and dispersion of the delay-line, energy calibration constant, propagation speed, etc.

For E-137 at SLAC, initially we stacked 48 1m x 1m chambers into 8 layers of 2m x 3m detector. All the old TDC's were replaced by new CCD's. We took data with 9.5 Coulombs of 20 GeV electrons in this configuration. Afterwards, the smaller chambers were replaced by eight new 3m x 3m ones.

Fig. 18 illustrate one example of the CCD information from one of the 1m x 1m cathode planes. Pulse trains from the 5 readout ports of one continuous delay line are shown. Each bucket represents ~ 8 mm in real transverse space (the propagation speed is ~ 5 nsec/m, one CCD bucket is 20 nsec wide, and the delay line spacing is 2 mm). Since we can determine the centroid of each shower to the accuracy of a fraction of one CCD bucket, in principle the direction of the shower can be determined to the accuracy of $\sim \pm 2$ mr by using 5 chambers at an inter-chamber spacing of 15" from a pure geometric point of view. However, one always wonders what other factors, such as the shower fluctuations, may effect the angular resolution. The best answer is that we should make a direct measurement of the angular resolution with an electron beam, like what we once did in 1974 at Cornell with the 1m x 1m chambers and the TDC's. Unfortunately, we have not found an opportunity to do that yet at SLAC. In running E-137, essentially we were operating with low energy beam-related skyshines (mostly

muons), or cosmic rays which fell within the accelerator beam gate. It is difficult to find enough electromagnetic showers, up to this time, to determine experimentally the angular resolution. By using TDC's, we already achieved an angular resolution of $\sim \pm 5$ mr. With CCD's, we can compute the centroid positions of the shower much more accurately. Perhaps, the purely geometric estimate mentioned above is not out of line. It is beyond argument that we have to find an opportunity to do this measurement.

3. The 3m x 3m chambers

Eight 3m x 3m chambers were built by the same construction method as the 1m x 1m chambers. We quickly found that the 1/4" aluminum plates were not strong enough to prevent the mechanical deformation. "Spiders" of aluminum girders were welded to each plate to reinforce its rigidity against buckling. Also, the chambers were heavy, weighing $\sim 1,500$ lbs each. It made the handling job rather inconvenient. Nevertheless, they were installed at SLAC in the summer of 1982. During the period of Oct-Dec, 1982, they were used successfully in taking data with ~ 20 Coulombs of 20 GeV electrons.

After building the initial eight 3m x 3m chambers, we changed the construction method. The 1/4" aluminum plates were replaced with home-made "Hexcel" boards. They are hard styrofoam board with 20 mil thick aluminum sheets epoxied on both sides. After the G-10 delay-line board is glued on, it becomes unusually rigid against buckling. Also, the total weight of a single chamber is reduced to ~ 350 lbs. As of February, 1983, 5 new chambers for this construction were already complete.

For the 3m x 3m chambers, we subdivide the delay-line on one cathode plane into 23 independent pieces. Only one end of each section is connected to a CCD digitizer. The other end is properly terminated to eliminate the reflections. (In principle, a second CCD can be used instead of termination. It can provide either redundancy, or wider dynamic range by using an amplifier of different gain). Since the signals are all traveling along the delay line in same direction, there will be no left-right ambiguities in sorting out their positions. Because of the use of delay-lines in conjunction with CCD digitizers, the multiple particle/shower capability of this device is intrinsic as the track positions manifest themselves as pulse trains. An example is shown in Fig. 19.

Because the propagation speed of the signal on the delay-line is ~ 5 nsec/m, the 20 nsec width of one CCD bucket represent ~ 1.3 times of a 3 m wire length. Therefore, the transverse spatial resolution is going to be better than 2mm, which is the delay line spacing. This corresponds to an angular resolution of approximately ± 1 mr. Again, this is an estimate based on geometry.

The pattern recognition and particle identification problems are helped enormously by the pulse height information and its correlation with the track. Once the straight line track of a particle/shower is recognized, its longitudinal and transverse distribution of pulse heights can be immediately displayed. This is most useful for particle identifications.

If the tracks of a multiple-particle event do not overlap, one can follow each individual track to determine its energy by summing up the pulse heights along the track. In case the tracks are overlapping, the direction of the energy flow can be properly determined because informations are available on the transverse energy distribution at each layer of the detector. This

method opens up a possibility of doing multi-particle physics with a non-magnetic detector. It can be very helpful in measuring the x -distribution, where $x \equiv q^2/2M\nu$, of hadronic neutral current in neutrino interactions.

In Fig. 20, we show an event measured at SLAC with the 3m x 3m chambers. In this display, all 23 sections of delay lines on one cathode plane of a single chamber are combined together. There are 1 r.l. thick iron plates between chambers. The shower track, its pulse height distribution along the track, and the quality of measurement can be seen at a glance.

As a last remark, there have been increasing interests in applying chambers similar to that described here in electromagnetic calorimetry.³⁹ In most of these applications, individual strips are used on the cathode planes instead of continuous delay-lines. Otherwise, they are similar.

Appendix 3

Cost Estimate

In this appendix, we only include the estimate for the new equipment cost. Part of the 50-modules detector already exists or is currently under construction, their costs are excluded. Components which have impact on the Laboratory, such as laboratory space, utilities, iron toroid, PREP electronics, etc., are also excluded here.

1. Construction of 28 3m x 3m MWPC's, labor and material included @ \$14,500/chamber	\$406,000
2. Amplifiers and CCD digitizers for 38 3m x 3m MWPC's	\$256,880
3. 42 layers of plastic scintilla- tion counters	\$604,000
4. 45 aluminum plates, 3m x 3m x 9.2 cm each, total weight ~100 tons.	\$165,000
5. Cables, power supplies gas manifolds, etc, etc.	\$ 80,000
6. Contingency (6.6%)	\$100,000

Total \$1,612,680

References and Footnotes

1. Y. Nambu, Phys. Rev. Lett. 4, 380 (1960).
Y. Nambu and G. Jona-Lasinio, Phys. Rev. 122, 345 (1961).
2. J. Goldstone, Nuovo Cim. 19, 154 (1961).
3. SLAC Experimental Proposal (E-56), by D. Dorfan, D. Fryberger, J. M. Gaillard, D. Kreinick, A. Mann, A. Rothenberg, M. Schwartz and T. Zipf.
For the experimental results, see A. F. Rothenberg, SLAC Report No. 147, 1972 (unpublished).
4. R. D. Peccei and H. R. Quinn, Phys. Rev. Lett. 38, 1440 (1977);
Phys. Rev. D16, 1971 (1977).
F. Wilczek, Phys. Rev. Lett. 40, 279 (1978).
S. Weinberg, Phys. Rev. Lett. 40, 223 (1978).
5. T. W. Donnelley, et al., Phys. Rev. D18, 1607 (1978).
6. SLAC Experimental Proposal (E-137), by A. Abashian, J. D. Bjorken, S. Ecklund, L. W. Mo, W. R. Nelson and Y. S. Tsai.
7. P. Fayet, Phys. Lett. 86B, 272 (1979); also see Proceedings of 21st International Conference on High Energy Physics, July 26-31, 1982, Paris, France, eds. P. Petiau and M. Porneuf.
J. Wess and B. Zumino, Nucl. Phys. B78, 1 (1974).
8. Y. Declais, Proceedings of the 21st International Conference on High Energy Physics, July 26-31, 1982, Paris, France, eds. P. Petiau and M. Porneuf. It is an up to date review which includes also the reactor experiments, rare decay modes and nuclear transitions.
9. T. Yamazaki, paper contributed to the 1982 Paris Conference on High Energy Physics. In this experiment at KEK, both $K^+ \rightarrow \pi^+ X^0$ and $K^+ \rightarrow \mu^+ N^0$ are searched. For the search of heavy neutrino, N^0 , see Phys. Rev. Lett. 49, 1305 (1982).

10. C. Edwards et al., Phys. Rev. Lett. 48, 903 (1982).
11. J. Lee-Franzini, Proceedings of the 21st International Conference on High Energy Physics, July 26-31, 1982, Paris, France, eds. P. Petiau and M. Porneuf.
12. J. D. Bjorken, review talk given at the Institute for Theoretical Physics, UC at Santa Barbara, Calif., 1981 (unpublished).
13. M. Veltman, Nucl. Phys. B123, 89 (1977).
14. Detailed reviews can be found from the following articles:
M. Davier, Proceedings of the 21st International Conference on High Energy Physics, July 26-31, 1982, Paris, France, eds. P. Petiau and M. Porneuf, p. c3-471.
S. M. Bilenky and J. Hösek, Physics Reports 5, 75 (1982).
J. E. Kim et al., Rev. Mod. Phys. 53, 211 (1981).
I. Leide and M. Roos, Proceedings of Neutrino 79, June 18-22, 1979, Bergen, Norway, eds. A. Haatuft and C. Jarlskog, Vol. 1, p. 309; Phys. Lett. 82B, 89 (1979).
15. E. A. Paschos and L. Wolfenstein, Phys. Rev. D7, 91 (1973).
16. C. Gewinger et al., Proceedings of Neutrino 79, June 18-22, 1979, Bergen, Norway, eds. A. Haatuft and C. Jarlskog, Vol. 2, p. 392.
17. M. Jonker et al., Phys. Lett. 99B, 265 (1981).
18. A. Entenberg et al., Phys. Rev. Lett. 42, 1198 (1978).
19. J. Blietschau et al., Phys. Lett. 73B, 232 (1978).
20. A. E. Asratyan et al., Proceedings of Neutrino 79, June 18-22, 1979, Bergen, Norway, eds. A. Haatuft and C. Jarlskog, Vol. 2, p. 246.
21. H. Faissner et al., Phys. Rev. Lett. 41, 213 (1978).
22. A. M. Cnops et al., Phys. Rev. Lett. 41, 357 (1978).
23. P. Alibrán et al., Phys. Lett. 74B, 422 (1978).

24. R. H. Heisterberg et al., Phys. Rev. Lett. 44, 635 (1980).
25. M. Jonker et al., Proceedings of Neutrino 79, June 18-22, 1979, Bergen, Norway, eds. A. Haatuft and C. Jaruskog, Vol. 2, p. 219.
26. J. Blietschau et al., Nucl. Phys. B114, 189 (1976).
27. N. Armenise et al., Phys. Lett. 81B, 385 (1979).
28. J. P. Berge et al., paper contributed to Neutrino 79, June 18-22, 1979, Bergen, Norway.
29. A. Pullia et al., Proceedings of Neutrino 79, June 18-22, 1979, Bergen, Norway, eds. A. Haatuft and C. Jaruskog, Vol. 2, p. 230.
30. M. Jonker et al., Phys. Lett. 105B, 242 (1981).

At the 1982 Paris Conference (see M. Davier of ref. 14), J. Allaby reported the new CHARM results: $46 \pm 21 \nu_\mu e$ events and $77 \pm 19 \bar{\nu}_\mu e$ events (above ~50% background). The individual cross sections were given as

$$\sigma(\nu_\mu e \rightarrow \nu_\mu e) = [2.1 \pm 0.55 \text{ (Stat)} \pm 0.49 \text{ (Syst)}] \times 10^{-42} \text{ cm}^2/\text{GeV},$$

and

$$\sigma(\bar{\nu}_\mu e \rightarrow \bar{\nu}_\mu e) = [1.6 \pm 0.35 \text{ (Stat)} \pm 0.36 \text{ (Syst)}] \times 10^{-42} \text{ cm}^2/\text{GeV}.$$

From their ratio

$$\frac{\sigma(\nu_\mu e \rightarrow \nu_\mu e)}{\sigma(\bar{\nu}_\mu e \rightarrow \bar{\nu}_\mu e)} = 1.37_{-0.44}^{-0.65},$$

it was extracted

$$\sin^2 \theta_w = 0.215 \pm 0.040 \text{ (Stat)} \pm 0.015 \text{ (Syst.)}.$$

31. F. Reines, M. S. Guir and H. W. Sobel, Phys. Rev. Lett. 37, 315 (1976).

32. C. Y. Prescott et al., Phys. Lett. 77B, 347 (1978); 84B, 524 (1979).
33. M. Davier, 1982 Paris Conference (see M. Davier of ref. 14).
34. J. G. Branson, Proceedings of the 1981 International Symposium on High Energy Lepton and Photon Interactions, Bonn, Germany, 1981, p. 279; DESY preprint No. 82-078, 1982 (it contains the most up to date results).
35. H.-J. Behrend et al., DESY preprint No. 82-063 (1982). This CELLO collaboration preprint also contains a tabulation of all the e^+e^- colliding beam results.
36. W. J. Marciano and A. Sirlin, Phys. Rev. Lett. 46, 163 (1981); BNL preprint No. 32028 (1982).
37. T. Kitagaki et al., Phys. Rev. Lett. 49, 98 (1982).
38. T. A. Nunamaker et al, Nucl. Instr. and Meth. 175, 331 (1980).
39. A. Barbaro-Galtieri, W. Carithers, C. Day, K. J. Johnson, W. A. Wenzel, and H. Videau, University of California at Berkeley preprint No. LBL-15030, 1982.

Figure Captions

- Fig. 1. Regions of parameter space in F_X-M_X which have been explored by various astrophysical processes and experiments. The sensitive region for P-635 is also shown.
- Fig. 2 The enlarged version of Fig. 1
- Fig. 3 (a) Production of axion coupled to $\gamma\gamma$.
(b) Electroproduction of axion coupled to e^+e^- .
(c) Single lepton production by positron annihilation.
(d) Lepton pair production by positron annihilation.
- Fig. 4 Hadroproduction of axion coupled to quarks and leptons.
- Fig. 5 Schematic arrangement of the experimental apparatus.
- Fig. 6 Region of the F_X-M_X parameter space which can be explored by P-635.
- Fig. 7 Spectrum of neutrino flux from the Tevatron beam dump when the production target is made of
(a) 104 cm of copper,
(b) 72 cm of tungsten,
(c) 200 cm of beryllium.
- Fig. 8 Resolution in longitudinal position, ΔZ , of the X^0 decay vertex as a function of θ_μ when the decay happens at a distance of (a) 300 m, (b) 200 m, (c) 100 m, before the detector.
- Fig. 9 Invariant mass resolution of the mu-pair, $\Delta m/m$, as a function of muon momentum, P_μ , for an axion decays into two symmetric muons.
- Fig. 10 Schematic arrangement of the non-magnetic detector.
- Fig. 11 Spectrum of neutrinos produced by 1 TeV protons. A single-horn train-load is used.

- Fig. 12 P_T -distributions of $\nu_\mu e \rightarrow \nu_\mu e$ and $\nu_e n \rightarrow pe$ events, assuming that $\nu_e/\nu_\mu = 1\%$ and $\theta_e \lesssim 10$ mr. The neutrinos are produced by 1 TeV protons and single-horn train-load is used.
- Fig. 13 Schematic arrangement of the magnetic muon spectrometer.
- Fig. 14 Geometry for the muon sky-shine calculation.
- Fig. 15 Muon spectrum at the P-635 detector due to muon sky-shine
- Fig. 16 Schematic diagram of the 1m x 1m MWPC.
(a) Electrical connections, (b) Mechanical arrangement of the anode wires and the cathode plane delay-line board.
- Fig. 17 Schematics of the CCD digitizer.
- Fig. 18 An example of the CCD data from one cathode plane of a 1m x 1m MWPC. They are readout from 5 equi-distance tap points of one continuous delay-line. The signals are the redundant measurement of a single shower.
- Fig. 19 An example of the CCD data from 8 independent and consecutive delay-lines on one cathode plane of a 3m x 3m MWPC. It illustrates the multi-particle capability of the chamber.
- Fig. 20 An example of the CCD data from one view of eight 3m x 3m MWPC's. Between chambers, there are 1 r.l. thick iron plates. Each view of the chamber is 3 m long, and there are 23 independent delay-lines on it.

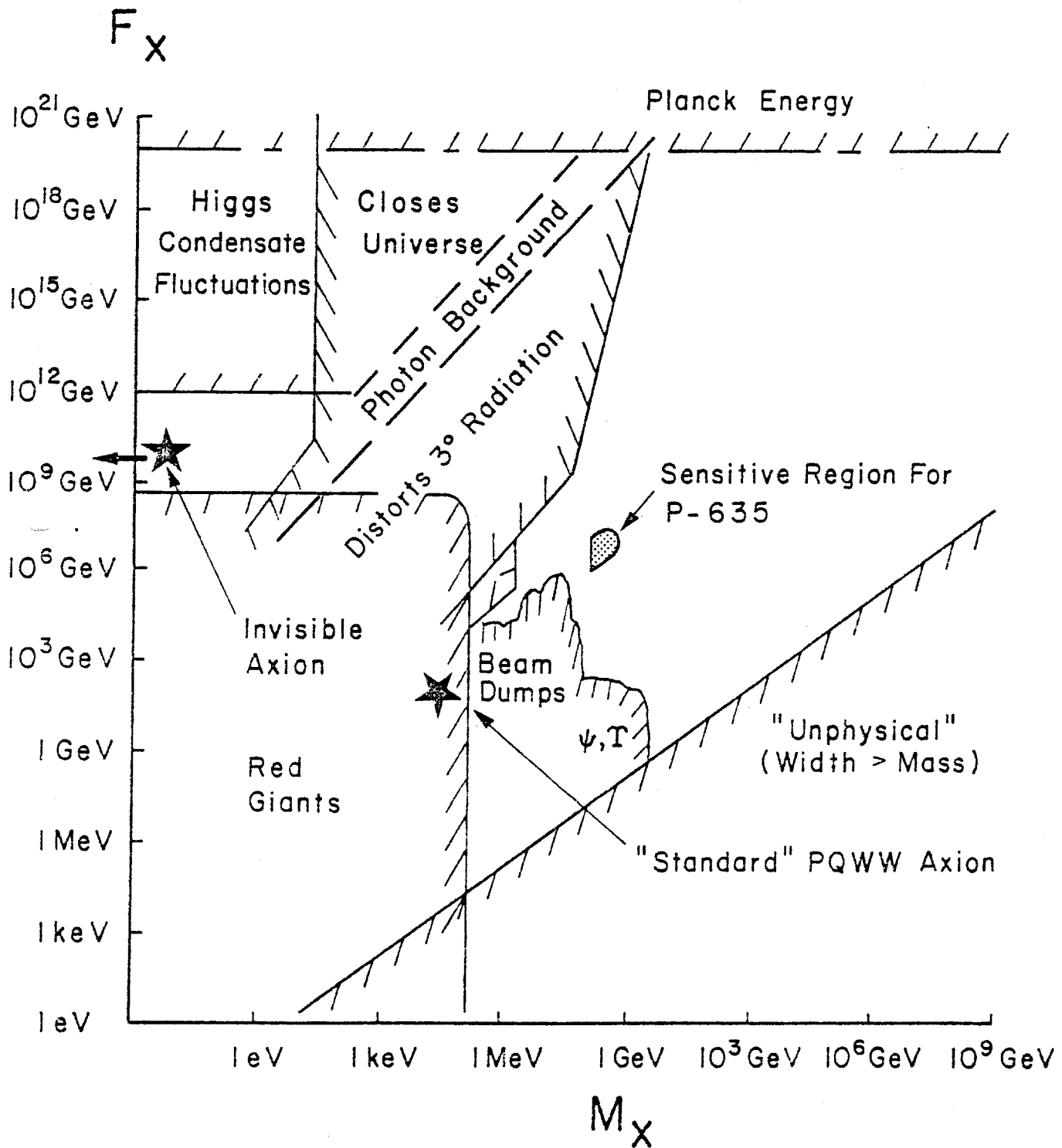


Fig. 1

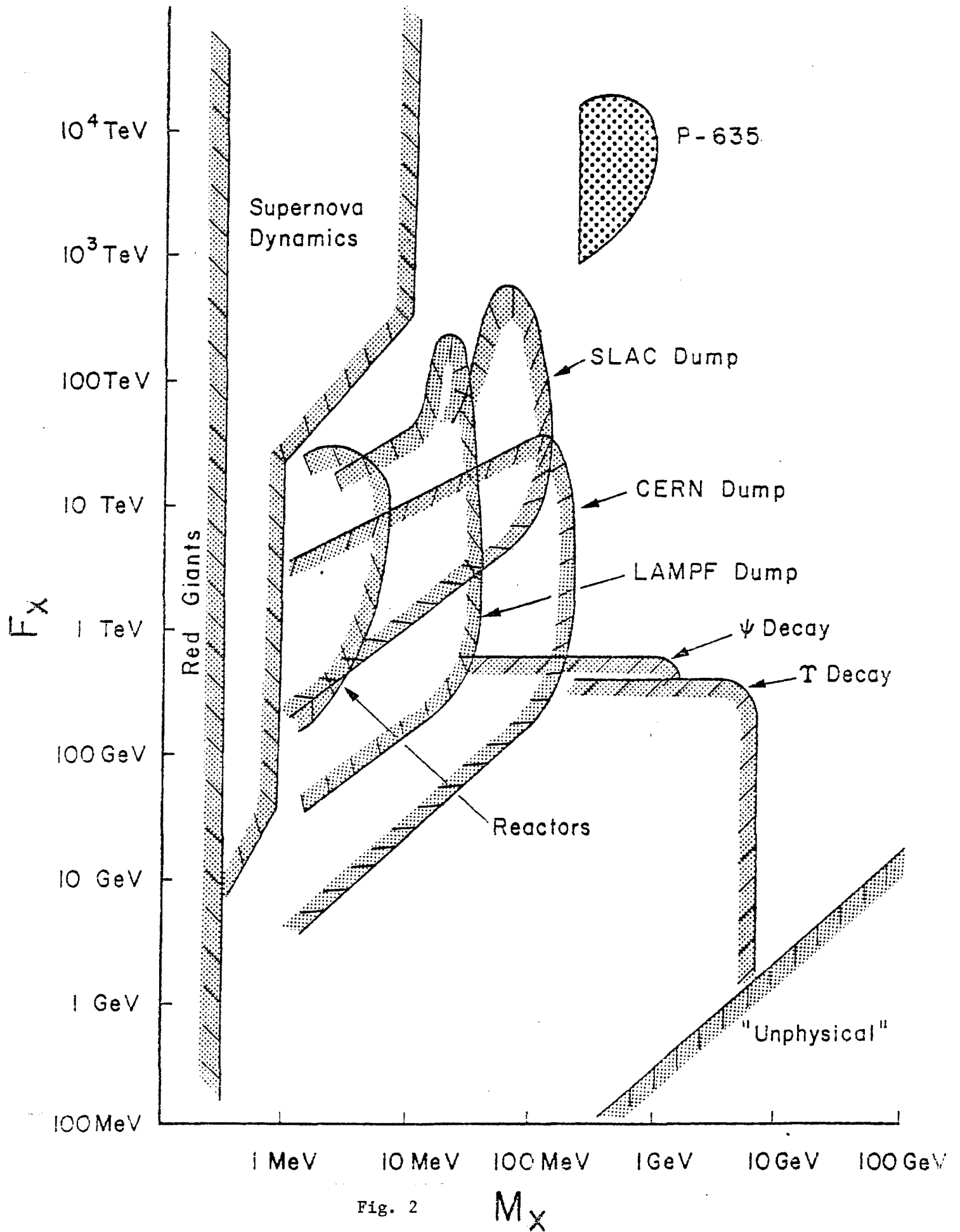


Fig. 2

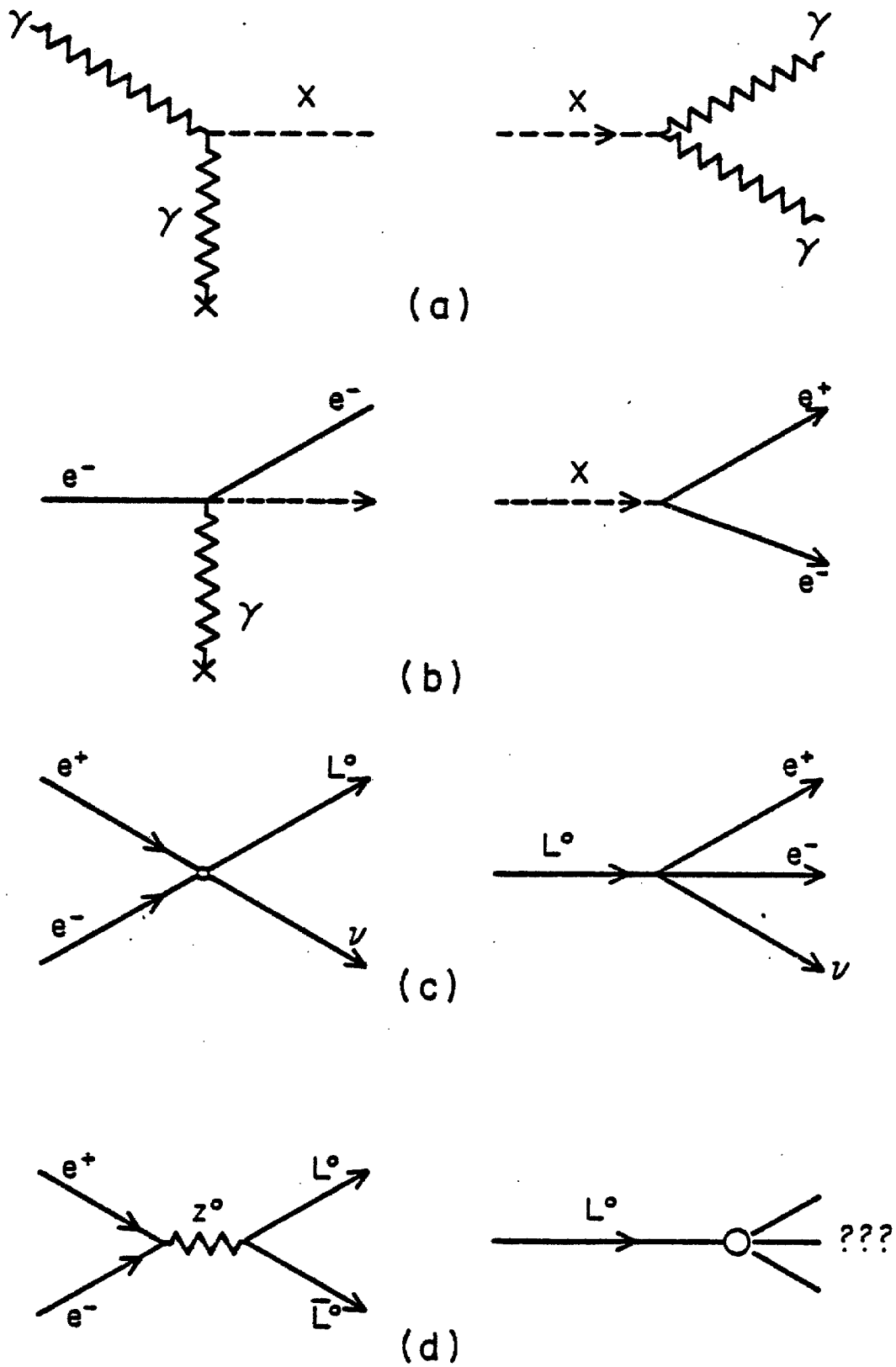


Fig. 3

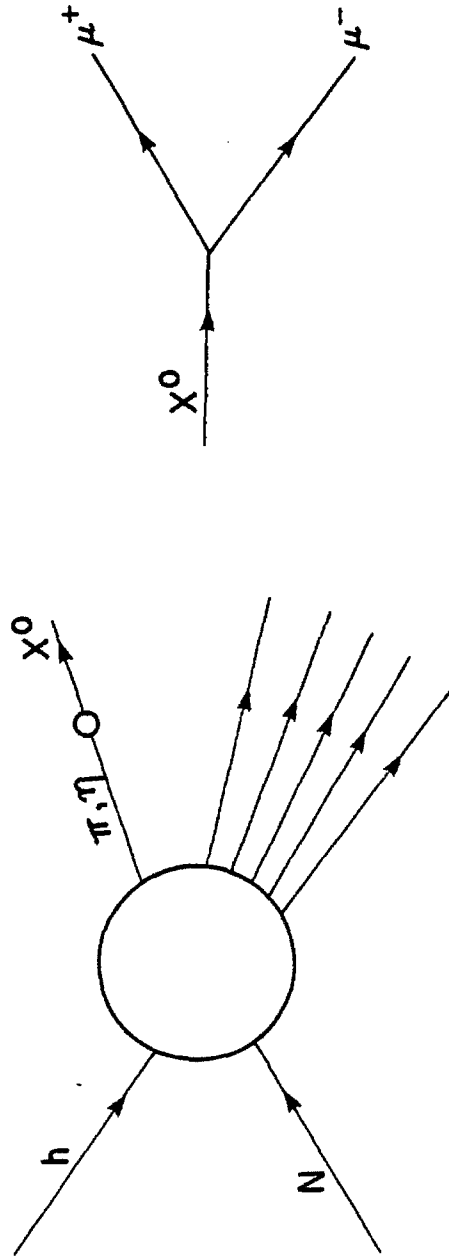
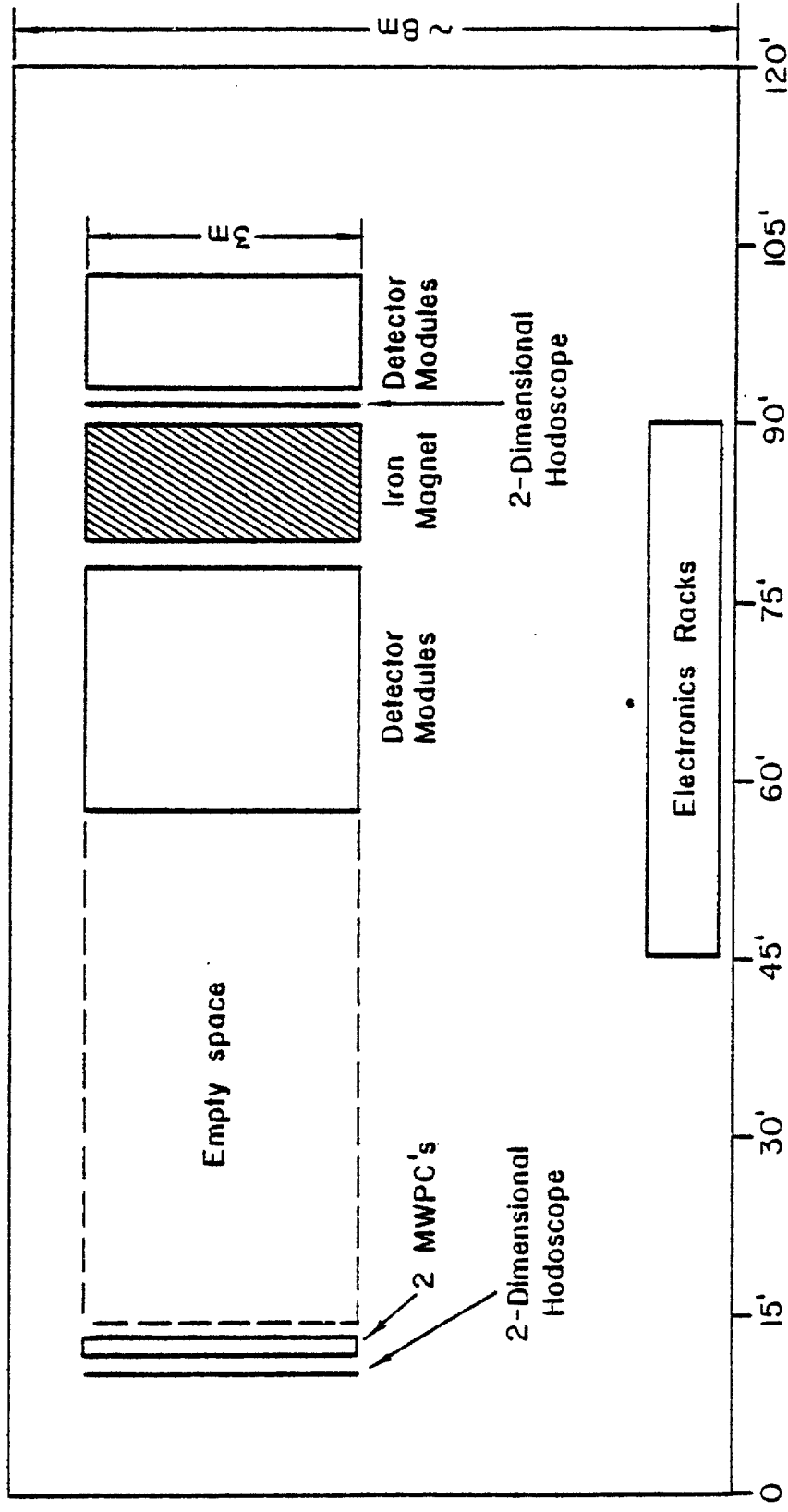


Fig. 4



Schematic Arrangement of the Experiment

FIG. 5

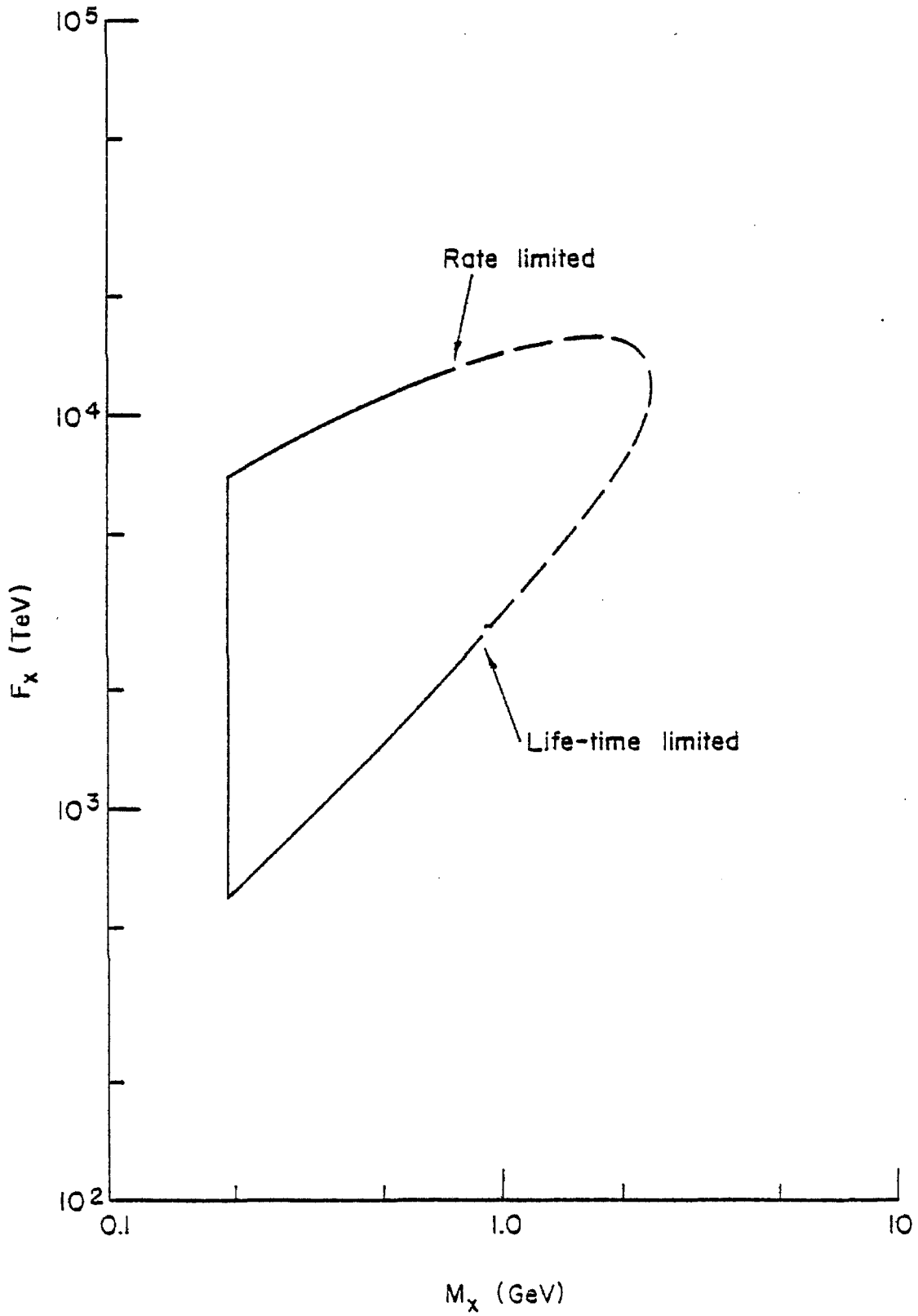


Fig. 6

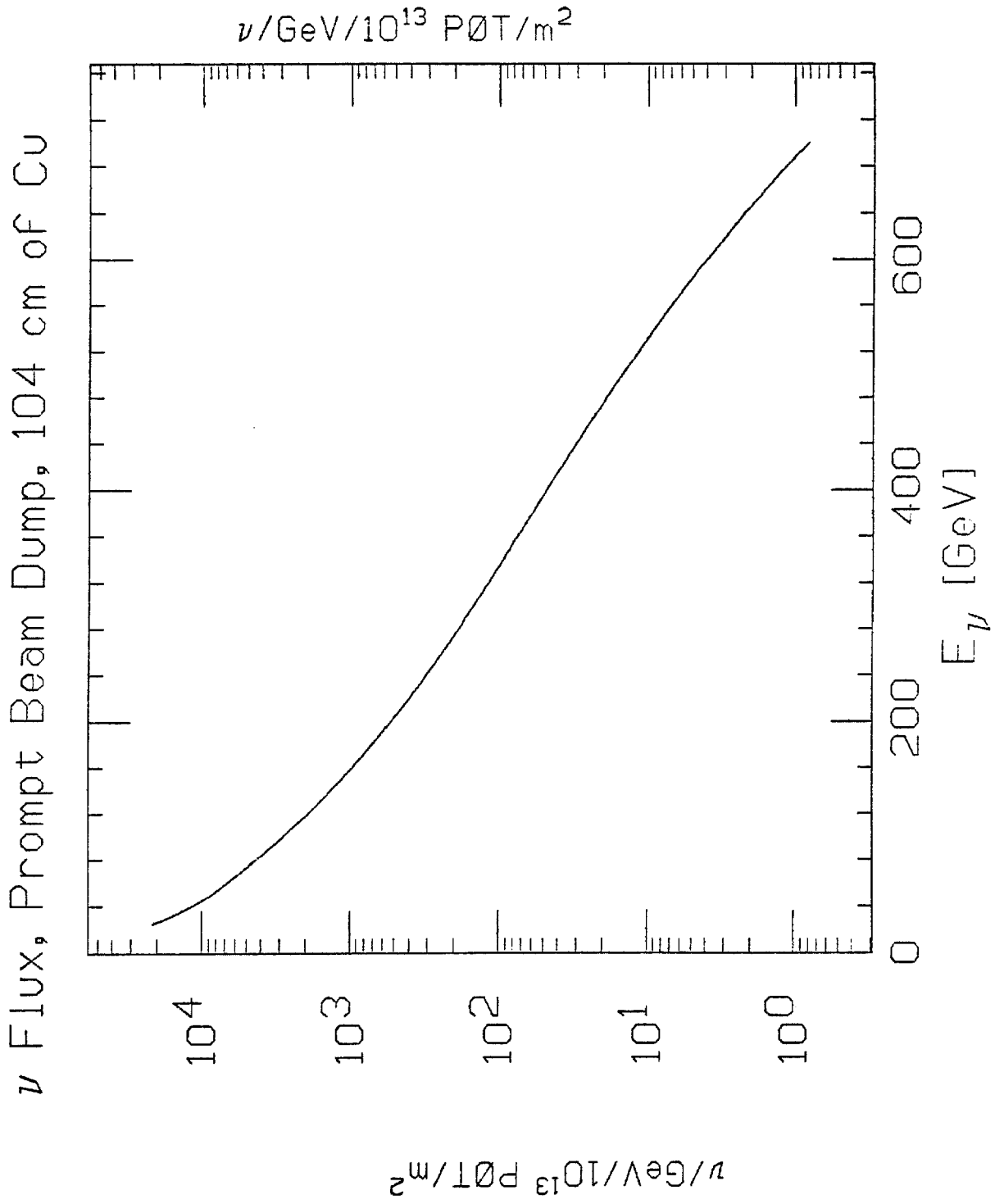


Fig. 7(a)

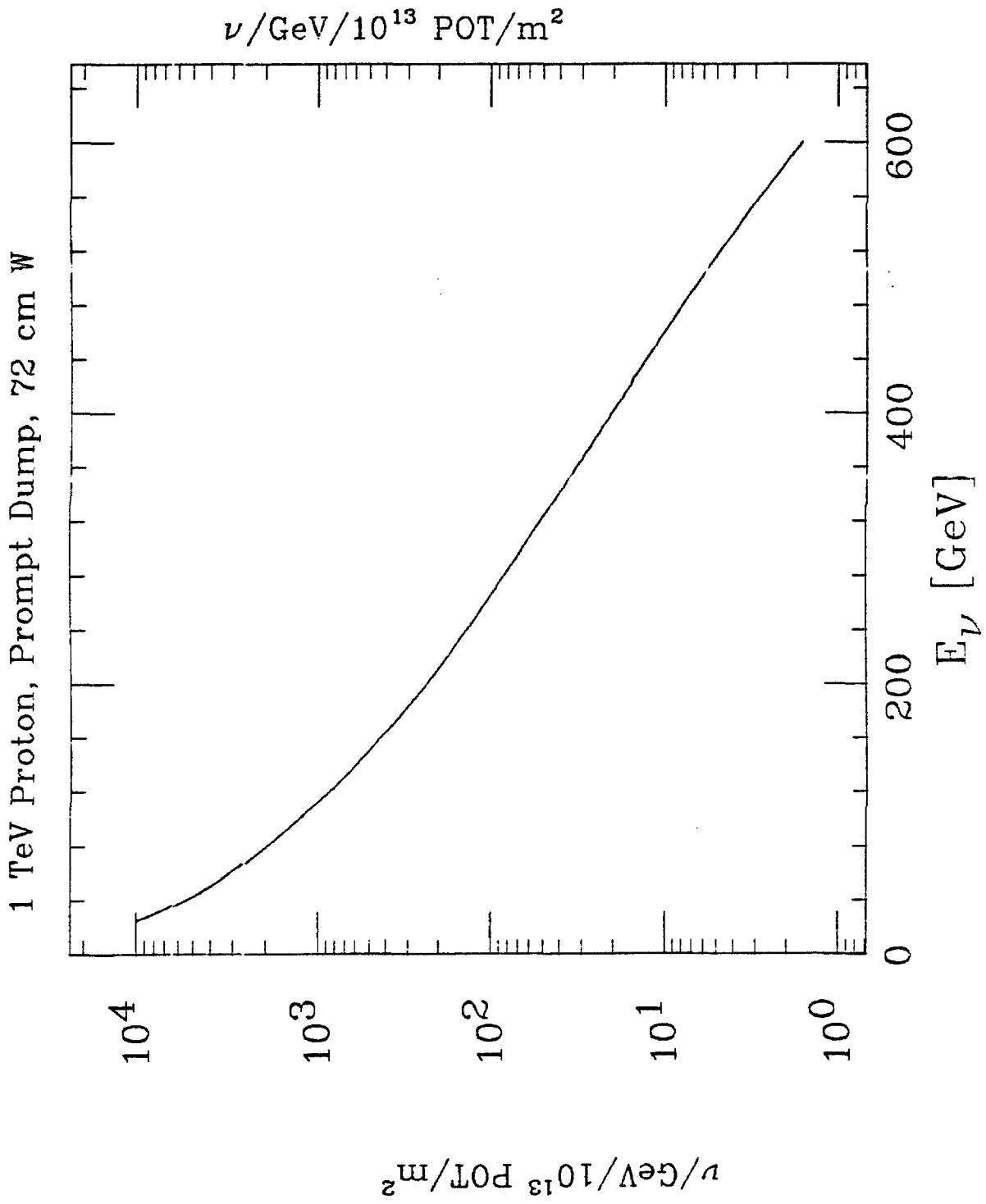


Fig. 7(b)

ν Flux, Prompt Dump, 200 cm Be

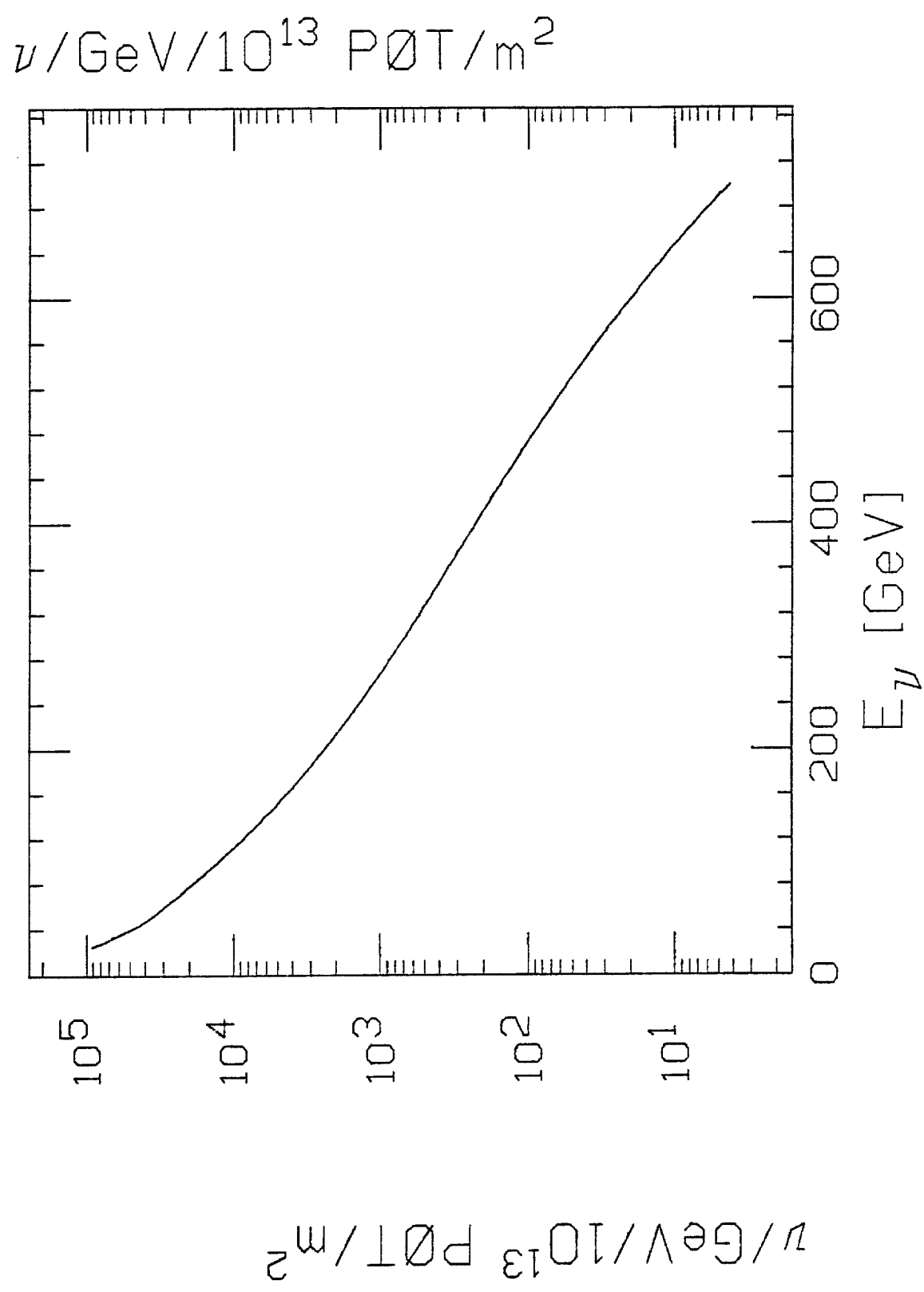


Fig. 7(c)

Vertex 300 m From the Detector

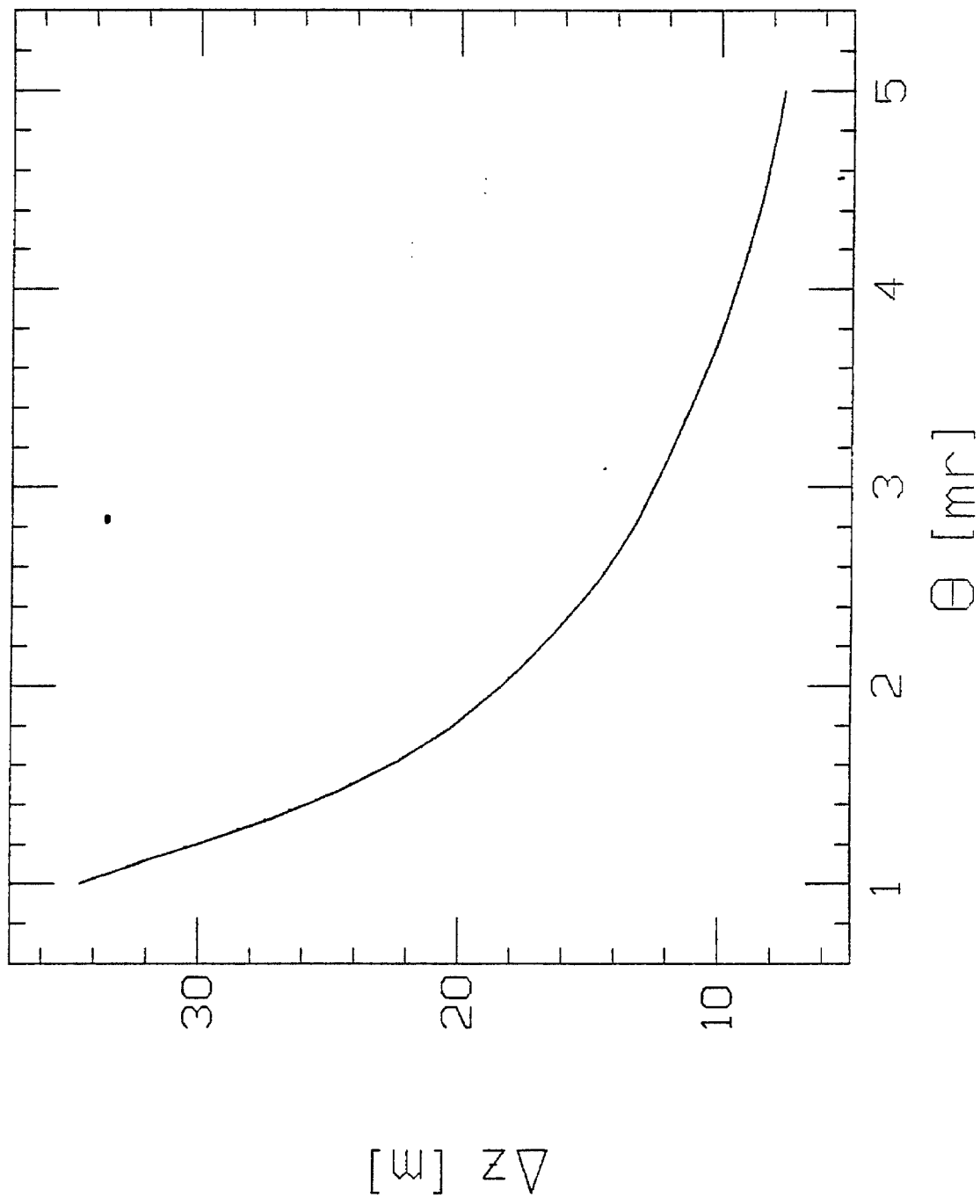


Fig. 8(a)

Vertex 200 m from the Detector

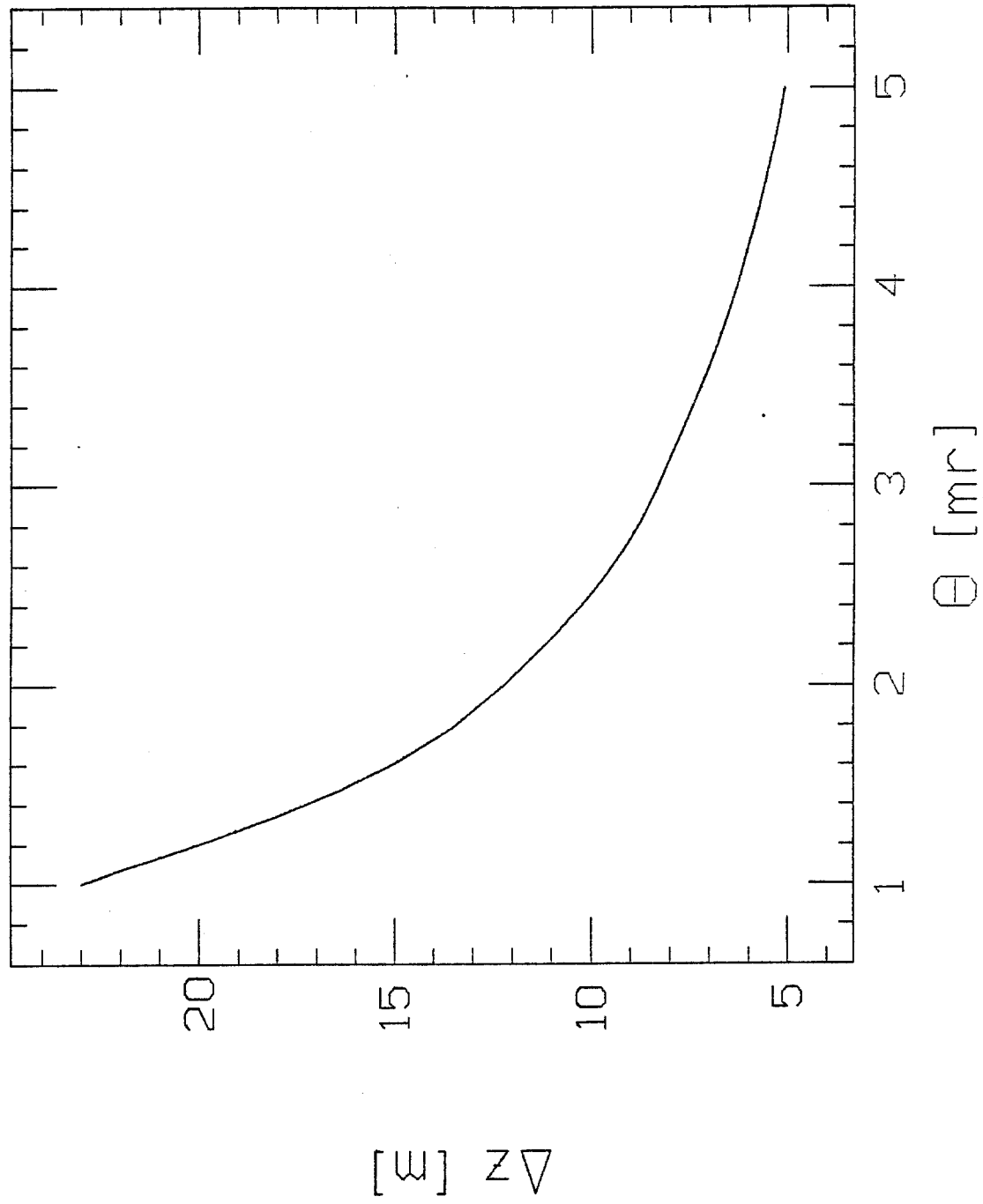


Fig. 8(b)

Vertex 100 m from the Detector

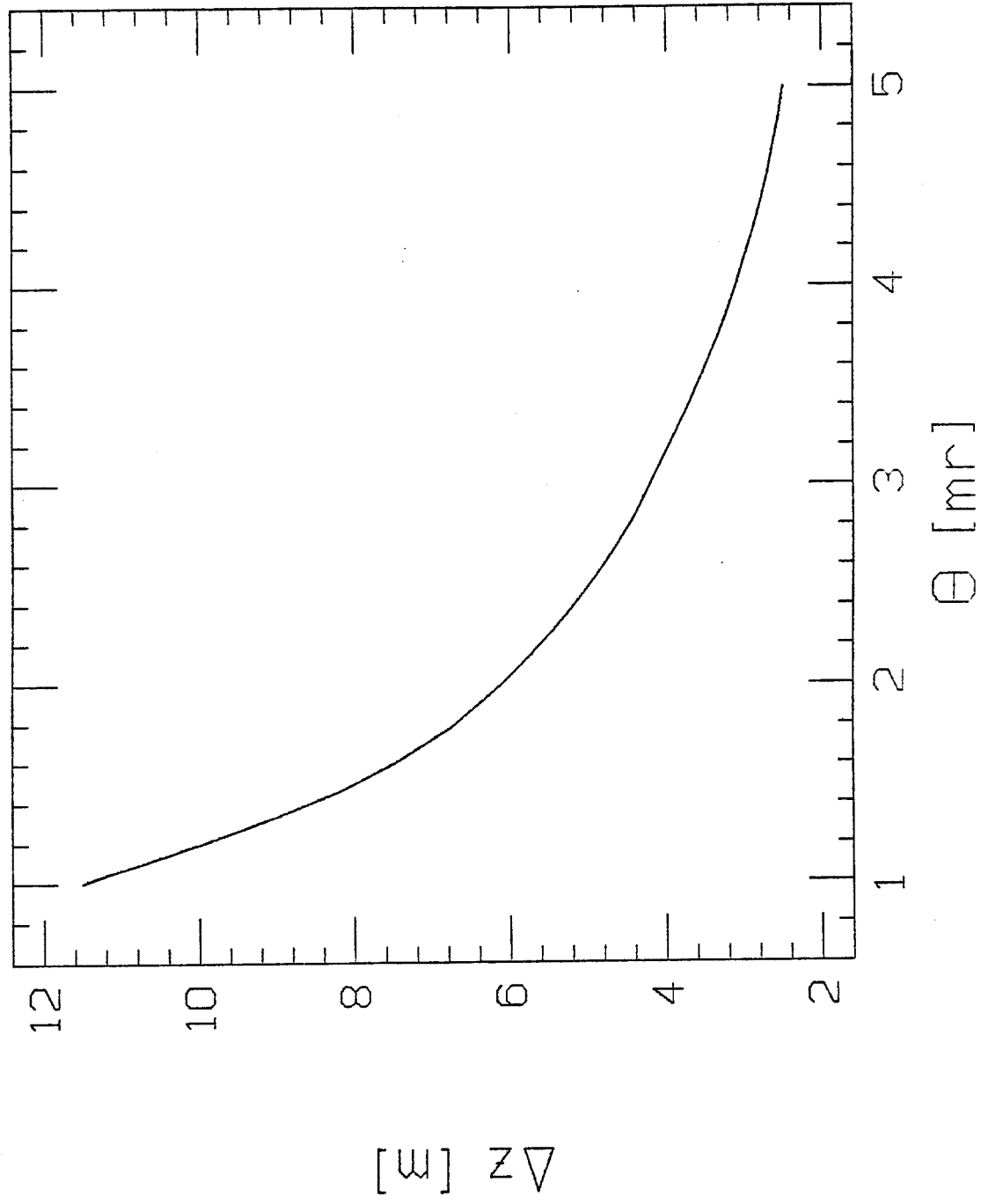


Fig. 8(c)

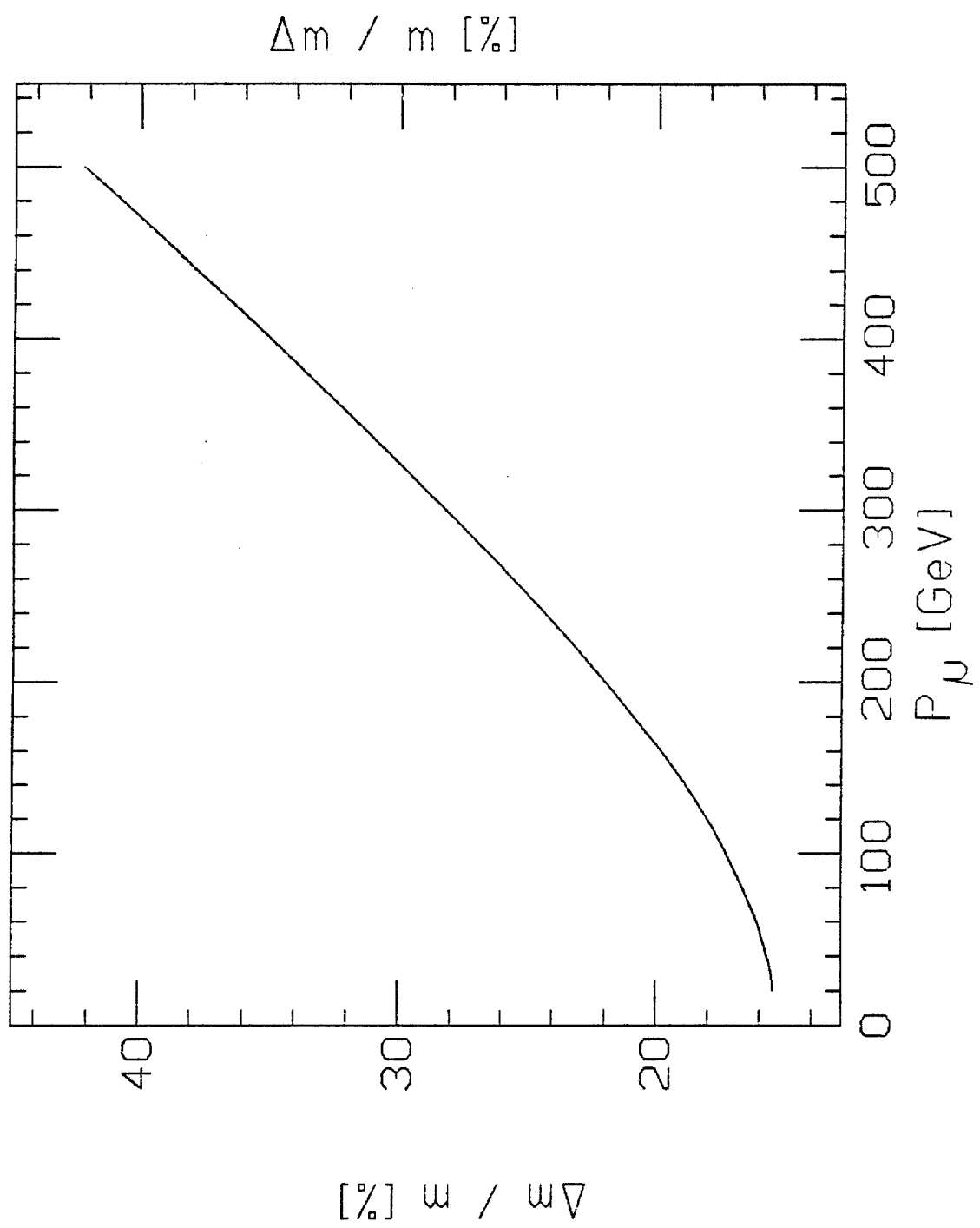


Fig. 9

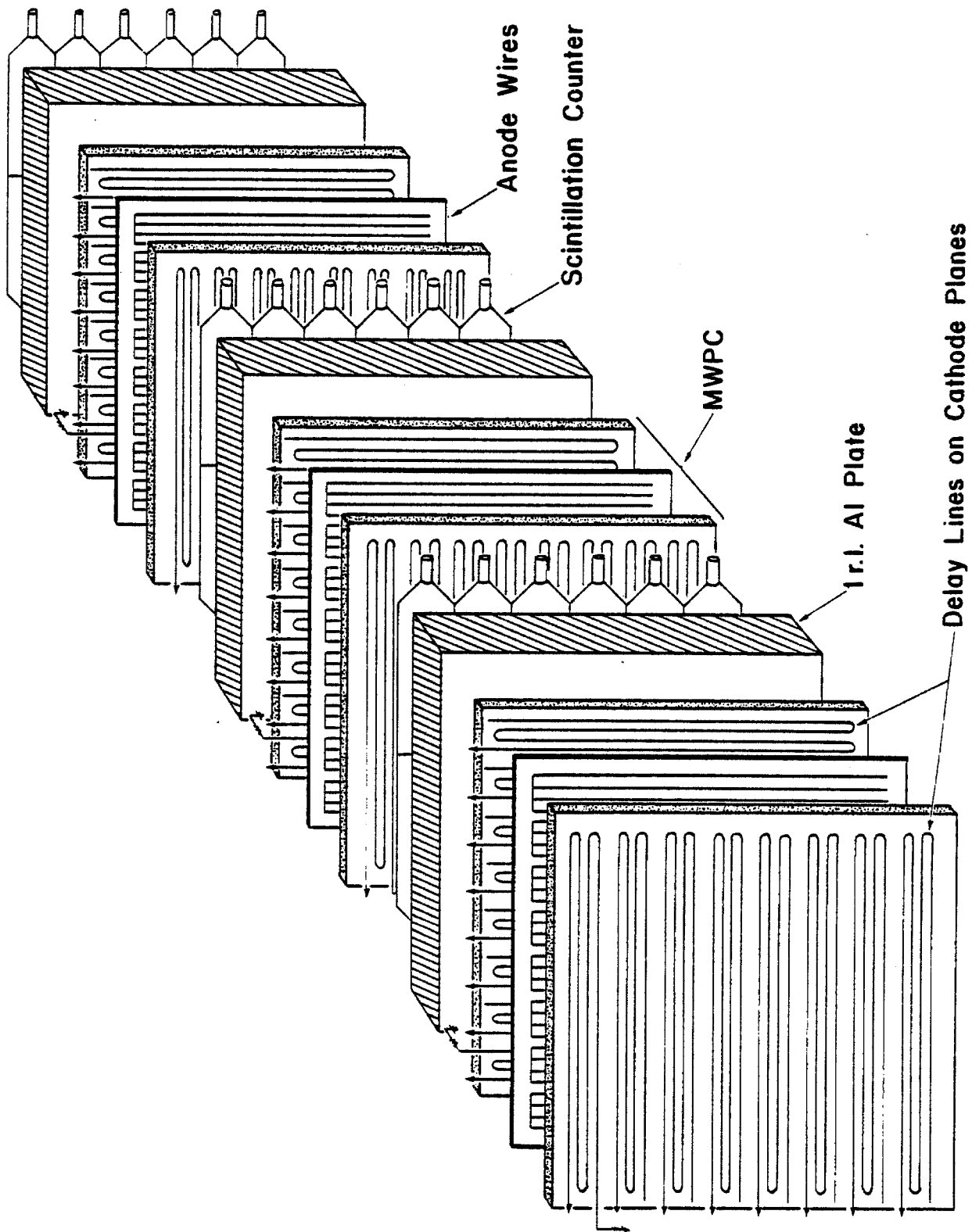


Fig. 10

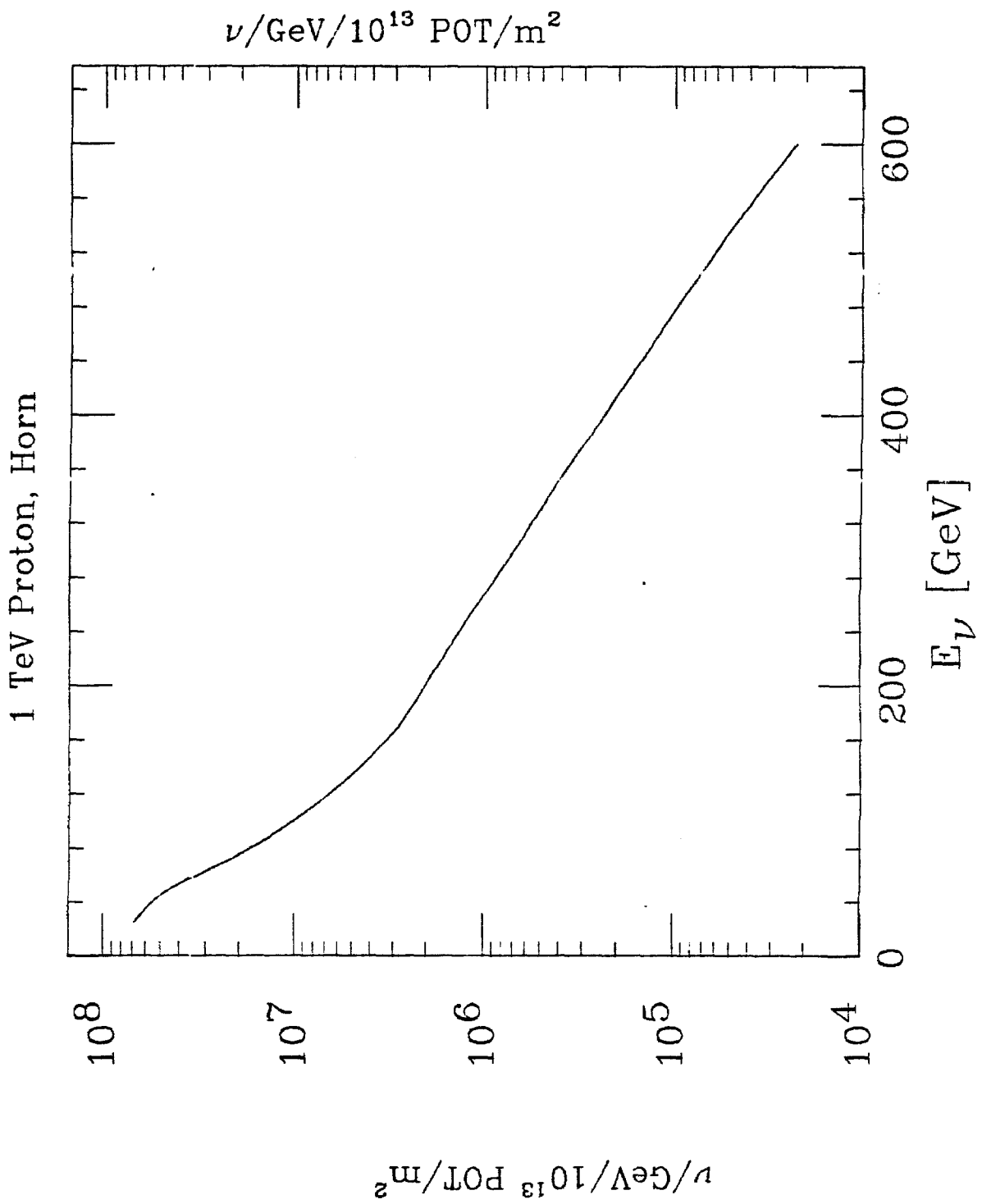


Fig. 11

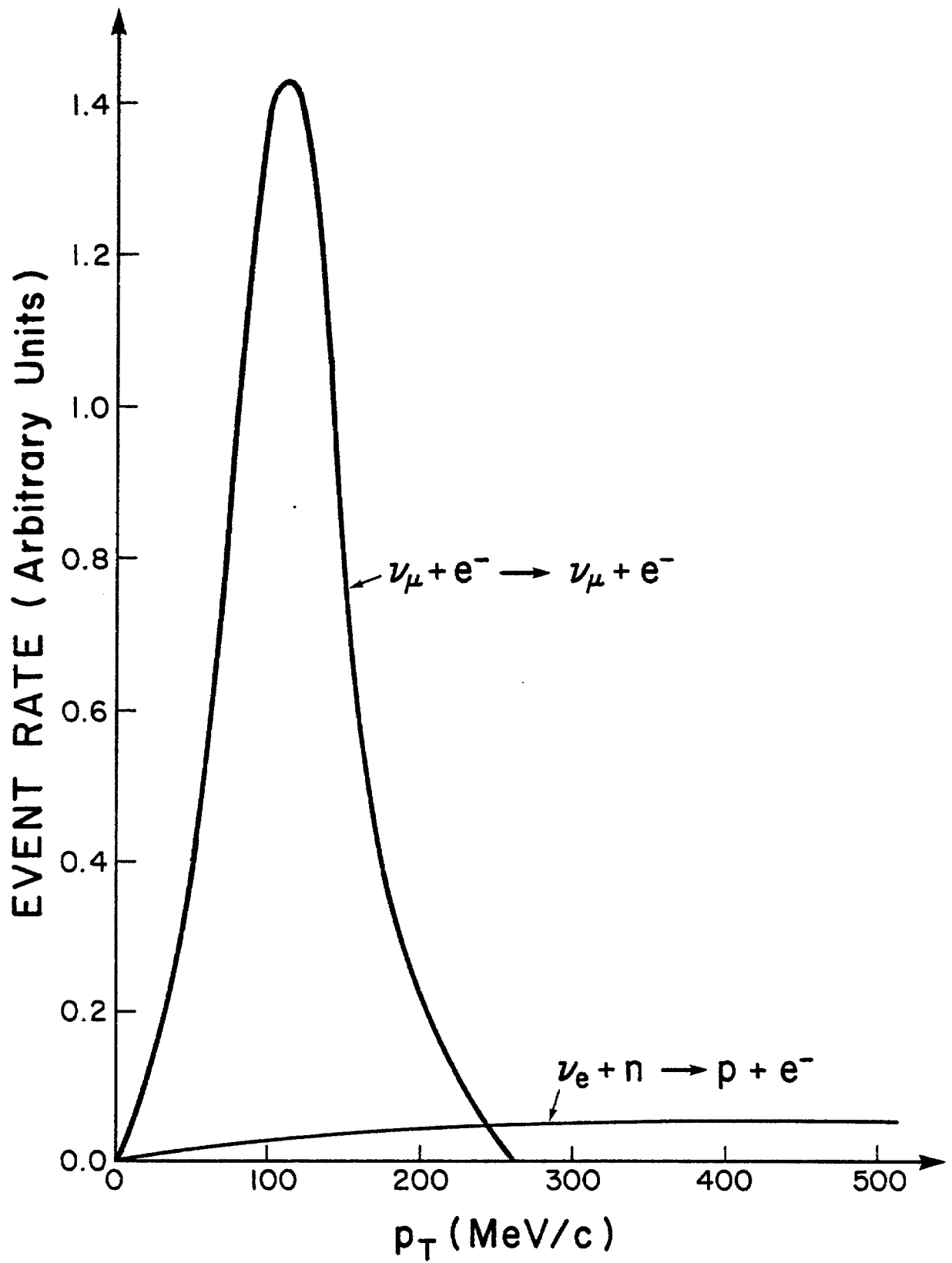


Fig. 12

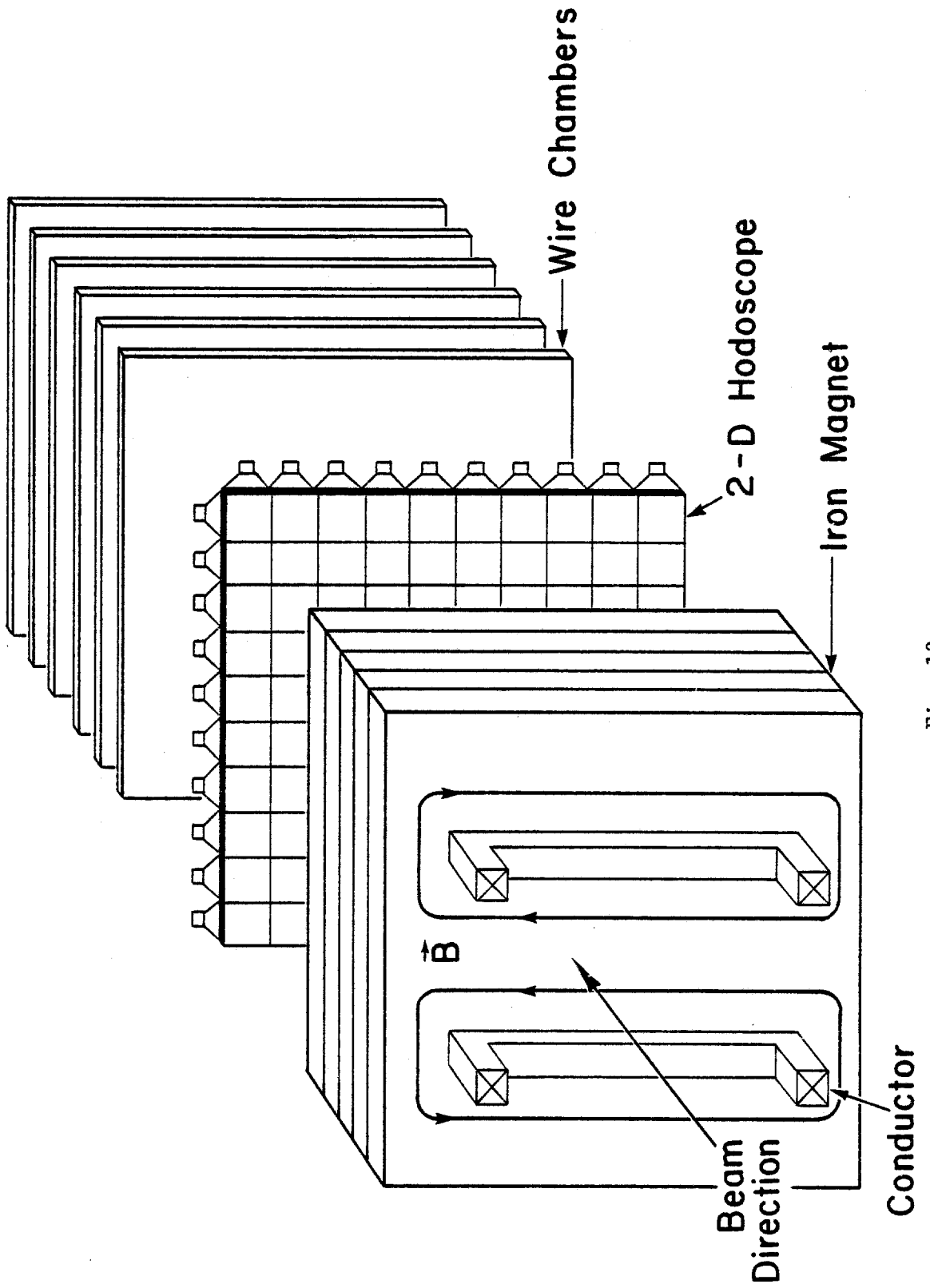
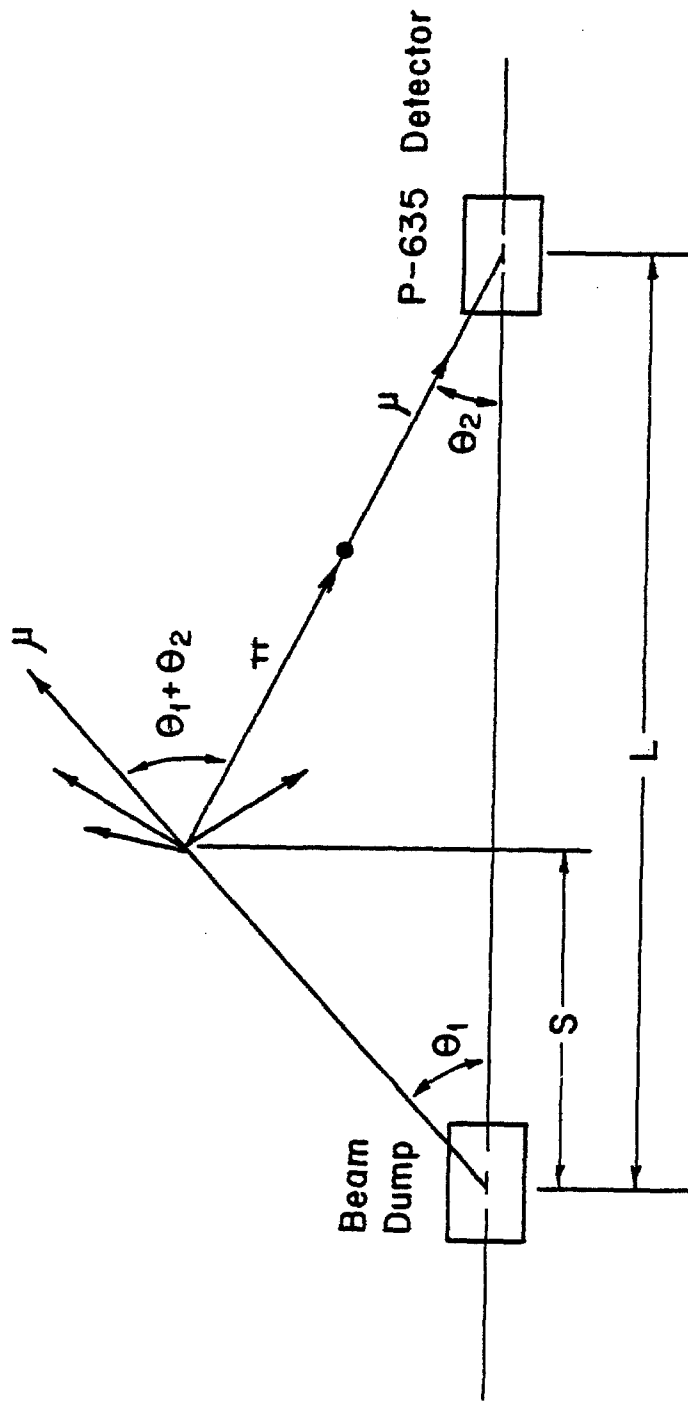


Fig. 13



$L \approx 600 \text{ m}$
 $\theta_1 \geq \theta_{\min} = 25 \text{ mrad}$
 $\theta_2 \leq \theta_{\max} = 50 \text{ mrad}$

Fig. 14

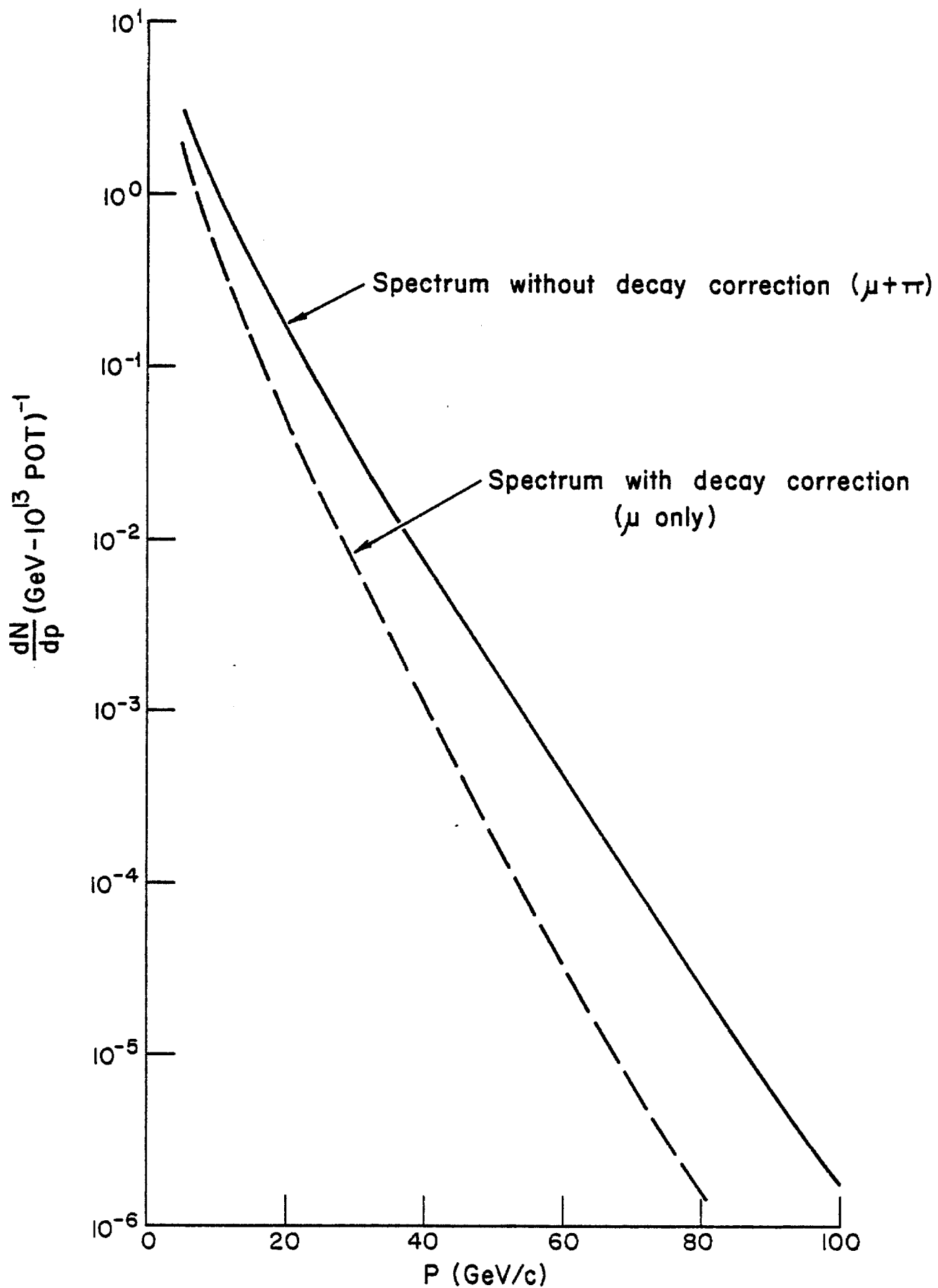


Fig. 15

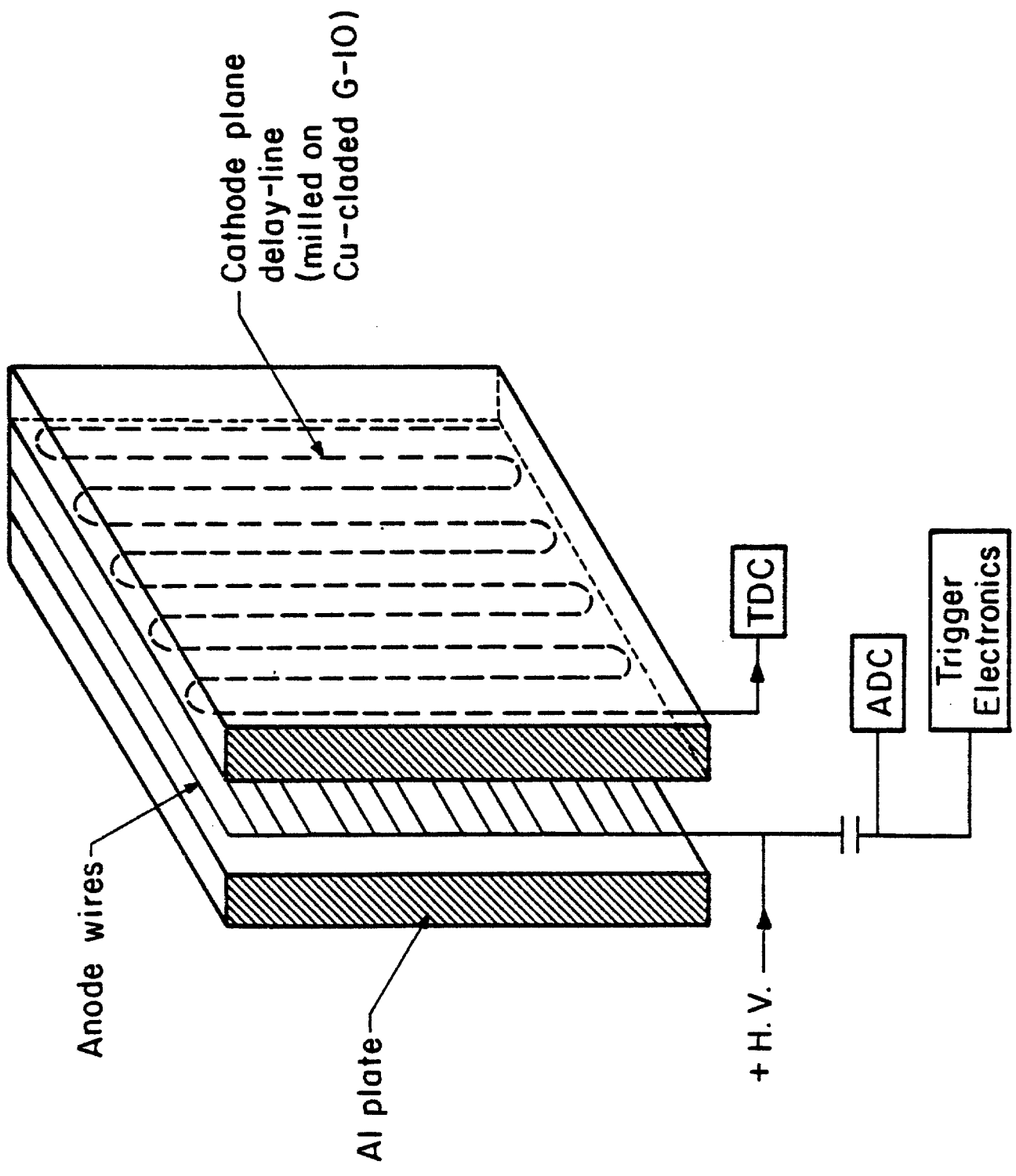


FIG. 16(a)

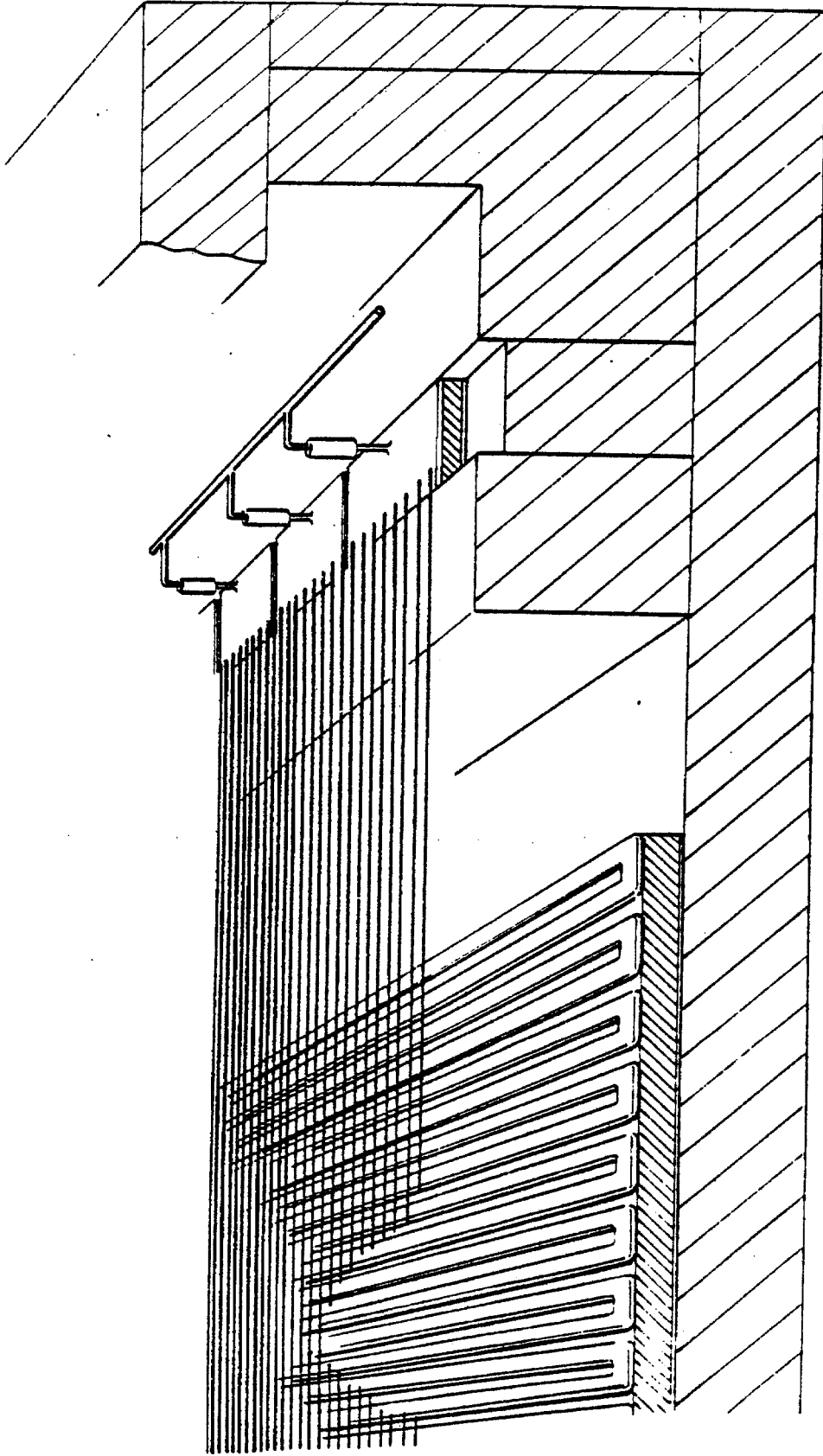
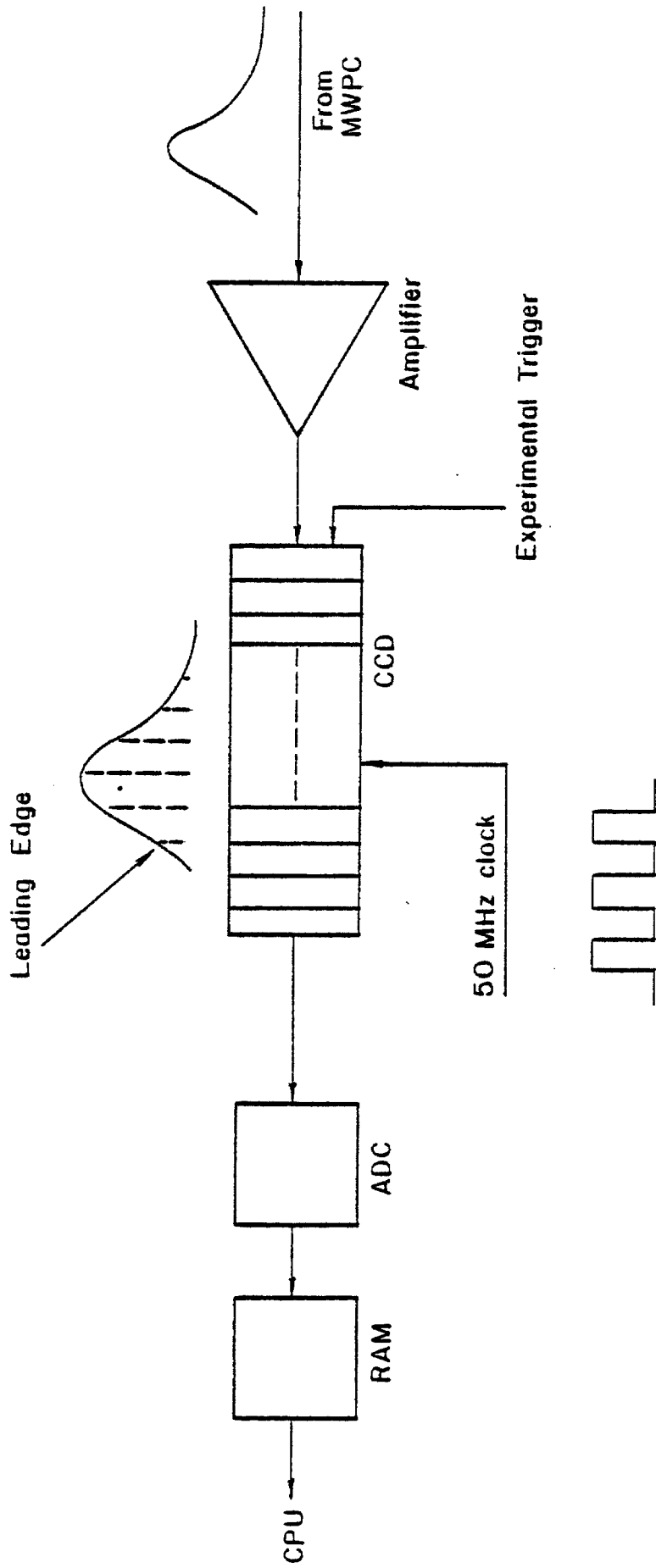


Fig. 16(b)



Schematics of CCD Digitizer

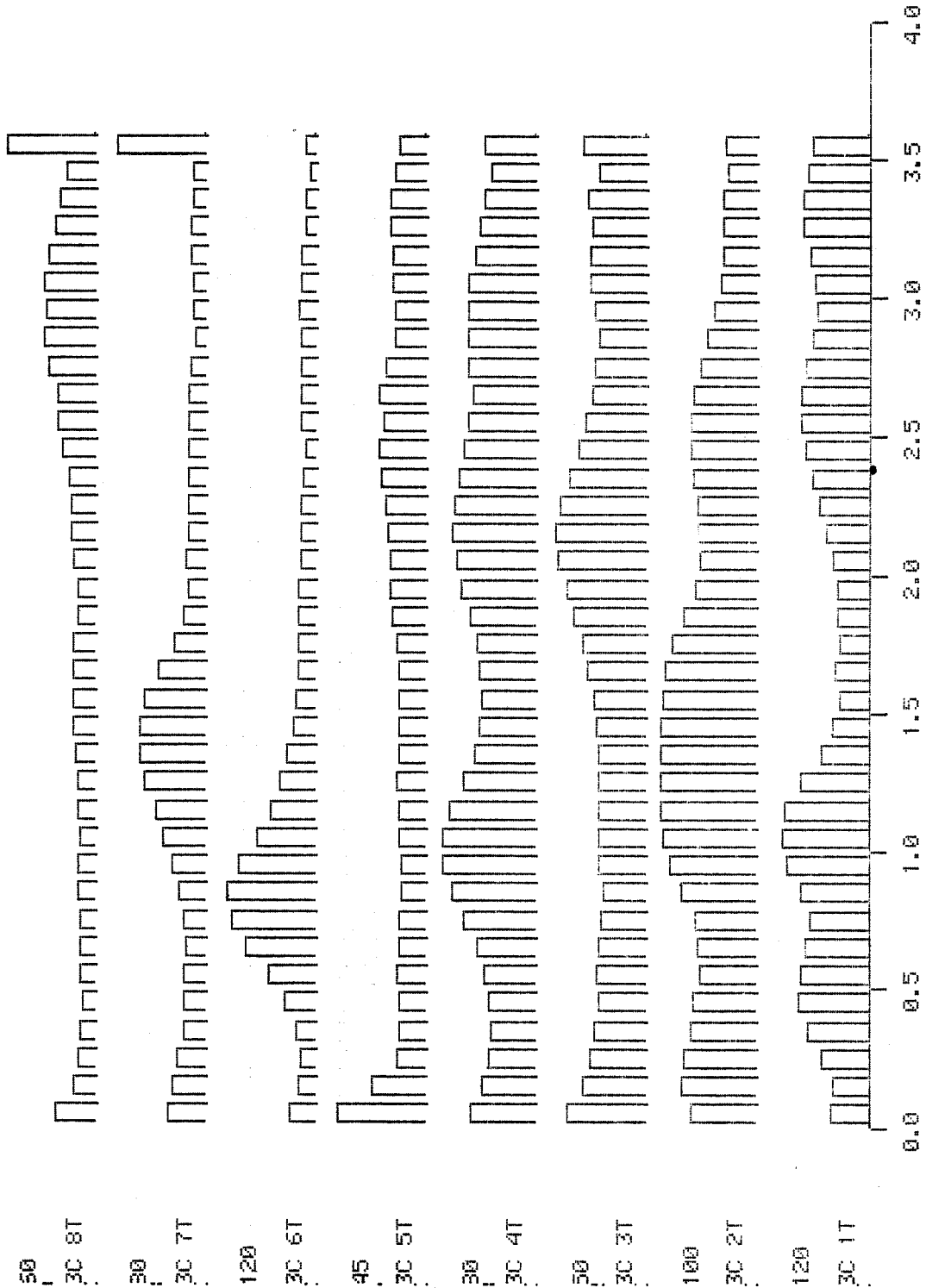
Fig. 17

BUCKET (101)



BUCKET (101)
Fig. 18

TAPE 52 RUN 132 TR6R 96 11/4/82 5:31:40 VERTICAL TAPS



BUCKET (10¹)

Fig. 19

TAPE 52 RUN 133 TRGR 188 11/5/82 21:19:50 EVERY TAP (X) (PPED ADJ)

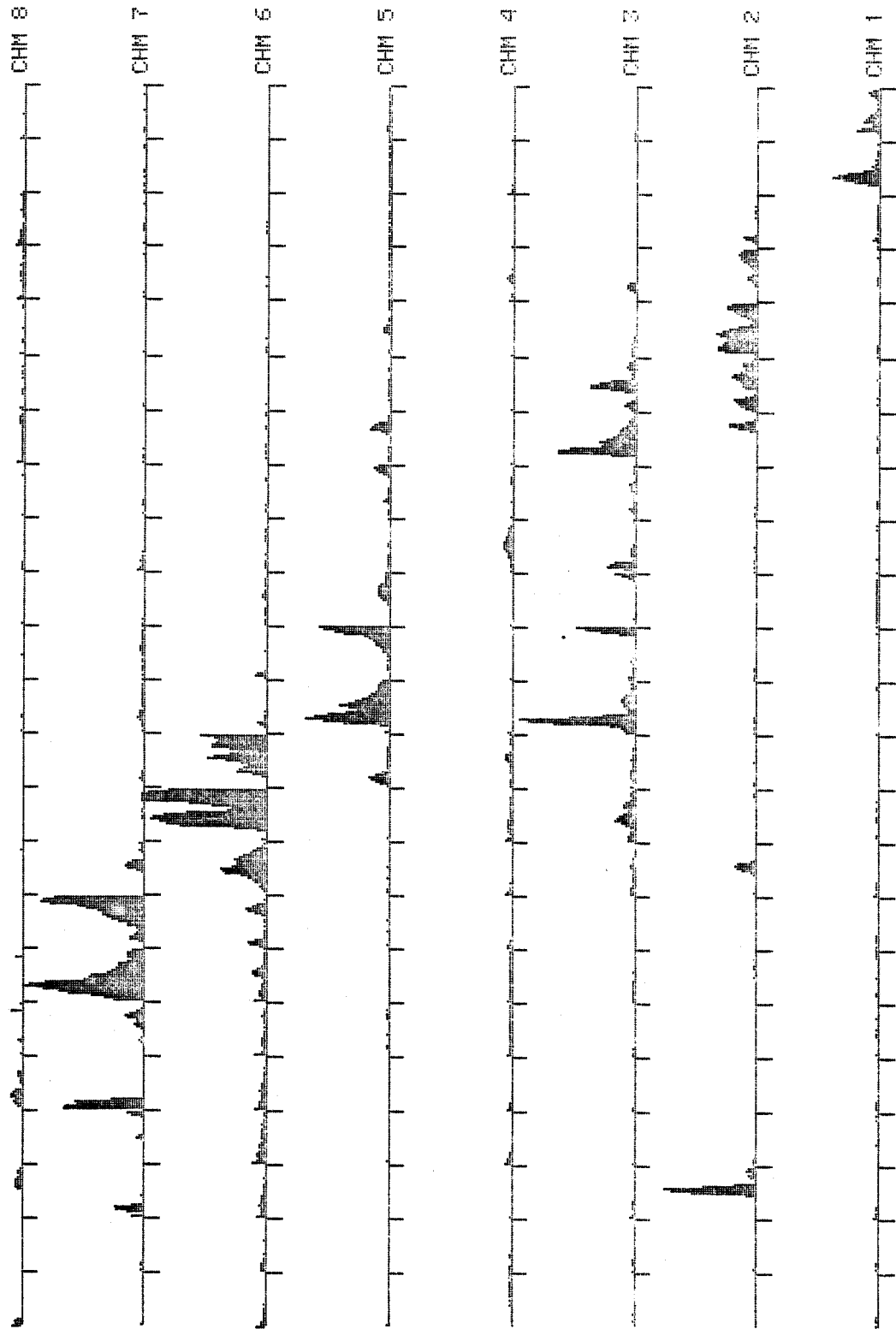


Fig. 20